Temporal Disaggregation of Daily Precipitation Data in a Changing Climate

by

Karen M. Wey

A thesis

presented to the University of Waterloo

in fulfillment of the

thesis requirement for the degree of

Master of Applied Science

in

Civil Engineering

Waterloo, Ontario, Canada, 2006

Author's Declaration

I hereby declare that I am the sole author of this thesis. This is a true copy of the thesis, including any required final revisions, as accepted by my examiners. I understand that my thesis may be made electronically available to the public.

Karen Wey

Abstract

Models for spatially interpolating hourly precipitation data and temporally disaggregating daily precipitation to hourly data are developed for application to multisite scenarios at the watershed scale. The intent is to create models to produce data which are valid input for a hydrologic rainfall-runoff model, from daily data produced by a stochastic weather generator. These models will be used to determine the potential effects of climate change on local precipitation events. A case study is presented applying these models to the Upper Thames River basin in Ontario, Canada; however, these models are generic and applicable to any watershed with few changes.

Some hourly precipitation data were required to calibrate the temporal disaggregation model. Spatial interpolation of this hourly precipitation data was required before temporal disaggregation could be completed. Spatial interpolation methods were investigated and an inverse distance method was applied to the data. Analysis of the output from this model confirms that isotropy is a valid assumption for this application and illustrates that the model is robust. The results for this model show that further study is required for accurate spatial interpolation of hourly precipitation data at the watershed scale.

An improved method of fragments is used to perform temporal disaggregation on daily precipitation data. A parsimonious approach to multisite fragment calculation is introduced within this model as well as other improvements upon the methods presented in the literature. The output from this model clearly indicates that spatial and

temporal variations are maintained throughout the disaggregation process. Analysis of the results indicates that the model creates plausible precipitation events.

The models presented here were run for multiple climate scenarios to determine which GCM scenario has the most potential to affect precipitation. Discussion on the potential impacts of climate change on the region of study is provided. Selected events are examined in detail to give a representation of extreme precipitation events which may be experienced in the study area due to climate change.

Acknowledgements

I would like to express gratitude to my supervisor, Dr. Don Burn, whose expertise, understanding, and patience added considerably to my graduate experience. I would also like to thank the Canadian Foundation for Climate and Atmospheric Sciences without whose funding this work would not have been possible. I want to communicate my appreciation of the entire project team, Mohammed Sharif, Dr. Slobodan Simonovic, Predreg Prodanovic, Linda Mortsch and Mark Helsten, for their input and guidance through my work. Finally I want to thank Brett McAllister for helping debug my computer code and editing this thesis.

Dedication

To David, my one true love.

Table of Contents

List of Tables

List of Figures

1   Introduction

Climate change is a contributor to increasing temperatures; however, global warming

also causes change in the amount of precipitation that is received. This changes the

amount of precipitation and the amount of fresh water that is available worldwide. While

climate change is creating drought in some parts of the world (United Nations

Environment Programme, 1996), Canada and other northern regions have experienced

increasing rates of precipitation, as can be seen in Figure 1-1.
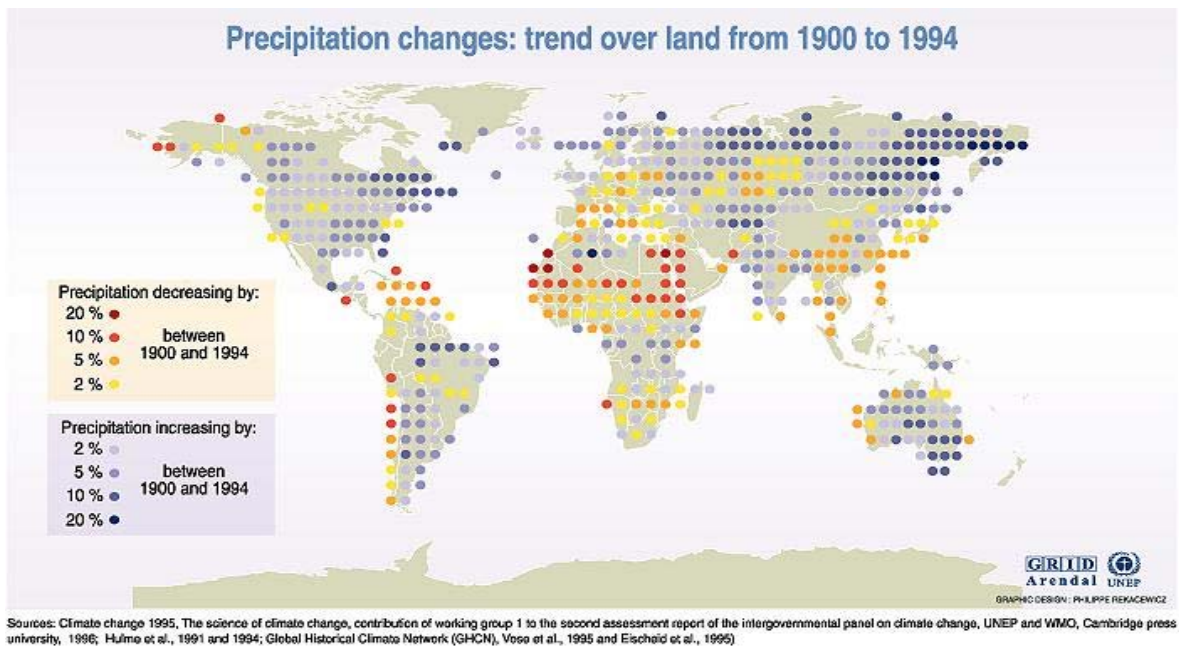
Figure 1-1: Global change in precipitation from 1900 to 1994
(United Nations Environment Programme, 1996)

Society relies on water resources infrastructure to protect urban and agricultural centers

from the hydrological hazards of both flood and drought events. Design of this

infrastructure is based on specified design events to ensure that it will be able to

withstand extreme hydrological events. For this infrastructure to operate properly,

designers need to be able to accurately predict the extent to which extreme events will affect the location for which the infrastructure is being designed. Without proper prediction of extreme hydrological events, these water resources systems could fail at unacceptable high rates, putting society at risk.

There are two methods currently used to forecast these hydrological events: statistical frequency analysis and streamflow simulation. Statistical frequency analysis is the more common of the two methods (Watt et al., 1989). It is based on historical precipitation records and therefore is only valid for forecasting purposes if precipitation trends are stationary (Watt et al., 1989). However, as shown above, due to climate change, precipitation data can no longer be considered stationary and therefore this method is not accurate in a changing climate. Streamflow simulation is a relatively new method and requires estimations of precipitation data which are used in the simulation of potential streamflow conditions. Since urban floods are almost always dominated by precipitation (Watt et al., 1989), good precipitation data are required to properly simulate streamflow. The focus of this thesis is to generate precipitation data which are acceptable for use in streamflow simulation.

1.1   Project Overview

This thesis is part of a larger project aimed at assessing the risk of damage by flood or drought while taking into account the changing climate. The various components of this project are shown in Figure 1-2, which also identifies the components of the project that compose this thesis. The aim of this thesis is create models for spatially interpolating

hourly precipitation data and temporally disaggregating daily precipitation data to an

hourly time scale for a multisite scenario. These models will be used to create data

which are valid for input to the event based hydrologic model used in this project.
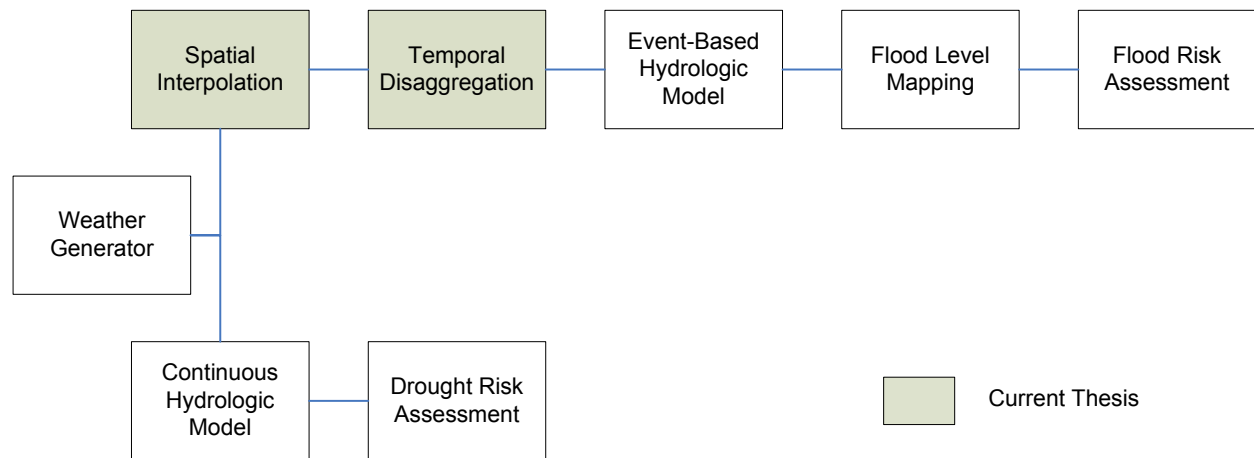
Figure 1-2: Project flowchart

The first segment of this project involves the development of a statistical weather

generator. This is a statistical model that generates synthetic meteorological data for

given climate scenarios. This particular weather generator creates data on a daily time

step. More information on the workings of this weather generator can be found in

Section 2.2.

The next part of this project is to simulate streamflow using the meteorological data

created by the weather generator as input. While the daily weather generator data can

be input directly to the continuous hydrological model used in this project, some

manipulations of the data, namely spatial interpolation and temporal disaggregation, are

required before these data can be input to the event-based hydrologic model used in

this project. The models for interpolation and disaggregation of the precipitation data will be the focus of this thesis.

The hydrologic event model requires hourly precipitation data to properly simulate streamflow during significant precipitation events. It was determined to be more advantageous to disaggregate the weather generator output into hourly data than it would be to modify the weather generator to generate hourly weather data. Therefore a model to disaggregate daily precipitation data to a finer timescale is required.

The spatial interpolation model is required to facilitate the application of the temporal disaggregation. Calibration of the temporal disaggregation model requires a small amount of hourly precipitation data at the same locations as the daily data being disaggregated. Since hourly precipitation gauges were not available at the locations requiring disaggregation for the project, spatial interpolation was required to acquire this input.

The streamflow output from the continuous hydrologic model is used to assess the risk and potential damage of drought in the region of study. The streamflow output from the event hydrologic model is used to map flood levels of potential extreme hydrologic events. These potential flood levels are then used to assess the risk and potential damage of floods in the region of study.

1.2 Scope of the Thesis

The purpose of this study is to convert the daily data, which are output from the weather generator, into hourly data that can be used for streamflow simulation by the event based hydrologic model. There are three main components to this study. The first component is the development of a model for the spatial interpolation of hourly precipitation data. The second portion of this study is the development of a model to disaggregate daily precipitation data into hourly precipitation data. The third part of this study is the application of these two models to a case study. The first two components comprise the shaded portions of Figure 1-2.

The chapters of this thesis are presented as follows. Chapter 2 is a review of literature as it applies to the different aspects of this research. Chapter 3 covers the spatial interpolation method that was used, along with some basic results. Chapter 4 describes the methods used in the temporal disaggregation model. Chapter 5 reviews a case study applying the models presented in the previous two chapters. Chapter 6 provides the results of the models and an analysis thereof. The final chapter covers the conclusions and outcomes of this research.

2   Literature Review

This literature review is comprised of four main sections: general circulation models, weather generators, spatial interpolation methods and temporal disaggregation methods. The first two sections discuss some of the background information required to understand the input data used for this study. The latter two sections examine previous studies that have been completed in the fields of spatial interpolation and temporal disaggregation, which are the main areas of study for this thesis.

2.1   General Circulation Models

General circulation models (GCMs), which have been in use since the mid 1990s are the main tool for predicting future global climate. GCMs are three-dimensional models of global air and water circulation patterns. There currently exist both atmospheric GCMs (AGCMs) and ocean GCMs (OGCMs) as well as the more complex atmosphere-ocean GCMs (AOGCMs) also known as the coupled GCM (CGCM) (Canadian Institute for Climate Studies 2005; Intergovernmental Panel on Climate Change, 2001).

GCMs are finite element models which divide the entire atmosphere (and/or ocean) into cells that are approximately 3° square and 1km high (Masters, 1998). Figure 2-1 provides a visual interpretation of how GCMs work. The models are designed to track changes in climate by location, time of year and climate change scenario. These changes are compared to the normal values from 1961-1990, which is known as the GCM baseline climate.
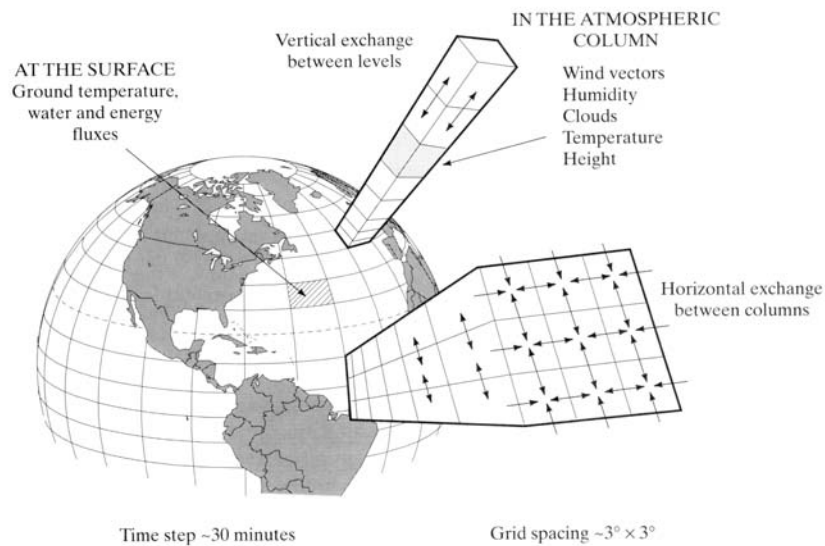
Figure 2-1: Schematic of GCM model (Masters, 1998)

2.1.1   GCM Storylines and Scenarios

The Intergovernmental Panel on Climate Change (IPCC) has suggested an ensemble of

possible scenarios or storylines describing how the world could look for the next

century. These scenarios include predictions of global population, economy and

pollutant emissions among other things. The scenarios are split into four main

categories known as the A1, A2, B1 and B2 storylines, which are discussed in detail in

the IPCC Special Report on Emission Scenarios (2000). The commonly known outline

of each storyline is given here for reference.

A1
The A1 storyline and scenario family describes a future world of very rapid economic growth, global population that peaks in mid-century and declines thereafter, and the rapid introduction of new and more efficient technologies. Major underlying themes are convergence among regions, capacity-building, and increased cultural and social interactions, with a substantial reduction in regional differences in per capita income. The A1 scenario family develops into three groups that describe alternative directions of technological change in the energy system. The three A1 groups are distinguished by their technological emphasis: fossil intensive (A1FI), non-fossil energy sources (A1T), or a balance across all sources (A1B; where balanced is defined as not relying too heavily on one particular energy source, on the assumption that similar improvement rates apply to all energy supply and end use technologies).

A2
The A2 storyline and scenario family describes a very heterogeneous world. The underlying theme is self-reliance and preservation of local identities. Fertility patterns across regions converge very slowly, which results in continuously increasing population. Economic development is primarily regionally oriented and per capita economic growth and technological change more fragmented and slower than other storylines.

B1
The B1 storyline and scenario family describes a convergent world with the same global population that peaks in mid-century and declines thereafter, as in the A1 storyline, but with rapid change in economic structures toward a service and information economy, with reductions in material intensity and the introduction of clean and resource-efficient technologies. The emphasis is on global solutions to economic, social and environmental sustainability, including improved equity, but without additional climate initiatives.

B2
The B2 storyline and scenario family describes a world in which the emphasis is on local solutions to economic, social and environmental sustainability. It is a world with continuously increasing global population, at a rate lower than A2, intermediate levels of economic development, and less rapid and more diverse technological change than in the B1 and A1 storylines. While the scenario is also oriented towards environmental protection and social equity, it focuses on local and regional levels.

(Intergovernmental Panel on Climate Change, 2000)

2.1.2   Statistical Downscaling

GCMs predict state variables and fluxes for each cell within the model; as described in Section 2.1 these cells are on the order of 3° square. The size of these grid cells is limited by computational expense. Most applications utilizing GCM predictions, including hydrologic models, require detail at much finer scales. Therefore in order to

obtain data at the finer spatial scale, methods known as downscaling are required

(Intergovernmental Panel on Climate Change, 2001).

There are three main types of statistical downscaling: weather generators, transfer

functions and weather typing. Weather generators, which are discussed in more detail

in Section 2.2, create sequences of synthetic weather on a regional scale (i.e.

subregions of a GCM cell). Transfer functions use direct relationships derived through

regression, kriging or Artificial Neural Networks to develop spatially varying weather

data within a GCM cell. Weather typing attempts to relate the GCM cell data to a set of

local climate variables based on synoptic climatology. More information on the latter

two methods can be found in IPCC (2001), these are not discussed in detail here

because they were not used in this study.

2.2   Weather Generators

Weather generators are stochastic models which create synthetic weather sequences in

a specific region of interest. Weather generators are employed because the historical

data record at most weather stations is not long enough, especially for the purposes of

statistical testing and forecasting. There are two main types of weather generators.

The first and most common type is parametric weather generators. The second type is

non-parametric weather generators.

Parametric weather generators such as the one created by Richardson (1981) are

based on a first order Markov chain process. Many of these models create precipitation

data first and then use this generated data to drive the generation of other parameters such as maximum and minimum temperature (Intergovernmental Panel on Climate Change, 2001; Richardson, 1981). The Markov process of parametric weather generators utilizes a probability distribution function of the data being generated. Since the probability distribution of precipitation is not well defined, assumptions regarding its form are required. Also, many of these models intrinsically assume that the data are normally distributed (Sharif and Burn, 2004; 2006); since this is not necessarily the case, transformations may be required during pre-processing of the data. Another downfall of this type of model is that it does not necessarily maintain spatial and temporal dependencies (Sharif and Burn, 2004; 2006), even when using the multisite extension by Wilks (1998; 1999). Finally, these models are not portable as they require this site specific data processing before being used in a different region. Non-parametric weather generators overcome many of the issues experienced through the use of parametric models.

The weather generator used in this project was created by Sharif and Burn (2004; 2006). It is a non-parametric stochastic weather generator based on a k-nearest neighbours (k-nn) algorithm. The k-nn algorithm is a selective resampling approach that uses chosen days from the historical record to represent the required days in the generated set. This model can be used to simulate historical data or to show the effects of specific global change phenomenon (e.g. global warming, wet springs, dry summers etc.) A quick overview of the workings of this model will be given here, for a full explanation of the weather generator see Sharif and Burn (2004; 2006). This model

generates synthetic precipitation, minimum temperature and maximum temperature for a specified number of years. Resampling is performed in the following manner (as given in Sharif and Burn (2004; 2006)):

1. First day in the generated sequence (e.g. January 1) is randomly chosen from all of the historical data, i.e. all January 1sts would have equal probability of being chosen.

2. Regional means are calculated for each parameter (minimum temperature, maximum temperature and precipitation) for each day of the historical record.

3. In order to maintain the seasonal variations in temperature and precipitation a subset of the historical data is identified as potential neighbours. This is accomplished through the use of a moving temporal window of 14 days (w=14) across all years.

4. The covariance matrix of all potential neighbours to the current generated day must be calculated for use in the next step.

5. The Mahalanobis distance is calculated for each potential neighbour. The Mahalanobis distance is used instead of the more common Euclidian distance because the Euclidian distance is based on the scale of the measurements. This makes the Euclidian distance difficult to use in this case because temperature and precipitation have different units and therefore weights would have to be assumed. The Mahalanobis distance is given by Equation 2-1, where $\bar{X}$ is the vector of regional means for each parameter and C is the covariance matrix calculated in step 4.

$$d_i = \sqrt{\left(\bar{X}_t - \bar{X}_i\right)C_t^{-1}\left(\bar{X}_t - \bar{X}_i\right)^T}$$

<div align="right">(2-1)</div>

t = current day of simulated data   i= potential neighbour

6. Using the Mahalanobis distances, the closest k neighbours are selected. The choice of the value for k is important because if k is too low there will be a tendency for repetition in the data and if k is too large data that is too different from the original day could be chosen. This could create patterns that do not match those from the historical record.

7. At this point each of the k-nearest neighbours is weighted according to its closeness of fit (or distance) to the original data.

8. The stochastic component of the model comes in the random selection of one of the weighted k neighbours. The day immediately following this chosen neighbour in the historical set is used to represent the next day in the synthetic sequence.

9. Steps 4 through 8 must be repeated for each day of the synthetic data set.

A graphical representation of a k-nn model is given in Figure 2-2. In this figure, each axis can be viewed as one of the parameters to be generated (minimum and maximum temperature and precipitation) and each red dot is a historical data point. The Wójcik and Buishand (2003) model, from which this figure was taken, did not use a moving window to maintain seasonality. If it had, each seasonal window would be represented by a subset of the red points, causing a different subset to be generated for each day. Starting at day one, the black dot is the randomly chosen first generated day. From a

seasonal subset of the red dots the k closest are identified (displayed in blue), one of

these is then randomly selected (shown in yellow with black outline). The historical day

immediately following this chosen day is used to represent the next day in the

generated set. This next day is displayed as the black dot in iteration two. The entire

process is then repeated from this new black dot (Wójcik and Buishand, 2003).
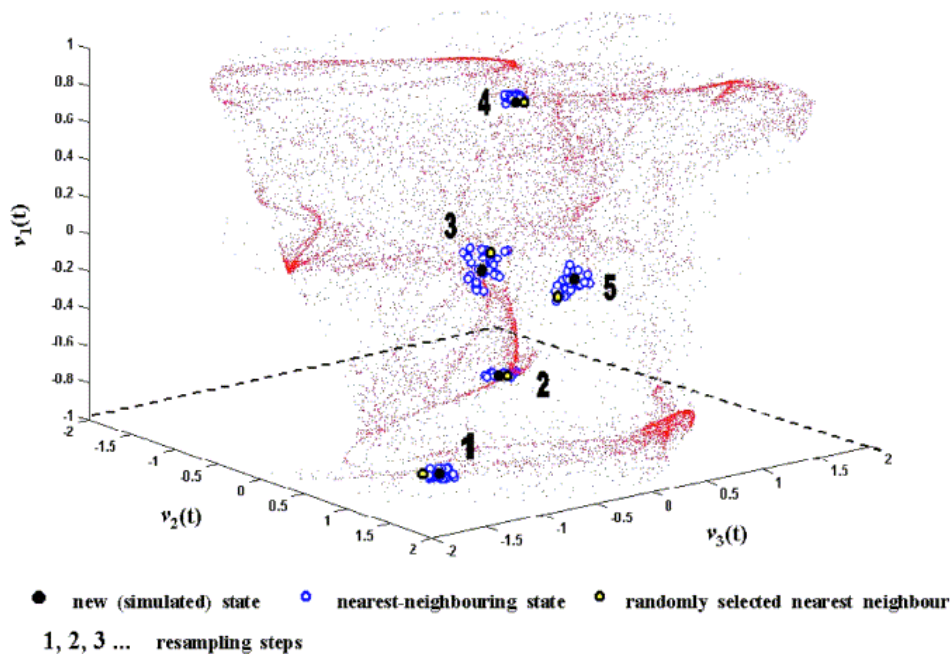
Figure 2-2: K-nearest neighbour diagram (Wójcik and Buishand, 2003)

By using the k-nn algorithm in this weather generator, Sharif and Burn (2004; 2006) and

others with similar models (i.e. Yates et al., 2003) were able to accurately reproduce

many statistical properties of the historical weather. Spatial dependencies which were a

known deficiency in parametric weather generators are automatically preserved by

resampling all stations simultaneously in the k-nn model. As well it has been shown

that temporal dependencies were maintained at daily, monthly and annual frequencies

(Sharif and Burn, 2004; 2006). The k-nn model required no assumptions regarding the

probabilistic distribution of any parameters. Furthermore, very few changes would be required to apply this model to another watershed since no calibration process is required.

2.3   Spatial Interpolation Methods

Spatial interpolation can be an important aspect of managing data. There are two main reasons for this. The first reason is to obtain data at locations where there is no historical record. The second is to generate data at a finer resolution than the historical record.

For this project it was required to have hourly data at the same locations as the daily data being disaggregated for calibration of the temporal disaggregation model. As hourly data was not available at many of these locations, spatial interpolation was used to generate the required hourly data. It is noted by the IPCC that "spatial and temporal scales in atmospheric phenomena are often related, approaches for increasing spatial resolution can also be expected to improve information at high-frequency temporal scales" (2001, p.751). This was an added benefit of the spatial interpolation for the project.

2.3.1   Method Options

There are numerous acceptable methods for spatially interpolating data. The reader is referred to Dingman (2002) and Tabios and Salas (1985) for a full review of many of these methods as they pertain to climatic data.

In the Thiessen polygon method every location is assumed to have data equal to the closest gauging station. As can be seen in Figure 2-3, polygons are a graphical method of determining which station is closest to a particular site. These polygons are created by connecting each station to neighbouring stations and then drawing the perpendicular bisectors. Drawing the polygons is not necessary however, if another way of determining the closest site is implemented. Although no reference was given to Theissen Polygons, Gutierrez-Magness and McCuen (2004) directly transferred hourly precipitation data from one site to another in their studies, assumedly using the closest gauge station for each site. Through their research Gutierrez-Magness and McCuen (2004) determined that direct transfer from one station to another gave poor results and the results deteriorated as the distance between the stations increased. Another downfall of this method is that weather trends can be lost by directly moving data from one location to another.
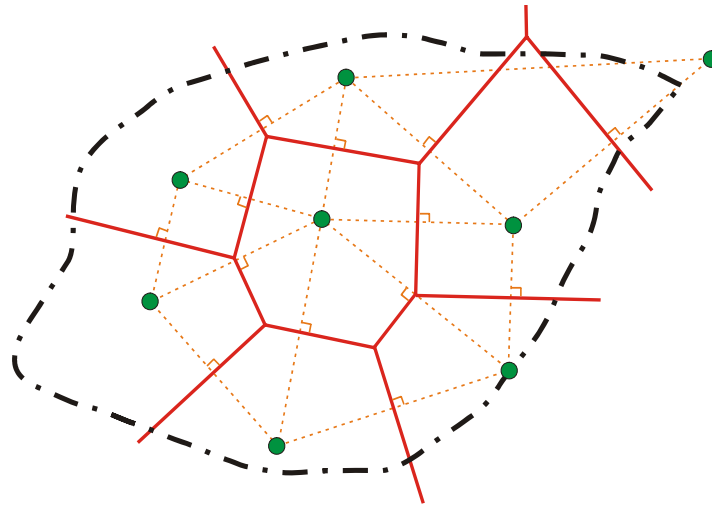
Figure 2-3: Example of Thiessen Polygons (adapted from Anhalt, 2004)

Another method for transferring precipitation data from a gauging site to other locations is known as the isohyetal method. This method is superior to Thiessen polygons because it transfers data from a site with potentially similar rainfall as opposed to transferring data from the closest site spatially. In this method, lines are drawn connecting locations of equal precipitation values. These lines, which are similar to contour lines on a topographical map, are known as isohyets. All locations are assigned a precipitation value according to the distance to each of the closest isohyets (i.e. a point halfway between isohyet 20 and isohyet 30 would be assigned a value of 25). This method is highly subjective as it does not lend itself well to computer programming and therefore the isohyets are generally drawn by hand. In order to accurately determine isohyet locations many gauge stations are required. This method becomes quite time consuming as isohyets must be determined for each precipitation event. Figure 2-4 shows an example of the isohyetal method, for further explanation see Hornberger (1998). Another method similar to the isohytal

method is the hypsometric method. This is only appropriate where topography is a major factor in precipitation patterns (i.e. in mountain ranges etc.) (Dingman, 2002).
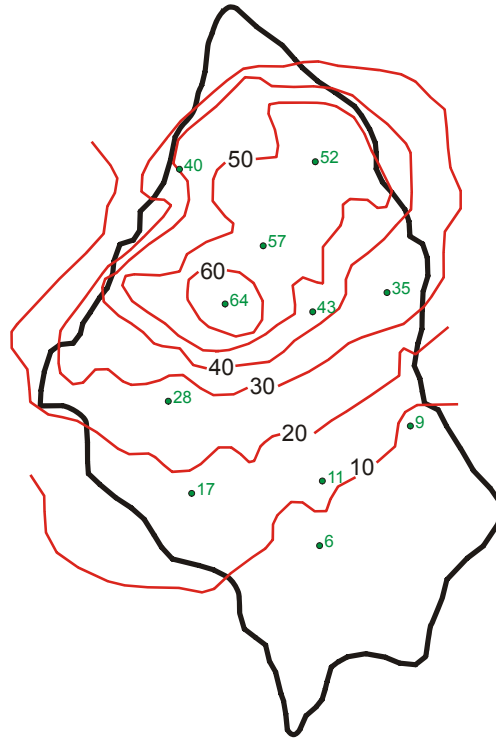
Figure 2-4: Isohyetal method schematic

There are many non-graphical methods of spatial interpolation available. The most basic of these is the inverse distance weighting method, which is discussed in more detail in Section 2.3.2. The other methods in this category are more complicated and will be discussed here only briefly as they are not implemented in this research. Multiquadratic interpolation uses quadratic relationships to determine cones of influence around each gauging station. At any location these cones of influence can be added together to determine the value at that point. Polynomial interpolation, which is also known as regression (Tabios and Salas, 1985), is a surface fitting method not an interpolation method, meaning that it may not reproduce the recorded

data at the gauging stations (Dingman, 2002). Surface fitting was not desirable for this project, so this method was not investigated further. The final two methods investigated are quite similar. Both optimal interpolation and kriging determine the weighting of each gauge station on the required site by minimizing the variance of error for the interpolation. The main difference between these two methods is that optimal interpolation is based on correlation between the stations while kriging is based on variograms (Tabios and Salas, 1985). Both of these methods assume isotropic conditions over the entire region.

2.3.2 Inverse Distance Weighting

Inverse distance weighting is a common method of spatial interpolation. It is popular because of its simplicity and accuracy in relation to other methods (Lapen and Hayhoe, 2003). Inverse distance weighting is based on the theory that precipitation measurements taken closer to the location requiring data should have more influence on the interpolation than stations which are farther away. Equation 2-2, below, shows how the interpolated data at a given location Z, is calculated from measured data.

$$Z = \frac{\sum_{i=1}^{n} Z_i w_i}{\sum_{i=1}^{n} w_i} \quad \text{where} \quad w_i = \frac{1}{d_i^{\,p}} \tag{2-2}$$

In this equation Z_i is the known data at station i and d_i^{P} is the distance from station i to the required location raised to the exponent P. In order to determine Z, both the numerator and the denominator are summed over all n stations. Historically the most

common value used for P has been two; this is a special case of inverse distance

weighting known as inverse distance squared. For the general case, as P increases

more precedence is placed on the stations closer to the required location.

Lapen and Hayhoe (2003) did an extensive study on spatial interpolation techniques

based on monthly data from southern Ontario, Canada. This study is of particular

importance because the study area coincides with the region of interest of the current

project. A summary of their results is presented in Figure 2-5. This figure compares the

relative mean square error of their outputs for each of the techniques tested.
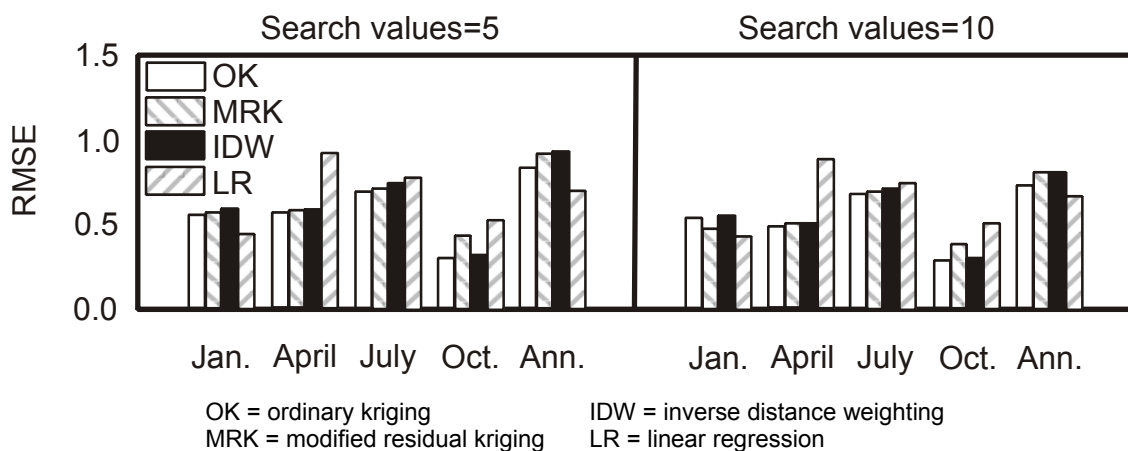
Figure 2-5:Comparison of spatial interpolation methods at South-Western Ontario
(Lapen and Hayhoe, 2003)

Through analysis of these results Lapen and Hayhoe (2003) determined that either

inverse distance weighting or modified residual kriging are the best options for climate

interpolations in this area. Lapen and Hayhoe (2003) used the distance to the coast of

Lake Huron as a secondary variable for the modified residual kriging. This was

because of the lake effect climate known to be present in this area (see Section 5.1.2).

This makes the modified residual kriging much more complicated to calculate than the

inverse distance weighting method; therefore since similar results were achieved the inverse distance weighting method appears to be the best method for this application.

A noted limitation of the inverse distance weighting method occurs if there are multiple gauge stations particularly close to each other. In this situation the inverse distance weighting method does not discriminate between this redundant data and the location with two stations will have twice as much influence on the output data as it should (Tabios and Salas, 1985).

2.4   Temporal Disaggregation Methods

Precipitation data are often required at a finer scale than what is measured, such as hourly rather than daily, for many hydrologic models. One option for creating data at this timescale is to modify the weather generator to produce hourly data, while another is to disaggregate the daily data, which are output from the weather generator, into hourly data. Porter and Pink (1991) recognized that generation of monthly data rarely preserves the annual statistics of the time series. They noted that disaggregation of generated annual data was a good way to maintain the necessary statistical properties of the data, at both the annual and monthly scale. Wòjcik and Buishand (2003) extended this theory to the disaggregation of daily climate data. They compared these two options for 6-hour precipitation and temperature data and determined that disaggregation of daily data preserved the second order statistics much better than directly generating data at the finer timescale.

2.4.1   Methods Formerly Used

The most basic disaggregation method is uniform disaggregation. This method simply takes the daily data and divides it evenly into 24 hours. As is intuitively assumed this method does not produce data that compared well to actual rainfall (Gutierrez-Magness and McCuen, 2004). This is because precipitation events do not last for 24 hours with equal intensity in all hours. Another method tested by Gutierrez-Magness and McCuen (2004), known as weather pattern disaggregation, uses weather patterns based on site specific meteorological studies. The weather patterns used still spread the precipitation values across all 24 hours; however the uniform distribution was replaced. This method was not deemed to be much better than the uniform distribution (Gutierrez-Magness and McCuen, 2004). This method is also not desirable as it is not transferable to other locations, because the weather patterns which are developed by the USGS are site specific.

Socolofsky et al. (2001) produced a stochastic disaggregation which divided daily rainfall into a random number of events each starting at a random time throughout the day. The random number generators for this model were based on the cumulative density function of selected events at an hourly station near the daily station being disaggregated. In the case that events overlapped the intensities that fell in the same hour were added together. However, events were not permitted to crossover from one day to the next, which would cause problems in the case of events that lasted longer than one day. There is no way to extend this model to a multisite scenario as there would be no way to preserve the correlations between stations.

21

The scaling based cascade model presented by Olsson and Berndtsson (1998) is a stochastic model based upon empirical observations of rainfall events. Figure 2-6 gives a visual representation of this model. This model splits the rainfall at each level based on patterns determined by calibrating the model with actual data and estimating the probability distribution of rain in each section. Through this method the model was able to accurately reproduce a variety of statistics for the rainfall at the study site (Olsson and Berndtsson, 1998). While there is no way to extend this model to a multisite scenario, it may be functional at other sites. However, Olsson and Berndtsson (1998) did not discuss how portable the probability distributions would be to other locations. This model has been shown to work at timescales as fine as 45 minutes and so could be effective in this study, however this method does not provide for maintaining correlations between stations. Olsson and Berndtsson (1998) do not mention overnight storms or the model's ability to handle such events.
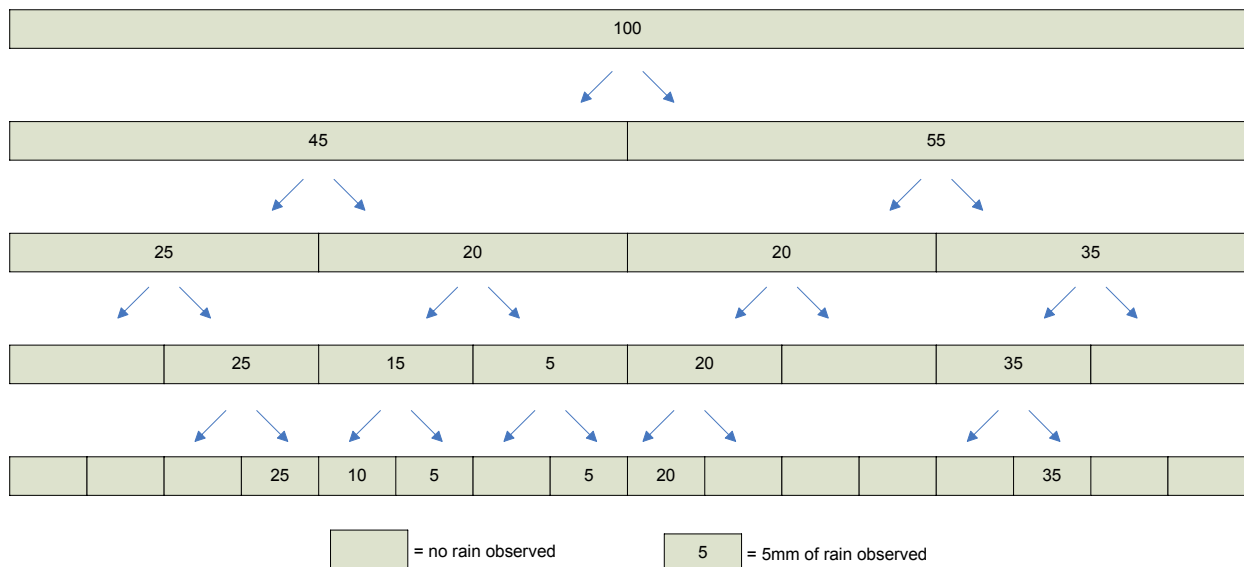

Figure 2-6: Diagram of scaling based cascade model (Olsson and Berndtsson, 1998)

Along similar lines of thought, Kottegoda et al. (2003) proposed a method which used geometric distributions to determine wet and dry periods. An advancement they made over Socolofsky et al. (2001) is that Kottegoda et al. (2003) were able to utilize their model in a multisite scenario. This model was based on historical hyetographs and disaggregated daily rainfall based on a beta distribution. Although this model was used for a multisite application, due to the statistical nature of the model, it was not able to ensure events maintained consistent start times across the region, and station cross correlations were not well preserved. It was noted, however, that even with these spatial deficiencies, downstream hydrographs were reproduced well.

The above models are parametric in nature and therefore would require determination of site specific parameters in order to be used at locations other than the one they were originally developed for. These models therefore are not very portable. Since the objective of this project is to create a set of models that will be adaptable to other watersheds for future use, these parametric models are not desirable for use on this project. The following paragraphs detail some of the non-parametric models available for temporal data disaggregation.

Although methods had previously been employed for data disaggregation (eg. the Thomas-Fiering Method), they "never caught on because of very obvious theoretical shortcomings" (Salas et al., 1980, p.421). Valencia and Schaake (1973) proposed a model that became the first well accepted method for this purpose. The basic form of this model has linear dependence as given in Equation 2-3.

$$Y = AX + B\underline{\varepsilon}$$ **(2-3)**

In this equation Y is a matrix of the disaggregated data, X is the data being disaggregated, A and B are matrices of estimated parameters and ε is a matrix of random numbers. A and B are estimated from the covariances of X and Y in the following manner, as presented by Valencia and Schaake (1973).

$$\hat{A} = \sigma_{YX}\sigma^{-1}_{XX}$$
$$\hat{B}\hat{B}^T = \sigma_{YY} - \sigma_{YX}\sigma^{-1}_{XX}\sigma_{XY}$$
(2-4)

From these equations it is apparent that there are infinite solutions for B. This model is computationally expensive because beyond the parameter estimates this method also requires all data to be normal with a mean of zero. This means that data transformations may be necessary before the model can be used. There are several other drawbacks to this method. Despite the number of required parameters, this model is not able to maintain relationships from one original data point, X, to the next. If data transformation is required to achieve normal data with a mean of zero, then the sum of the disaggregated data will not equal the original data (Salas et al., 1980). Since this is not generally acceptable in disaggregation, further adjustments to the data must be made.

In an attempt to improve Valencia and Schaake's method, Mejia and Rouselle (1976) made revisions to maintain the temporal relationships from one data point to another. This extended model is similar in form to the original, with an extra term. Equation 2-5 shows the form of the extended model (Mejia and Rouselle, 1976).

$$Y = AX + B\underline{\varepsilon} + CZ \tag{2-5}$$

In this new term, Z is a matrix of previously disaggregated data. As can be seen in the following equation (Salas et al., 1980) the parameter terms become markedly more complex in this model.

$$\hat{A} = \left(\sigma_{YX} - \sigma_{YZ}\sigma^{-1}{}_{ZZ}\sigma_{ZX} \right)\left(\sigma_{XX} - \sigma_{XZ}\sigma^{-1}{}_{ZZ}\sigma_{ZX} \right)^{-1}$$
$$\hat{C} = (\sigma_{YZ} - \hat{A}\sigma_{XZ})\sigma^{-1}{}_{ZZ} \tag{2-6}$$
$$\hat{B}\hat{B}^{T} = \sigma_{YY} - \hat{A}\sigma_{XY} - \hat{C}\sigma_{ZY}$$

A third variation on this model was provided by Lane (1983). This variation is a condensed version of the model to reduce the number of parameters required. The form of this model is given by Equation 2-7. The subscript τ in this equation refers to the period currently being generated (i.e. the current season, hour etc.). Due to the nature of this model significantly less parametric estimation is required, however, it does not maintain cross-correlations and the sum of the disaggregated parts still does not equal the whole (Salas et al., 1980). The formula for the condensed model as presented by (Lane, 1983) is given in Equation 2-7.

$$Y_{\tau} = A_{\tau}X + B_{\tau}\underline{\varepsilon} + C_{\tau}Y_{\tau-1} \tag{2-7}$$

Commenting on the computer package written to perform his model Lane notes:

> While the programs were developed with streamflow in mind, they could be applied to other variables, such as rainfall, evaporation, water quality, sediment, and crop water requirements, either alone or in combination… This package is not presently designed to be applicable to event dominated series such as daily rainfall or runoff. (Lane, 1983, p. I-1)

This shows that although models may be written for streamflow, they may well be valid with respect to precipitation data. As well the user of any model must be aware of the impacts of working at a small scale, particularly with daily precipitation data. In further studies it was determined that this set of methods performed poorly for data with high variance (Srikanthan and McMahon, 1982). Therefore, while they may be valid for annual stream flow data they are not appropriate for use with daily precipitation data.

Another model was proposed by Gutierrez-Magness and McCuen (2004). This model is known as satellite ratio disaggregation. In this model hourly data are generated at a daily gauge station by using the distribution of hourly data at an hourly gauge station from a nearby watershed. This requires data sets at two sites for the same time period as it simply transfers data from one site to another, using ratios. This model created a negative bias in the data because there is no way to accommodate for days with data at only one site, if there was no precipitation at either site, a dry period was created in the disaggregated data. This model cannot be extended to a multisite situation, but is mentioned here for reference only.

2.4.2   Method of Fragments

The method of fragments was first introduced in the early 1960's by G.G. Svanidze. This method was an improvement upon previous statistical disaggregation methods as it did not require the assumptions and vast amounts of data associated with probability distribution fitting that was required by the previous methods (Svanidze, 1977). From a

survey of the literature, it appears that the method of fragments is currently the most popular method for disaggregation of precipitation data.

2.4.2.1 *Basic Method*

In order to perform the method of fragments, data at both the original and the disaggregated time scale are necessary. The benefit is that the amount of data required at the smaller time scale is much less than the amount of data that is being disaggregated.

For each piece of daily data that is to be disaggregated, a set of fragments must be formed. The fragments are the fraction of daily precipitation that occurred in each hour of the day, thus the fragments sum to unity. Equation 2-8 and Equation 2-9 show the general form of the method of fragments. In Equation 2-8, w_i is the fragment to be calculated for hour i, h_i is the data from the series chosen to produce fragments (e.g. the chosen hourly data) and n is the number of data in that series (e.g. 24 hours).

$$w_i = \frac{h_i}{\sum_{i=1}^{n} h_i}$$ (2-8)

Each fragment is then multiplied by the daily data (d in Equation 2-9) being disaggregated such that the total precipitation in the day is not altered. This produces the new hourly values (h_i' in Equation 2-9).

$$h_i' = w_i * d$$ (2-9)

The series of hourly data to be used as fragments can be chosen by any number of methods. The original method involved choosing a random series for fragments; however, this was shown to inadequately reproduce the necessary statistics (Srikanthan and McMahon, 1982). It is better to choose the series which most closely matches the data being disaggregated (Srikanthan and McMahon, 1982). For instance, in the case of precipitation data, it is best to choose a series with a total daily precipitation that closely matches the daily data being disaggregated. This is because the shapes of large precipitation events are not the same as those of small events. Other factors that may be included in the matching process for precipitation data include time of year, temperature, humidity and air pressure. Choosing a closely matching set of fragments will ensure that precipitation events are generated with the proper shapes and characteristics.

2.4.2.2 *Method of Synthetic Fragments*

One problem that can occur with the method of fragments, especially if the data set being used for fragment generation is small in relation to the original data set, is fragment repetition causing a cyclic pattern in the output. Porter and Pink (1991) propose a method of synthetic fragments to be used in this case. Their method involves creating synthetic data at the time scale to be used for the fragments (i.e. generating an hourly data set to draw fragments from). This could be done using a k-nearest neighbour or any other reasonable approach. This synthesized data set should be long enough to allow the selection of different fragments for each disaggregation period, thus removing the repetitive pattern occurring in the basic method of fragments. Porter and

Pink also note that this method will improve the accuracy of disaggregation of large events as events of this magnitude may not be seen in the short historical record of (hourly) data, but are more likely to be present in the generated fragment set. Since extreme events are one of the main interests of hydrologic models, this is a key feature. The synthetic fragments will create more options for the disaggregation of large events.

Wòjcik and Buishand (2003) propose another method for reducing repetition in the chosen fragments. They suggest choosing a randomly selected fragment set from the k closest matches instead of choosing the fragment set that most closely matches the data being disaggregated for each day. This adds the stochastic aspects of a k-nearest-neighbour approach to the fragment selection process and could potentially reduce the amount of repetition in the final output.

2.4.2.3   *Smoothing Methods*

Svanidze's original model, which disaggregated stream flow from annual data to monthly data, reproduced monthly statistics well, but was not able to satisfactorily maintain annual moments (Svanidze, 1977). Porter and Pink (1991) note that even with the use of synthetic fragments some statistical properties are not maintained in their output. Their study also involved the disaggregation of annual data into monthly data. They identified that although they managed to maintain the monthly statistics, they were not able to maintain the correlation between the first month of the year and the last month of the preceding year.

Maheepala and Perera (1996) improved upon this design by adding a smoothing factor into selecting the series to be used as fragments. Along with matching the total of the chosen fragments to the value of the data being disaggregated, they compared the data directly preceding the fragments to the last data point previously disaggregated. Their smoothing method is presented in Equation 2-10 for use at a single site (adapted from Maheepala and Perera, 1996). By doing this they were able to preserve the correlation between the disaggregated data at the larger time scale.

$$\min(\alpha_j + \beta_j)$$
$$where$$

$$\alpha_j = \left(\frac{D_k - \sum_{j=1}^{24} H_j}{S_D} \right)^2 \quad and \quad \beta_j = \left(\frac{h_{k-1} - h_{j-1}}{S_h} \right)^2 \tag{2-10}$$

D=generated daily data   j=day of hourly data
H=historical hourly data   k=day of daily data
h=last hour of hourly data (example 11pm)   S=standard deviation

2.4.2.4   *Multi-Site Tactics*

The selection of fragments becomes more complicated when a study area of more than one site is considered. In this case the process for matching a set of fragments to the data being disaggregated is no longer well defined. This is still a developing field, "the use of method of fragments for the temporal disaggregation of multisite weather data requires further study" (Wójcik and Buishand, 2003).

One solution to this problem is to treat each site individually and choose a set of fragments for each site. This approach is known as random selection. This approach is

reasonable only if the cross-correlation between stations is low because it does not maintain the correlations among stations (McMahon and Mein, 1986, p.262). This approach is implemented by running multiple cases of a single site analysis.

The key site approach is presented by McMahon and Mein (1986, p.262). This approach is acceptable if one site stands out from the others as being of greater importance or influence. Perhaps this key site has considerably better data than the others, or is the focus of interest in the study. If a key site is used in the selection process of the fragments, comparison of all fragment possibilities are made at this site alone. Once the selection of fragments has been completed at this site the fragments corresponding to the same historical period are used at all stations. This approach maintains cross-correlations among stations because the same historical period is used for all stations.

Porter and Pink (1991) determined that the key site approach was not valid in their study because of the variability between their sites. It was not deemed suitable to assume that one site could be representative of what was occurring at the other sites. In order to maintain station correlation without the use of a key site they performed a full analysis of all stations and chose a set of fragments that fit best with each site. This approach is computationally expensive, especially as the number of sites increases.

2.4.2.5   *Usage for Daily Precipitation Data*

Although the majority of studies in the literature using the method of fragments were disaggregating annual streamflow data, there is evidence that this method is applicable for use on daily precipitation data as well. Research completed at a fine timescale includes a study by Wójcik and Buishand (2003). They studied the disaggregation of daily precipitation into 6-hour segments. This is the finest timescale on which precipitation disaggregation was performed that could be found in the literature. Wójcik and Buishand (2003) disaggregated daily precipitation data (which had been generated through the k-nearest neighbour technique) into 6-hourly data using the method of fragments. Positive results were achieved through this method (Wójcik and Buishand, 2003), therefore, although the effectiveness on an hourly scale is still untested, these methods are acceptable for use with precipitation data on a sub-daily scale.

In summary, this literature review discussed the process utilized by the weather generator which was produced in earlier portions of this project. It was determined that the inverse distance weighting method is the most appropriate for the spatial interpolation of hourly precipitation data. Finally, although many options are available for temporal disaggregation of daily precipitation data, this review of the literature aided in deciding upon the use of the method of fragments for the disaggregation required in this project.

3   Spatial Interpolation

Spatial interpolation was required in this study to generate hourly data at the same locations as the daily precipitation gauge sites. Data at these locations was a required input for the temporal disaggregation of the future daily climate data from the k-nn daily weather generator. After considering the available methods, as discussed in Section 2.3, it was decided that the inverse distance weighting method would be used for this application.

3.1   Input Data

Historical hourly data composed the main input for this portion of the study. A small amount of preprocessing was performed on the historical hourly data. This preprocessing involved the removal of outliers from the data set; however data missing from the historical data set were not filled in. Since the nature of the spatial interpolation model did not require data at each station for all time steps, it was deemed more appropriate to leave the data missing than to create more uncertainty by filling in the missing data.

3.2   Methodology

3.2.1   Inverse Distance Weighting

Spatial interpolation for this study was performed by using the inverse distance weighting method. Inverse distance weighting was chosen because the method is fairly

simple to implement and the literature studied (refer to Section 2.3 for more detail) did

not provide any reason to assume that another method would provide superior results.

Furthermore, other portions of the project which this study was a part of, have also

employed inverse distance weighting for the interpolation of hourly precipitation data.

Therefore consistency was maintained throughout the project by choosing the same

method. More information including the formulae used in this method can be found in

Section 2.3.2.

3.2.2   Different Exponents

Inverse distance weighting may be more commonly referred to as inverse distance

squared because the most common exponent used in the formulation is two. No

literature could be found which used this method (or any method for that matter) with

hourly precipitation data and no reasoning for the use of the number two as an

exponent was found. Therefore, it was determined that more extensive modelling was

required to determine the value of the exponent to be used with the inverse distance

weighting method for this application.

A subset containing five of the historical hourly stations was used to calibrate the

exponent. For each station, interpolation was completed using the data from all stations

except the station in question. This process was repeated with various exponents for

each of the five stations. Statistical testing was then completed on the interpolated

hourly data to determine which exponent produced acceptable results. Once a

permissible exponent was chosen, interpolation was performed on the full set of

locations of daily stations for validation purposes. The interpolated data at the daily

station locations were then compared to the historical data to determine which exponent

best reproduced the historical data.

3.2.3　Distance Types

It was assumed that all precipitation events move in a common direction; therefore,

either the latitudinal or the longitudinal distance could be more significant than the

absolute distance to the interpolation. This reasoning was based upon examination of

the historical weather patterns over the watershed used in this study, as will be

discussed in Section 5.1. Because of these trends, interpolations were run for each of

the three distance types in order to determine which type reproduced the original data

most accurately. A schematic of these distance types can be seen in Figure 3-1.
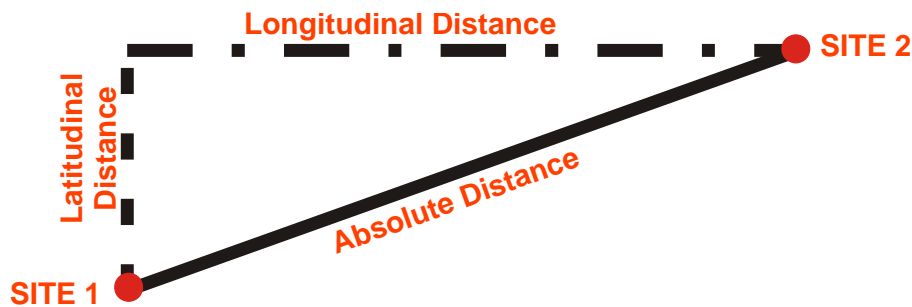
Figure 3-1: Diagram of distance types

3.3　Results

A paired t-test was used to compare the interpolated hourly data to the historical hourly

data for various interpolation runs during the analysis of the output from the spatial

interpolation model. The form of this test is given in Equation 3-1. Based on this

equation the best interpolated data will minimize the absolute value of t. To be

considered acceptable the calculated t value must be within the range of some specified

critical t-values. Examples of widely used critical values are the 10% critical t-value and

the 1% critical t-value. When determining the critical values used for assessing the

calculated t-value, the parameter n was assumed to be infinite due to the large data set.

For further details on this test see Montgomery (2001).

$$t = \frac{\overline{(X-Y)}}{\sigma_{(X-Y)}/\sqrt{n}}$$

(3-1)

X=spatially interpolated hourly data   Y= historical hourly data
σ=standard deviation   n=number of data points

3.3.1   Exponent

To determine the proper exponent to use in the inverse distance weighting equations, a

t-test was used to compare the interpolated data to the historical hourly data for a

variety of possible exponents. As can be seen in Figure 3-2 the traditionally used

inverse distance squared method (with an exponent value of two) did not produce

results that fell within the 1% critical t-value range for the majority of the sites tested.

Thus an exponent of two is not acceptable for use in the case of hourly precipitation

data (at least in the region used in this study).

Upon examination of Figure 3-2 it was determined that the most appropriate exponent

for this application was either five or six. When exponents of less than five were used in

the inverse distance method, t values that were too large were calculated at most of the

sites, and when an exponent of seven was used, t values began to drop significantly

below zero. This downward trend in the value of t continued as the exponent was

increased.
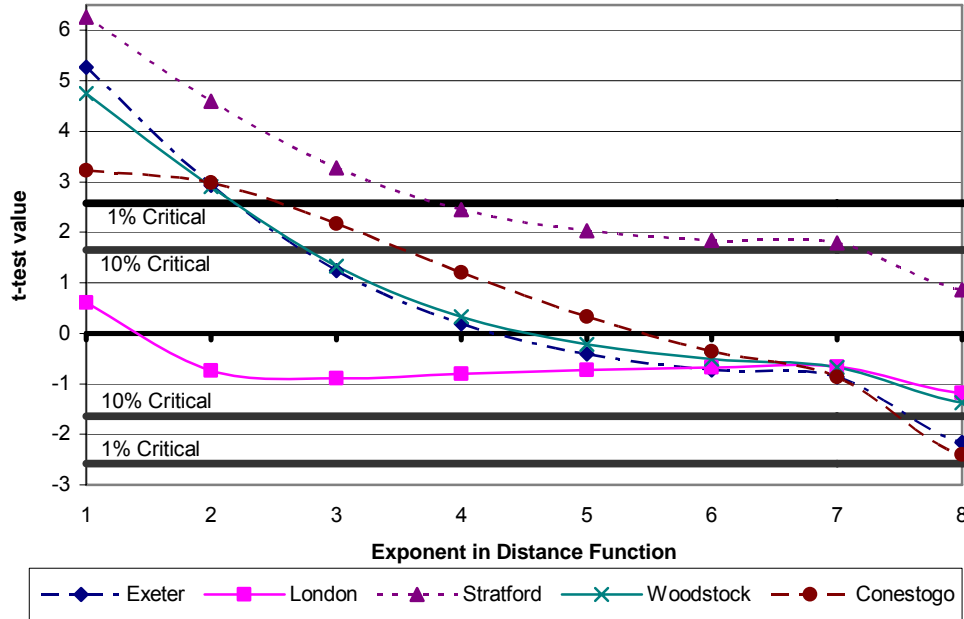
Figure 3-2: Paired T-Test comparison for different exponents

After it was determined which exponents were permissible based on the t-test

comparison, it was necessary to determine which exponent produced data with

correlations that reasonably matched those of the historical data. Interpolations on the

entire set of required daily station locations were completed for exponents of both five

and six. The autocorrelation and the spatial correlations of the interpolated data were

compared visually to those of the original data set. Figure 3-3 and Figure 3-4 show the

autocorrelation and spatial correlation of the historical and interpolated data sets

respectively with each exponent.
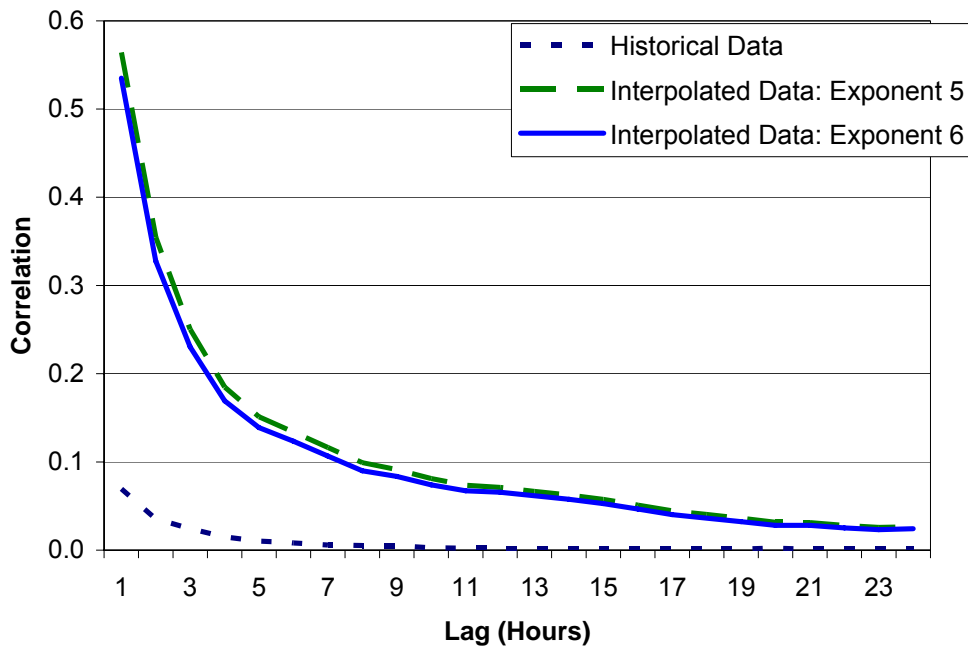
Figure 3-3: Autocorrelation results with different exponents
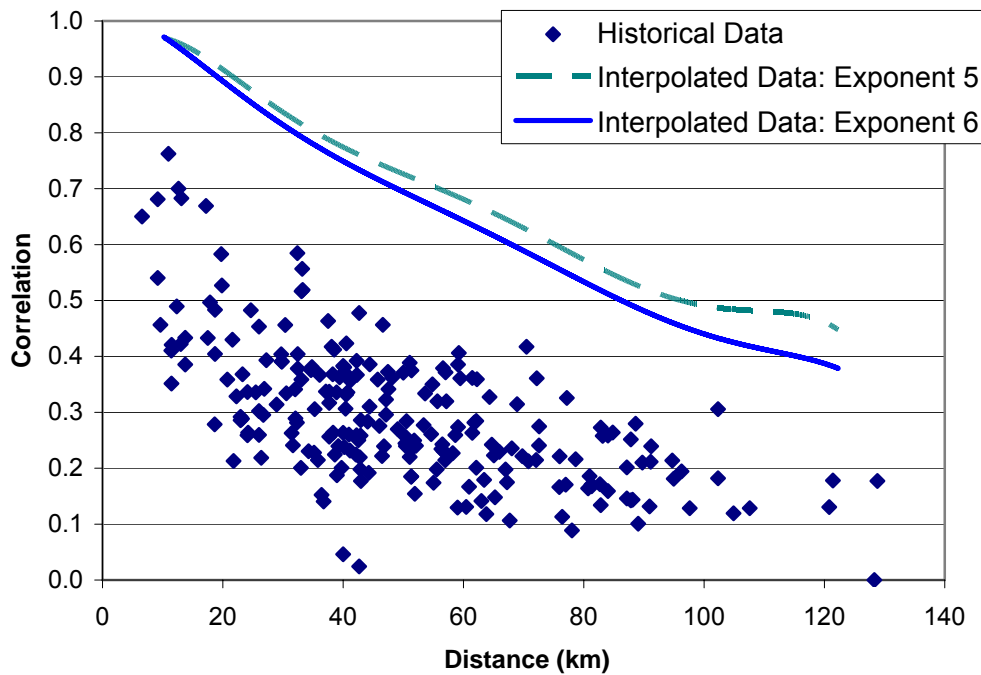
Figure 3-4: Spatial correlation of hourly data with different exponents

Figure 3-3 and Figure 3-4 are both based on interpolation by absolute distance. Further discussion on distance types is provided in Section 3.2.3 and Section 3.3.2. Figure 3-3 is averaged over all stations and Figure 3-4 shows only the trend line of the interpolated data using each exponent for clarity purposes.

As can be seen in the above figures, neither an exponent of five nor six was able to reproduce the correlations of the historical data. This prompted the calculation of correlations through the use of various other exponents. The results of this test showed that the correlations of the interpolated data were similar and therefore the exponent had little impact on the correlations. Based on these tests there does not appear to be a significant difference between using an exponent of five or six. Since an exponent of six appears to provide slightly better correlations, it was chosen as the exponent that would be used for the remainder of this study. A detailed analysis of these results can be found in Section 6.1

3.3.2 Distance Types

Once an exponent was decided upon, the type of distance used for interpolation was examined. Interpolation was completed for each of the three distance types: latitudinal, longitudinal and absolute. This was done to determine which method of calculating the distance for the inverse distance formulae produced the most accurate interpolation results. The results of these interpolations are displayed in Figure 3-5. The exponent value determined in the previous section was checked in this step by visually comparing

a variety of exponents with each distance type. This test confirmed the results noted in the previous section.

From Figure 3-5 it is obvious that using the absolute distance in the inverse distance formulae was acceptable for use with hourly data in the region of study. Using the longitudinal distance in the interpolation created erratic results in the spatial correlations. While using the latitudinal distance in the interpolation created data that followed the general downward trend in correlation with distance, it did not create as smooth a trend as was required. Therefore the absolute distance was chosen as the distance type for use in the inverse distance interpolation of hourly precipitation data.
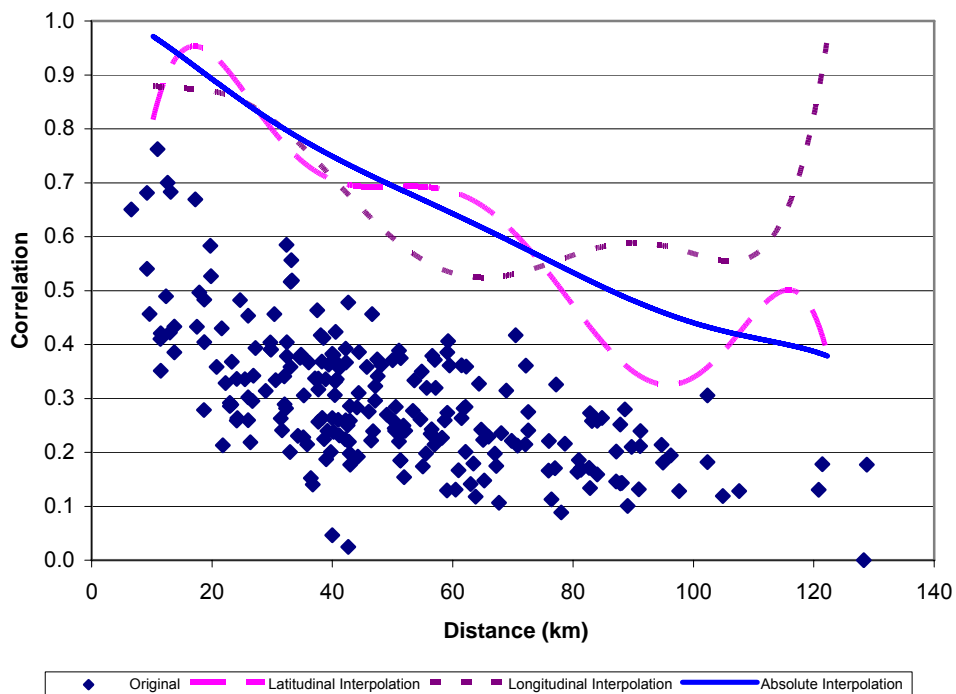
Figure 3-5: Spatial correlation of hourly data for interpolation with different distance calculations

3.3.3   Number of Stations Required for Interpolation

The number of data stations used within the inverse distance weighting method, when interpolating on an unknown site, can have an effect on the interpolated data. If there are not enough gauge sites with valid data then there will not be a proper distribution of precipitation across the entire watershed. An extreme case would occur if only one site was used during interpolation. In this case, interpolation at all desired locations would result in the same value being produced; this would result in no regional variation.

To determine the minimum number of sites required to achieve reasonable regional variation, interpolations were completed multiple times with an exponent of six utilized in the inverse distance formulae,. For each run, a constraint was implemented limiting interpolation to only the hours that had a minimum number of sites with data. For example, in 1960 only three hourly stations were operating within the study region; therefore the data from 1960 was not included in any run with a specified minimum number of stations more than three. However, by 1984 there were 12 operational hourly data stations in the study region; therefore the data from 1984 would be included in all runs with a specified minimum of 12 stations or less. The specified minimum number of sites used in this testing ranged from one (in which all available times were used) to twenty (only times that had twenty or more sites with valid data were used) at increments of five. The t-test depicted in Figure 3-6 was used to compare the interpolated data sets to the original data at the selected stations.
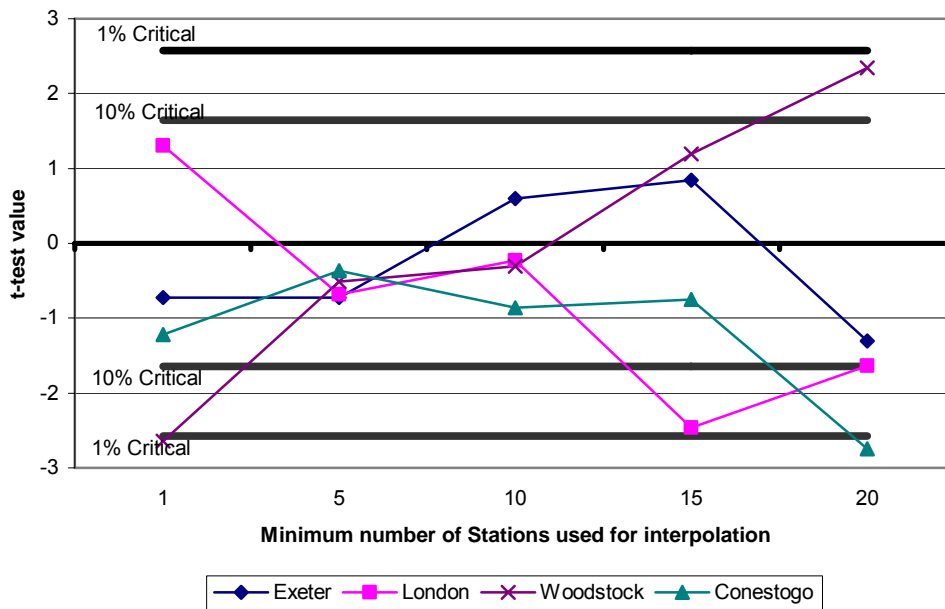
Figure 3-6: Number of sites required to have valid data for interpolation

It can be seen from Figure 3-6 that minimums of both five and ten produce acceptable results within the confidence interval limits. Figure 3-6 does not show a consistent increase in accuracy as the minimum number of sites increases. This is because the t-test value is also dependent on the number of data points available (refer to Equation 3-1). As the minimum number of gauge stations increased, the size of the overall data set decreased because not all of the gauge stations were operational for the entire historical record period (e.g. as noted in Section 5.1.2 gauges are prone to failure in winter), this can be seen in Table 3-1. This caused the data set to be smaller if fifteen or twenty gauge stations were required, which in turn caused an increase in the t-test value. Since a large data set was desirable for the upcoming temporal disaggregation and there did not seem to be a significant difference in the accuracy of interpolation when using a minimum of five or ten stations, a minimum of five stations was used in the remainder of this study.

Table 3-1: Number of data points used in the creation of Figure 3-6

Minimum Number of Stations	Exeter	London	Stratford	Woodstock	Conestogo
1	150123	336142	359426	359451	365943
5	150123	136816	144712	144737	151229
10	147506	130732	138279	138304	144796
15	102953	74944	77992	78017	85252
20	22642	15085	13833	13856	13855

4 Temporal Disaggregation

The main focus of this research was the temporal disaggregation model. Temporal disaggregation was performed on daily precipitation data to produce data at an hourly timescale for use in hydrologic models created in a later portion of the project which this thesis is a part of. Upon examination of the available methods for temporal disaggregation (see Section 2.4) it was determined that the method of fragments showed the most potential for success within this study. A diagram of data flow within this model is provided in Figure 4-1. Figure 4-1 is only a summary of the process, for a detailed flow chart of the model developed in this study refer to Appendix A.
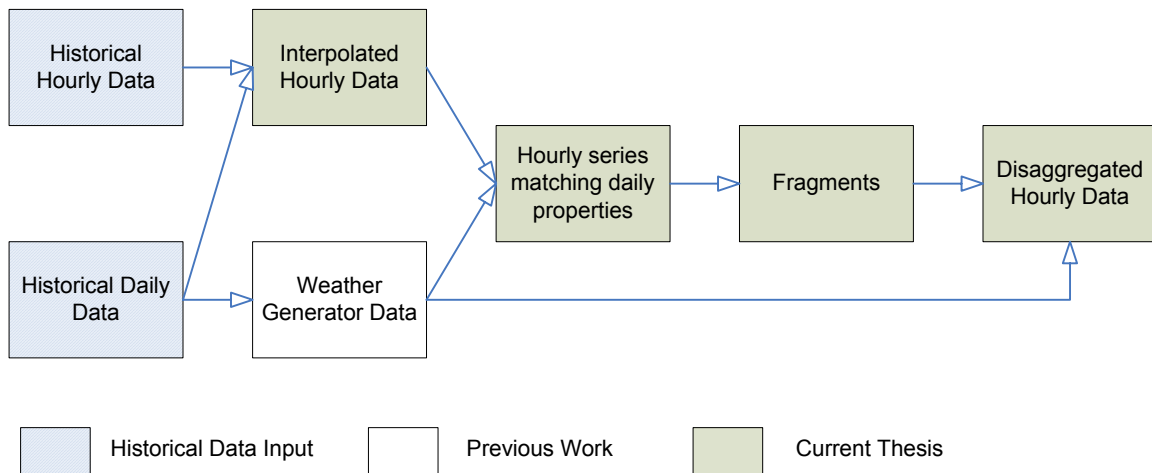
Figure 4-1: Flow chart of data in the temporal disaggregation model

4.1 Input Data

There were two main inputs used in the temporal disaggregation model for this study: daily and hourly data.

The daily data input for temporal disaggregation was produced by the K-nn weather generator as described in Section 2.2. This weather generator produced daily data sets for different climate scenarios as required for this portion of the project.

The hourly data input was produced by the spatial interpolation model discussed in Chapter 3. This data was required to reproduce the precipitation trends of the study region. For this study the hourly data used were created with the spatial interpolation method presented in Chapter 3. Although use of the spatial interpolation model is not ideal, it was used in this case because the hourly data were required to be at the same locations as the daily data that was output by the weather generator. Other potential sources of hourly data include the direct use of historical precipitation records. This is only possible if the locations of the hourly precipitation gauges coincide with the daily gauge sites.

4.2   Data Preprocessing

The time of day at which a daily gauge station is measured creates the definition of a day for that station. For example, if a daily station is measured and recorded at 8 a.m. every day, a day is defined as 8 a.m. to 8 a.m. the following morning, for that station. Therefore, the measurement time, (by Environment Canada, etc.) of the daily data had to be determined before temporal disaggregation could be performed. For all of the stations in this study that had both hourly and daily precipitation gauges, the hourly data were summed for each day using different definitions of a day (i.e. midnight-midnight, 1

a.m. to 1 a.m. etc.) in order to determine the measurement time of the data. These

sums were then compared to the historical daily data from the same period to determine

when the daily data were recorded. The standard deviation of the difference between

the daily data and the sum of the hourly data was minimized at the time the daily data

were recorded. The results of this test can be seen in Figure 4-2.
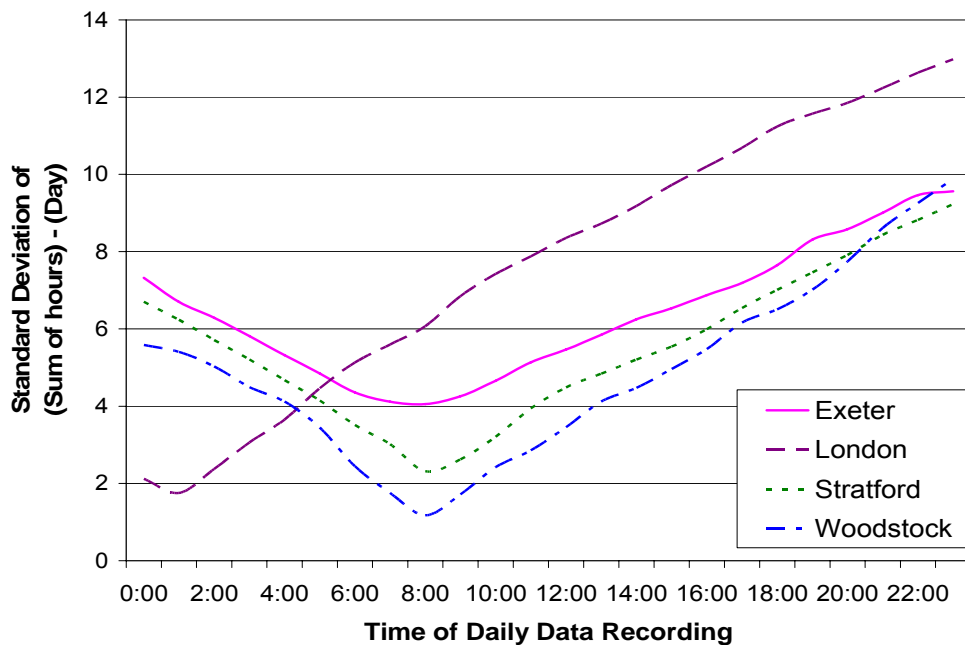
Figure 4-2: Daily data recording time

From Figure 4-2 it can easily be seen that the daily data used was recorded at different

times of the day; therefore the definition of a day, as measured by Environment

Canada, etc., was ill-defined. Because of this discrepancy, temporal disaggregation

was completed with both the actual daily recording times as determined for each

station, as well as with a common start time for all stations. These two methods were

then compared to determine the significance of the daily data recording time.

4.3   Methodology

The method of fragments was the temporal disaggregation method used in this study. More information on the method of fragments can be found in Section 2.4.2. A flow chart of the temporal disaggregation process developed for this research and described below is located in Appendix A for reference.

4.3.1   Event Model

It was determined that it would be infeasible to disaggregate the entire set of daily data produced by the weather generator due to the computational time required to run such a model. The time required for this model to run would increase dramatically with the number of stations involved as well as with the length of the generated daily data set. Since output from this model is intended to estimate potential floods only and not droughts, it was determined that only those days with significant amounts of precipitation needed to be disaggregated. This is sufficient because drought assessment can be completed with the generated daily data and does not require a finer timescale. The days with significant precipitation will herein be referred to as event days. By only disaggregating event days the time required to run the model was dramatically decreased. For the purposes of this thesis, an event is defined as all consecutive event days, with at least one non-event day separating events.

4.3.2 Multisite Approach

Although many methods are available for selecting a set of fragments in studies containing more than one gauge station (see Section 2.4.2.4 for a review of these methods), a new variation is proposed here. This new method is a hybrid between the key site approach (McMahon and Mein, 1986; Porter and Pink, 1991) and the method used by Maheepala and Perera (1996) which took every station into consideration when choosing fragments.

The key site approach is thought to be applicable in two scenarios. The first scenario occurs if one site has greater significance to the area than any other site. The second scenario occurs if there is very little spatial variation across the entire area under consideration, such that a single site could provide a good representation of the entire region. Maheepala and Perera's (1996) approach is applicable in more situations than the key site approach, but it is computationally expensive, because it includes every data station in the calculation. The proposed method is thought to maintain a balance between the key site approach and Maheepala and Perera's (1996) approach.

The proposed approach involves multiple key sites, thereby representing the distribution across the watershed without the expense of examining all sites in the study area. This multiple key site method requires the user to select the number of key sites to be used for a specific application. By increasing the number of key sites, the user decreases the ambiguity of the selection process; however, by decreasing the number of keys sites,

the user decreases the required computational time for fragment selection. It is important to select enough sites to accurately represent the region of study.

Key sites should be chosen so that the entire area being disaggregated is well represented. The key sites should be spread out across the study area and any geographically or climatically significant areas should be represented. Consideration of data quality should be made when determining the key sites to be used. Sites with good quality data should be used as these sites will be used to determine the fragments chosen for the entire study area.

In order to obtain credible results from the equations presented in Section 4.3.3, there must be precipitation at a minimum of one of the key stations on each event day. If there is no precipitation at any of the key sites on a specific event day, the results acquired from the disaggregation will be completely arbitrary. In this case it is proposed that all sites with recorded precipitation on that event day be temporarily used as key sites, regardless of these sites' ability to meet the criteria for key site selection as stated above. This will rectify the problem of having no precipitation at the key stations during an event day, without going to the extent of using all of the stations for comparison.

4.3.3   Method for Choosing Fragments

It was presumed that in order to produce acceptable results, the fragments should be created from the hourly data best suited to the daily data being disaggregated. Srikanthan and McMahon (1982) determined that using randomly selected fragments

did not produce desirable data, so randomly selected fragments were not applied in this study.

Although deterministic models using the method of fragments are known to be susceptible to repetition, this study employs a strictly deterministic approach. This approach was implemented for a variety of reasons including time constraints and the lack of evidence to support the success of stochastic methods. Wójcik and Buishand (2003) provided a method for performing a stochastic method of fragments, and suggest that it will remove the repetition in the output, but no results were published by the time the current study was completed. Since a large data set was available from the spatial interpolation model output, it was assumed that repetition would not be a great concern in this study and that the deterministic method would suffice.

4.3.3.1   *First Event Day of an Event*

During the disaggregation of the first event day of any event there is no hourly data in the previous day to compare it to because, by definition, the day prior to the beginning of an event must be a non-event day. Therefore, no smoothing methods are required on the first day of an event. Although there may have been some precipitation in the day previous to the first day of an event, the precipitation must not have been a large enough volume for the previous day to be considered an event day. Therefore it is not necessary to incorporate the previous day's precipitation into the pattern being produced for the event. There is no precedence put on the time of day when the precipitation occurs during the fragment selection process for the first event day of an

event. By selecting the fragments for the first day of an event in this manner, no

assumptions were made regarding the precipitation on the previous day.

That being the case, Equation 2-10 presented in Section 2.4.2.3 cannot be fully

calculated. The fragments for the first event day of each event were chosen by

Equation 4-1 which is a simplified version of the equations provided by Maheepala and

Perera (1996).

$$\alpha_j = \sum_{i=1}^{n} \left(\frac{D_{i,k} - \sum_{j=1}^{24} H_{i,j}}{S_{i,D}} \right)^2$$

(4-1)

D=generated daily data	i=gauge station
H=historical hourly data	j=day of hourly data
h=last hour of hourly data (example 11pm)	k=day of daily data
S=standard deviation	

The series of hourly data chosen to be used as fragments for disaggregation will be that

which provides the minimum value of α, calculated using all of the key sites, i. α is a

parameter created to determine the similarity of a series of hours (H_j) to the daily data

point (D) being disaggregated. While serving more functions if applying a smoothing

factor (refer to Section 4.3.3.2), the standard deviation in the denominator of Equation

4-1 standardizes all of the key stations to each other for a multi-site application.

Equation 4-1 used by itself without any smoothing factors is essentially the method

suggested by Srikanthan and McMahon (1982) with an extension added for multi-site

capabilities.

4.3.3.2   *Subsequent Event Days*

While the first event day to be disaggregated for an event is not influenced by preceding precipitation, all subsequent event days must maintain some continuity with the former portion of the event. This ensures that the event responds as a single unit with proper sequencing and not as multiple single day events that happen to occur in succession. For instance if a large event is occurring overnight, it should be able to continue itself into the next day and not just abruptly stop because that's when the next daily data were recorded. A method was proposed by Maheepala and Perera (1996) to maintain statistical properties at timescales larger than the intended disaggregated data.

All subsequent event days in this study had fragments chosen using the standard comparison methods presented in Section 4.3.3.1, with an added smoothing function to maintain any precipitation patterns that existed on the day turnover. This results in the use of Equation 2-10 (Maheepala and Perera, 1996) in its full form, for a multisite application. For a further explanation of the work by Maheepala and Perera (1996) including this equation refer to Section 2.4.2.3. The equation in its expanded form is given in Equation 4-2.

$$\alpha_j + \beta_j = \sum_{i=1}^{n}\left(\frac{D_{i,k} - \sum_{j=1}^{24} H_{i,j}}{S_{i,D}}\right)^2 + \sum_{i=1}^{n}\left(\frac{h_{i,k-1} - h_{i,j-1}}{S_{i,h}}\right)^2$$

(4-2)

D=generated daily data   i=gauge station
H=historical hourly data   j=day of hourly data
h=last hour of hourly data (example 11pm)   k=day of daily data
S=standard deviation

The optimal hourly series for fragment creation of event days after the beginning of an event will minimize the value of $\alpha + \beta$. As noted previously, α is used to compare a series of hours to a daily data point. However, β is a parameter created to determine the similarity between the last hour of historical data prior to the hourly series currently under examination (h_{j-1}) to the last hour of the disaggregated hourly series (h_{k-1}). In Equation 4-2 the standard deviation is used to standardize the key stations as well as standardize α to β. The beta portion of Equation 4-2 serves as the smoothing function for events that span over more than one day in the daily record.

4.3.3.3   *Seasonality*

Precipitation patterns vary depending on the season. As will be discussed in Section 5.1.2, in the region of study summer weather patterns tend to produce thunderstorms while spring and fall weather patterns tend to produce longer less intense rainfall events influenced by lake effects. In order to maintain this distinction in the disaggregated data, it is vital to choose fragments that originate in the correct season, thereby selecting precipitation patterns that correspond to the proper season. For this model a season was defined as 30 days in either direction of the day being disaggregated.

The literature suggested that historically a season in this region could be defined as three months; however, this study employed a season of 61 days. The season was decreased in order to ensure clearly defined seasonal patterns as well as to decrease computational expense. This shorter season could potentially increase fragment repetition due to a smaller effective data set, but this is not anticipated to be an issue because of the large historical data set created by spatial interpolation. During the

selection of an hourly series for the creation of fragments, only hourly series that fell within the required season were considered as potential fragments. A longer season would cause more hourly data to be examined as potential fragments for each event day and this would increase processing time.

Another point of interest regarding seasons is that in the literature (Ruhf and Cutrim, 2003) the three month seasons were the same three months all the time (i.e., December to February, March to May, June to August and September to November). Through the proposed method, the seasonal window is constantly changing based on the date of the event day. Therefore for an event day that would have occurred on the cusp of the seasons in former studies (i.e., Ruhf and Cutrim, 2003) the proposed method is assumed to provide more seasonal accuracy.

4.3.4   Closest Precipitation Model

While calculating hourly precipitation values after the fragments have been selected some special cases can occur. A discussion of these special cases and proposed methods for rectifying potential errors are presented below. The formulae used to calculate hourly precipitation values from fragments are repeated in Equation 4-3 for reference, more information on this Equation can be found in Section 2.4.2.

$$w_i = \frac{h_i}{\sum\limits_{i=1}^{n} h_i} \qquad \text{and} \qquad h_i^{'} = w_i \times d \qquad\qquad \textbf{(4-3)}$$

As can be seen from Equation 4-3, rational output occurs if there is precipitation in the fragments, even if there is none in the daily data being disaggregated. In this case there will be no precipitation in the disaggregated data because the fragments are multiplied by the zero precipitation of the daily data.

Complications do arise however if there is precipitation at a certain site on the day being disaggregated, but there is no precipitation in the fragments that were chosen for that site. This will cause irrational results since there will be division by zero during the calculation of the fragments. A similar case was discovered by Gutierrez-Magness and McCuen (2004) in their studies. To overcome this problem they assumed that if there was no precipitation in the fragments being used, then there would be no precipitation in the disaggregated data. This assumption resulted in a loss of precipitation volume, which was deemed unacceptable for the current study.

To correct this problem, the closest precipitation model is introduced here. The theory behind this model is that there must be precipitation at one or more sites, or this set of fragments would not have been chosen. That being the case, it is proposed that the fragments chosen for the closest site with precipitation be used for this site as well. By doing this two sites will have exactly the same pattern throughout the particular day, but each will maintain its proper daily precipitation value. This method is not perfect as some of the spatial patterns of an event may be lost; however, it is an improvement over the solution found in the literature. It is assumed that if a sufficient number of key sites are utilized, the closest precipitation model will not be utilized often.

5   Case Study Application

5.1   Thames River Basin

5.1.1   General Background

The study area for this research is the Upper Thames River basin. The Thames River

is located in south-western Ontario as shown in Figure 5-1.
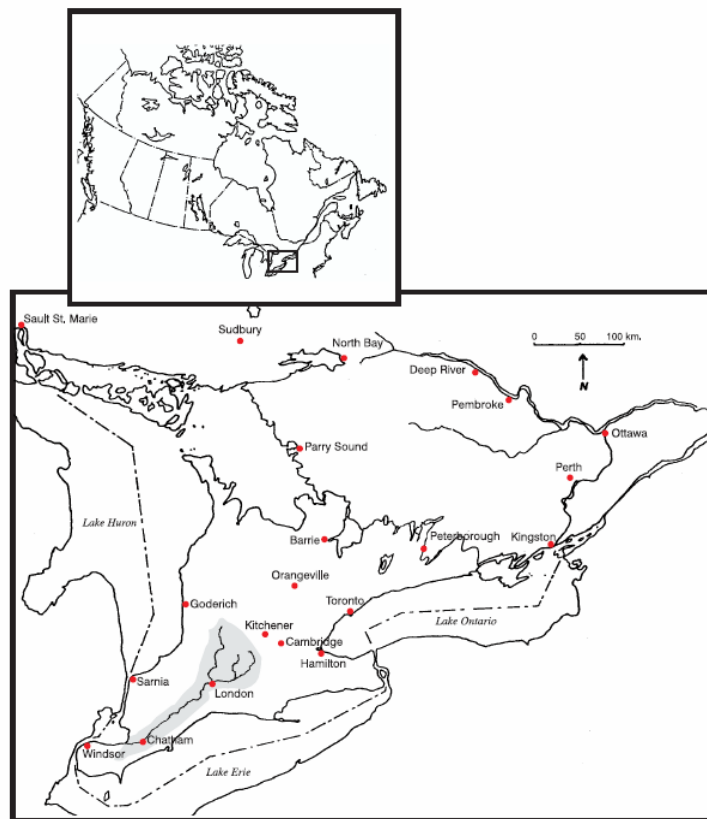
Figure 5-1: Location of Thames River Basin
(Thames River Background Study Research Team, 1998)

As can be seen in Figure 5-1, there are three main branches of the Thames River, the North Thames, Middle Thames and the South Thames. These branches originate at the towns of Mitchell, Hickson and Tavistock, respectively. The river is 273 km from source to outlet and has a catchment area of 5,825 square kilometres (Canadian Heritage Rivers System, 2006). The Thames carries an average of 30.8 cubic metres per second (May to October average) to its outlet at Lighthouse Cove in Lake St. Clair (Thames River Background Study Research Team, 1998).

The Thames River is often thought of as having two main sections, the Upper Thames and the Lower Thames, because the topography and therefore the river's properties are quite different in these two sections. The Upper Thames includes the area above and including London, while the Lower Thames consists of the region from below London to the outlet. As can be seen in Figure 5-2, the Upper Thames has a moderate profile while the Lower Thames is relatively flat. This difference in topography is also present in the river's cross-sections. Referring again to Figure 5-2 it can be seen that the Lower Thames may be prone to flooding due to its large floodplains and shallow banks. A map of the Upper Thames River watershed is provided in Figure 5-3. The majority of the data used in this study were recorded in this portion of the watershed.
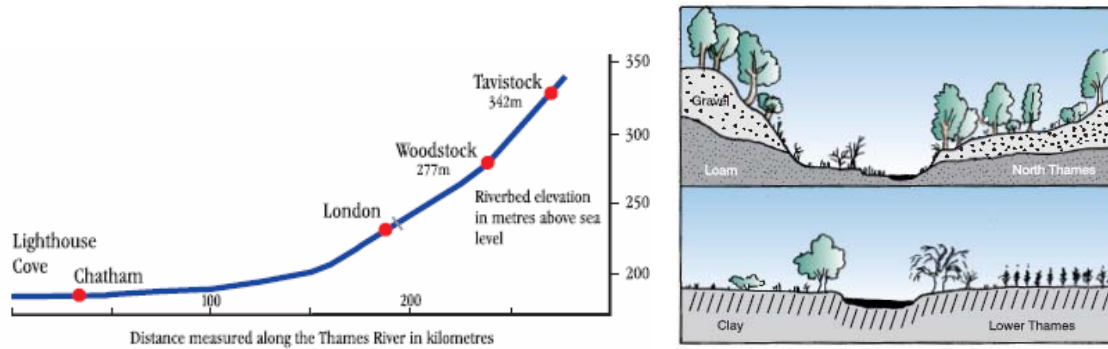
Figure 5-2: Thames valley profile and general cross sections
(Thames River Background Study Research Team, 1998)

The majority of land use in the Upper Thames basin is rural in nature; however, there are three main urban centers within the basin: London, Woodstock and Stratford. The Thames watershed contains some of the most prosperous farming land in Canada (Thames River Background Study Research Team, 1998). The largest human input to the river is from London sewage (Thames River Background Study Research Team, 1998). Sewage treatment in London began operations in 1901, and there are now six treatment plants in London with an output totalling 1500 m^3/day (City of London, 2006).
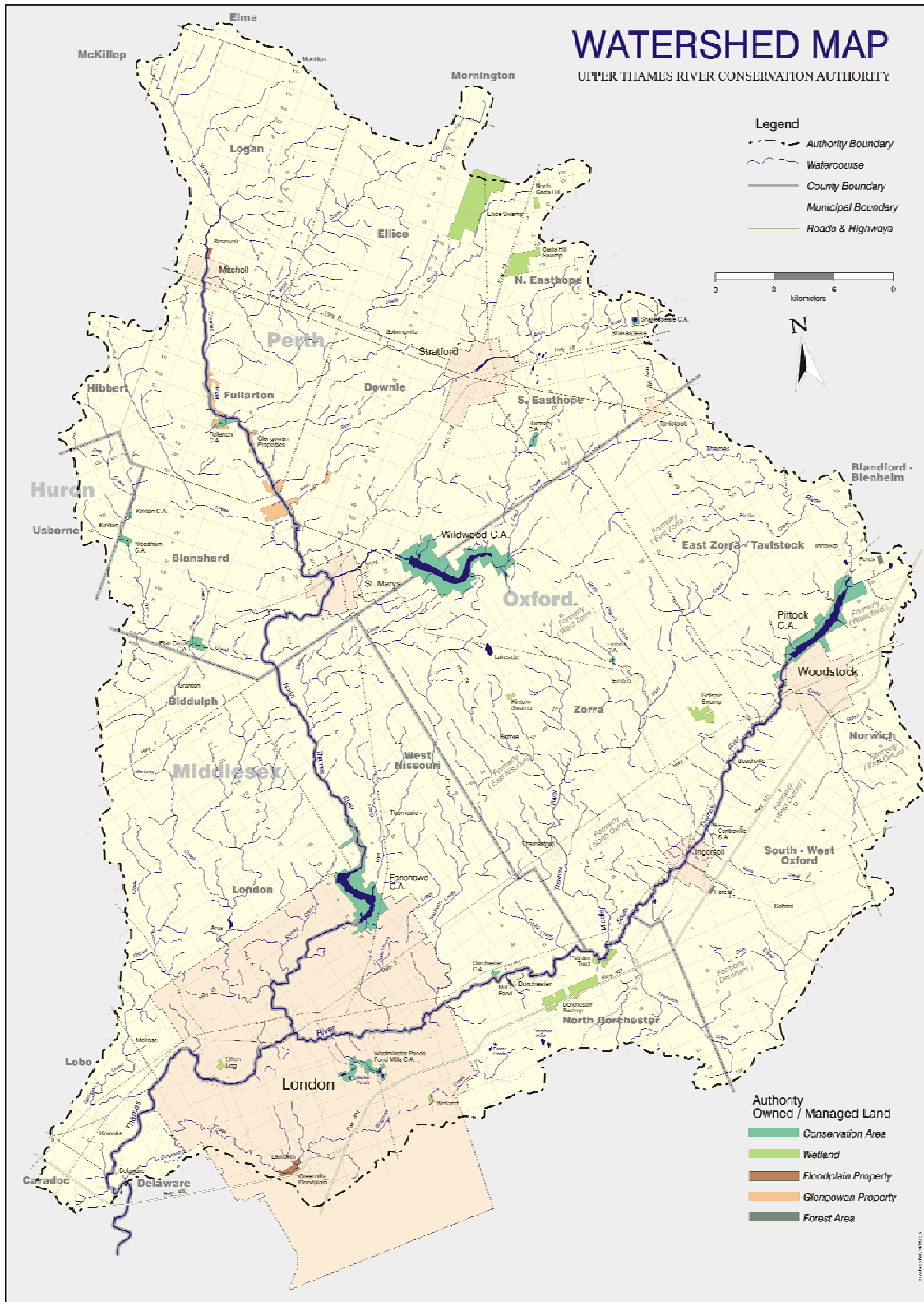
Figure 5-3: Map of the Upper Thames River Watershed (Upper Thames River Conservation Authority, 1995)

The Thames River is classified as having Category 1 flow, which is defined by the Canadian Heritage River System as extreme annual flow variation and a pronounced discharge peak with major year-to-year variation (as quoted in Thames River Background Study Research Team, 1998). According to the Thames River Background Study Team, 40% of the precipitation that falls on the Thames watershed flows to the outlet (1998). Historically (e.g., July 1883) severe floods on the Thames have occurred due to intense rainfall over a short period (Thames River Background Study Research Team, 1998).   However, the Thames is also susceptible to flooding because snowmelt on the watershed occurs before the outlet at Lake St. Clair melts.

5.1.2   Climate and Climate Change

The Thames River basin falls within the Carolinian Life Zone. It is the only river in Canada with the majority of its watershed in this zone (Thames River Background Study Research Team, 1998). The weather statistics displayed in Table 5-1 represent the mean value of the precipitation parameters for each month of the year. The sampling period for this data covers 30 years from 1961 to 1990 (The Weather Network, 2006), which coincides with the GCM baseline (see Section 2.1). It should be recognized that rain gauges in this region may not work properly in the winter due to freezing temperatures (Helsten, 2006).

Table 5-1: Climate normals for London Ontario (The Weather Network, 2006)

	J	F	M	A	M	J	J	A	S	O	N	D
Rain (mm)	25	27	53	70	74	82	77	90	86	74	73	50
Snow (cm)	55	42	26	10	1	0	0	0	0	3	21	55
Total (mm)	69	61	75	79	74	82	77	90	86	76	91	95
Snow Cover(cm)	15	9	1	0	0	0	0	0	0	0	2	9

Due to the nature of the Carolinian Life Zone in Canada, this region has a highly variable climate, both spatially and seasonally. Figure 5-4 shows the spatial variation of precipitation in a region including the Thames River. In their study of seasonal precipitation in southern Ontario, Lapen and Hayhoe (2003) determined that weather patterns in the region of the Thames River varied by season. They noted that the majority of summer events were of a convective thunderstorm nature while most autumn events were the results of lake effect precipitation from Lake Huron. Lake effect events tend to be less intense with longer durations than convective events. There is also a significant seasonal difference in the wind patterns over the river basin, as can be seen in Figure 5-5.
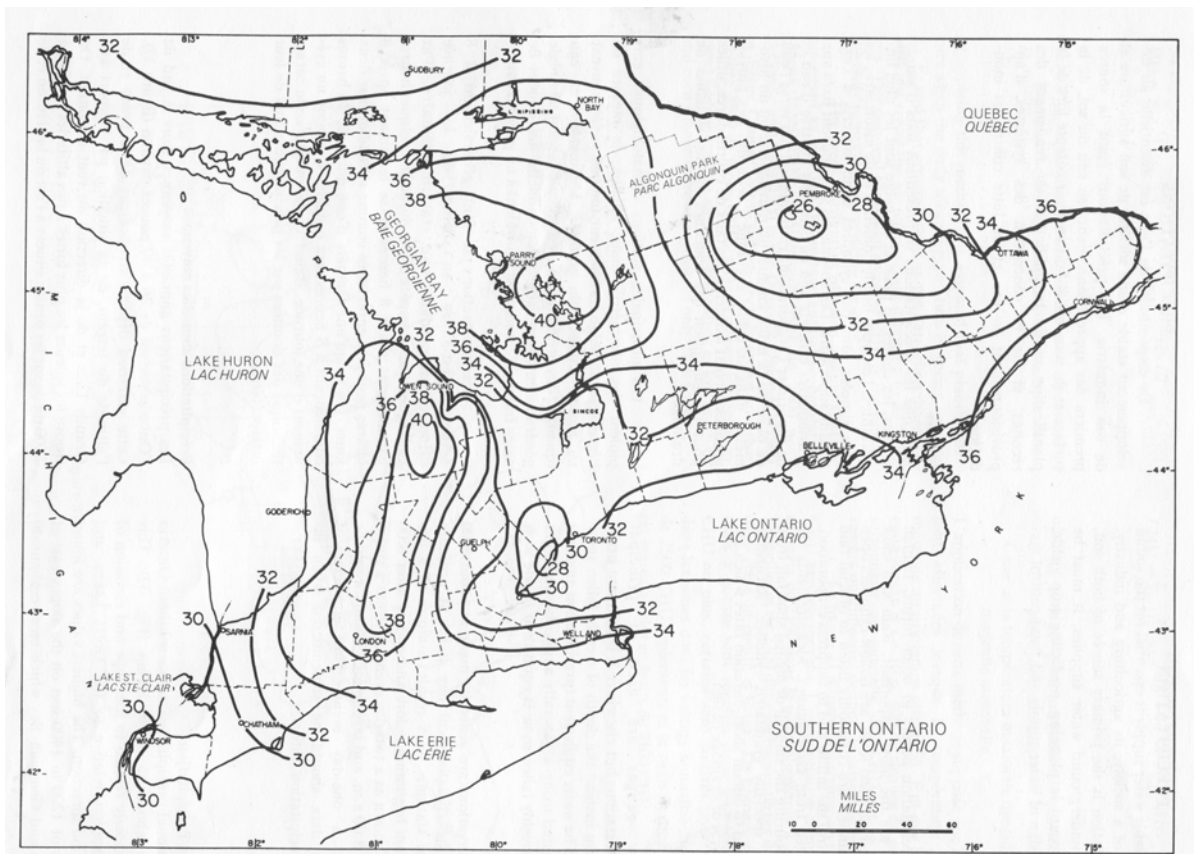
Figure 5-4: Southern Ontario mean annual precipitation in inches (Brown et al., 1980)
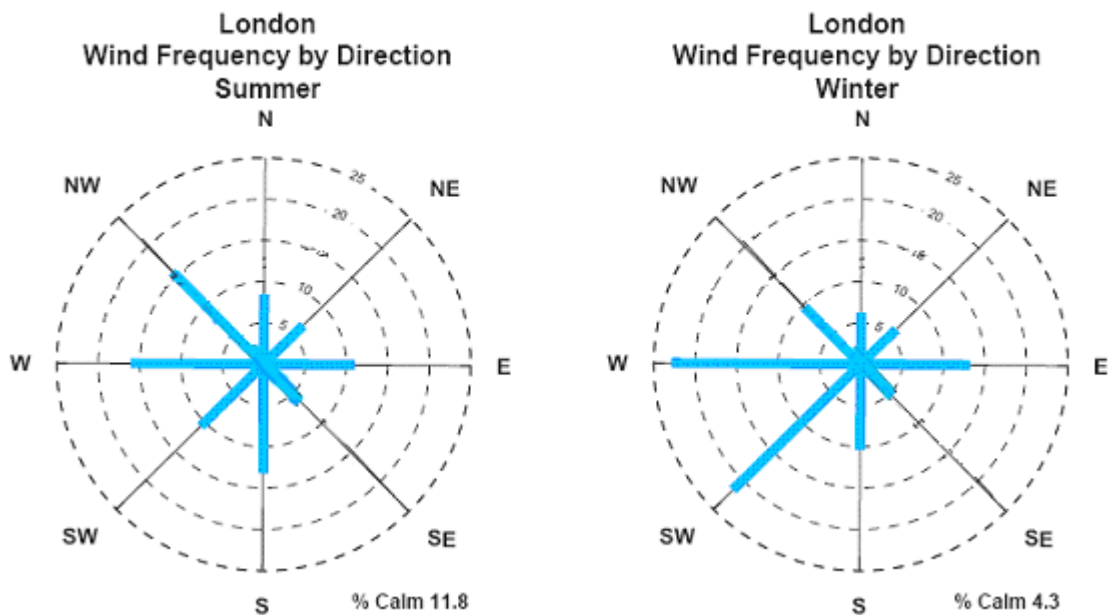
Figure 5-5: Wind patterns over London Airport (Klock et al., 2002)

The precipitation map shown in Figure 5-4 shows that over the Upper Thames basin there is a well defined ridge of high precipitation oriented from north to south and the wind patterns displayed in Figure 5-5 show that there are definite trends in the direction which precipitation events would be pushed.

From the literature, very little work has been done with precipitation at the hourly time scale, however, an analysis of hourly historical precipitation data was completed in southern Michigan (Ruhf and Cutrim, 2003). This study is referred to here because of its close proximity to the Upper Thames watershed. The southern Michigan study did not attempt to model data but rather was a detailed analysis of the characteristics of the measured data. Due to the proximity of the southern Michigan study to the Thames River, similar trends will be assumed in the present study.

Ruhf and Cutrim (2003) determined a season to be defined as three month spans.

Table 5-2 is a summary of their findings for each season; Figure 5-6A shows the annual

average of precipitation accumulation for each hour of the day while Figure 5-6B shows

the annual average of rainfall occurrences in each hour of the day.

Table 5-2: Summary of findings by Ruhf and Cutrim (2003)

	Highest Accumulation Time	*Highest Occurrence Time*
Winter	Morning	Late Afternoon
Spring	Night	Night
Summer	Morning	Morning
Autumn	Afternoon and evening	Morning

Along with the seasonal analysis, Ruhf and Cutrim (2003) also performed analysis on

extreme values in their data. The most notable finding in this section of their research is

that the highest single-hour rainfall that occurred in their dataset was 46mm.

It is known that climate change as a part of global warming is already occurring in the

area of the Thames River. Annual precipitation has increased 7-12% on average over

the 20th century in the 30°N to 80°N latitude zone(Intergovernmental Panel on Climate

Change, 2001). This mid-latitudinal region has had annual precipitation totals

exceeding the 1961-1990 normal every year since 1995.
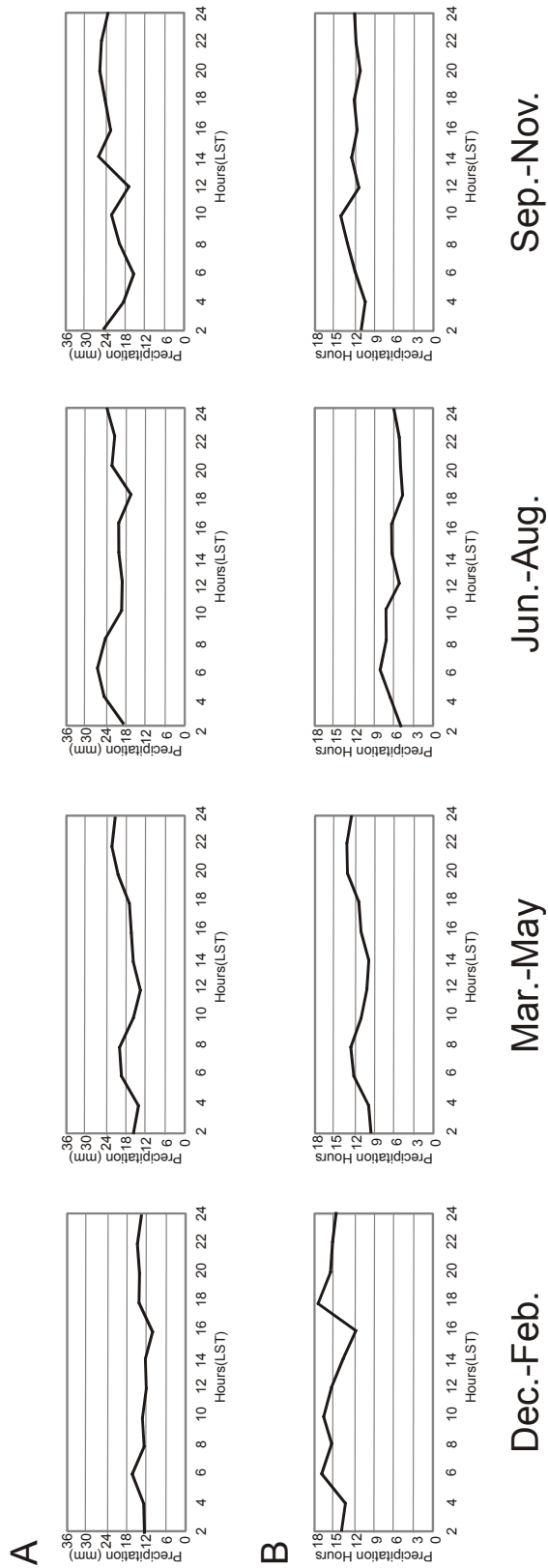
Figure 5-6: Daily rainfall cycle, (A) precipitation accumulation (B) precipitation occurrences (Ruhf and Cutrim, 2003)

5.2   GCM Scenarios Used

From the GCM scenarios presented in Section 2.1.1, two were selected for use within this study. The chosen scenarios were taken from the B1 and B2 storylines. The first chosen scenario is the first simulation with Australia's Commonwealth Scientific and Industrial Research Organisation model (CSIROM2kb) based on the B1 storyline (referred to simply as CSIROM2kb B11). The second scenario used is the first simulation using the Center for Climate System Research at the University of Tokyo's model (CCSRNIES) based on the B2 storyline (referred to as CCSRNIES B21). These scenarios and models were chosen based on the availability of data for all three of the required parameters for the weather generator.

Both of these scenarios provide information regarding the climate change that will have occurred by the year 2050. This climate change is expressed as change fields which are calculated by the GCM models for various weather parameters including temperature and precipitation as required for this study. These change fields are calculated by the equations given in Equation 5-1. The change field calculations were provided for the GCM cell centered at 43.01°N and 78.75°W because the study area is located in this cell. The change fields for each month in this cell as output by the CSIROM2kb B11 and CCSRNIES B21 models are provided in Table 5-3 and Table 5-4 respectively. It is recognized that along with the changes in these variables, changes in the variances could occur as well. An increase in variance would cause proportionately more change in the frequency of extreme events than a change in the mean values of the parameters would (Intergovernmental Panel on Climate Change, 2001).

Temperature: Precipitation:
                                                                                      (5-1)
change field = future period - base climate $\text{change field} = \dfrac{\text{future period - base climate}}{\text{base climate}} x\ 100$

Table 5-3: CSIROM2kb B11 (43.01, -78.75)(Mortsch, 2005)

Month	Mean Temperature	Minimum Temperature	Maximum Temperature	Precipitation
	°C	°C	°C	%
January	3.66	4.13	3.35	10.41
February	3.37	3.29	3.18	5.74
March	4.11	4.52	7.02	-0.98
April	6.09	5.78	4.77	-11.41
May	3.39	4.50	1.88	19.13
June	2.41	3.32	2.43	4.56
July	3.50	3.59	4.01	5.87
August	3.20	4.09	2.41	15.32
September	3.08	2.11	3.66	-6.65
October	3.17	3.11	2.51	5.39
November	3.55	4.64	3.34	-6.12
December	2.48	1.43	3.06	5.09

Table 5-4: CCSRNIES B21 (41.53, -78.75) (Mortsch, 2005)

Month	Mean Temperature	Minimum Temperature	Maximum Temperature	Precipitation
	°C	°C	°C	%
January	6.89	6.84	6.84	17.67
February	5.11	4.95	5.24	6.38
March	6.13	5.83	6.43	15.07
April	6.23	5.91	6.51	22.84
May	5.89	5.60	6.09	24.14
June	4.35	4.25	4.60	18.55
July	4.18	4.25	4.14	5.03
August	4.89	4.85	5.02	7.88
September	4.83	4.57	5.20	4.27
October	4.91	4.47	5.51	-11.51
November	5.63	5.26	6.13	-15.55
December	6.11	5.80	6.43	-3.10

5.3   Spatial Interpolation

5.3.1   Precipitation Gauge Stations

In this study of the Thames River watershed 15 daily and 28 hourly gauge stations were used. A list of these stations and their locations can be found in Table 5-5 for the daily stations and Table 5-6 for the hourly stations. The data from the daily stations was supplied by Environment Canada so the identification numbers for these stations have been included in Table 5-5. The data for the hourly gauge stations was supplied in part by Environment Canada and in part by the Upper Thames River Conservation Authority. Because of this, not all hourly stations have identification numbers associated with them and so these are not presented in Table 5-6.

Table 5-5: Daily data stations

Station Name	ID Number*	Latitude	Longitude
Blyth	6120819	43°43'	81°23'
Dorchester	6142066	43°0'	81°2'
Embro Innes	6142295	43°15'	80°56'
Exeter	6122370	43°21'	81°29'
Foldens	6142420	43°1'	80°47'
Fullarton	6142627	43°23'	81°12'
Glen Allen	6142803	43°41'	80°43'
Ilderton Bear Creek	6143722	43°3'	81°26'
London A	6144475	43°2'	81°9'
St. Thomas WPCP	6137362	42°46'	81°13'
Stratford MOE	6148105	43°22'	81°0'
Tavistock	6148212	43°19'	80°50'
Waterloo WPCP	6149386	43°29'	80°31'
Woodstock	6149625	43°8'	80°46'
Wroxeter	6129660	43°52'	81°9'

*Environment Canada identification number

Table 5-6: Historical hourly data stations

Station Name	Latitude	Longitude
Avon	43°21'	81°7'
Conestogo	43°33'	80°31'
Dingman Creek.	42°56'	81°21'
Dutton	42°40'	81°32'
Ethel	43°43'	81°7'
Exeter	43°21'	81°29'
Ingersoll	43°3'	80°53'
Innerkip	43°12'	80°41'
Listowel	43°45'	80°58'
London CS	43°2'	81°9'
Medway Creek	43°0'	81°17'
Millbank	43°35'	80°44'
Mitchell	43°27'	81°12'
New Hamburg	43°22'	80°43'
Orr dam	43°22'	80°59'
Oxbow Cr.	42°58'	81°25'
Parkhill	43°10'	81°42'
Pittock	43°16'	80°49'
Plover Mills	43°9'	81°11'
Reynolds	42°59'	80°57'
Springbank	43°4'	81°40'
St. Mary's	43°15'	81°11'
Stratford	43°22'	81°0'
Thamesford	43°4'	81°0'
Thamesville	42°32'	81°58'
Trout Creek	43°17'	80°58'
Waubuno	43°0'	81°7'
Woodstock	43°8'	80°46'

Figure 5-7 shows the location of each gauge station; the outline of the Upper Thames

basin has been included for reference purposes. The circles identify the key sites used

for temporal disaggregation (see Section 5.4)
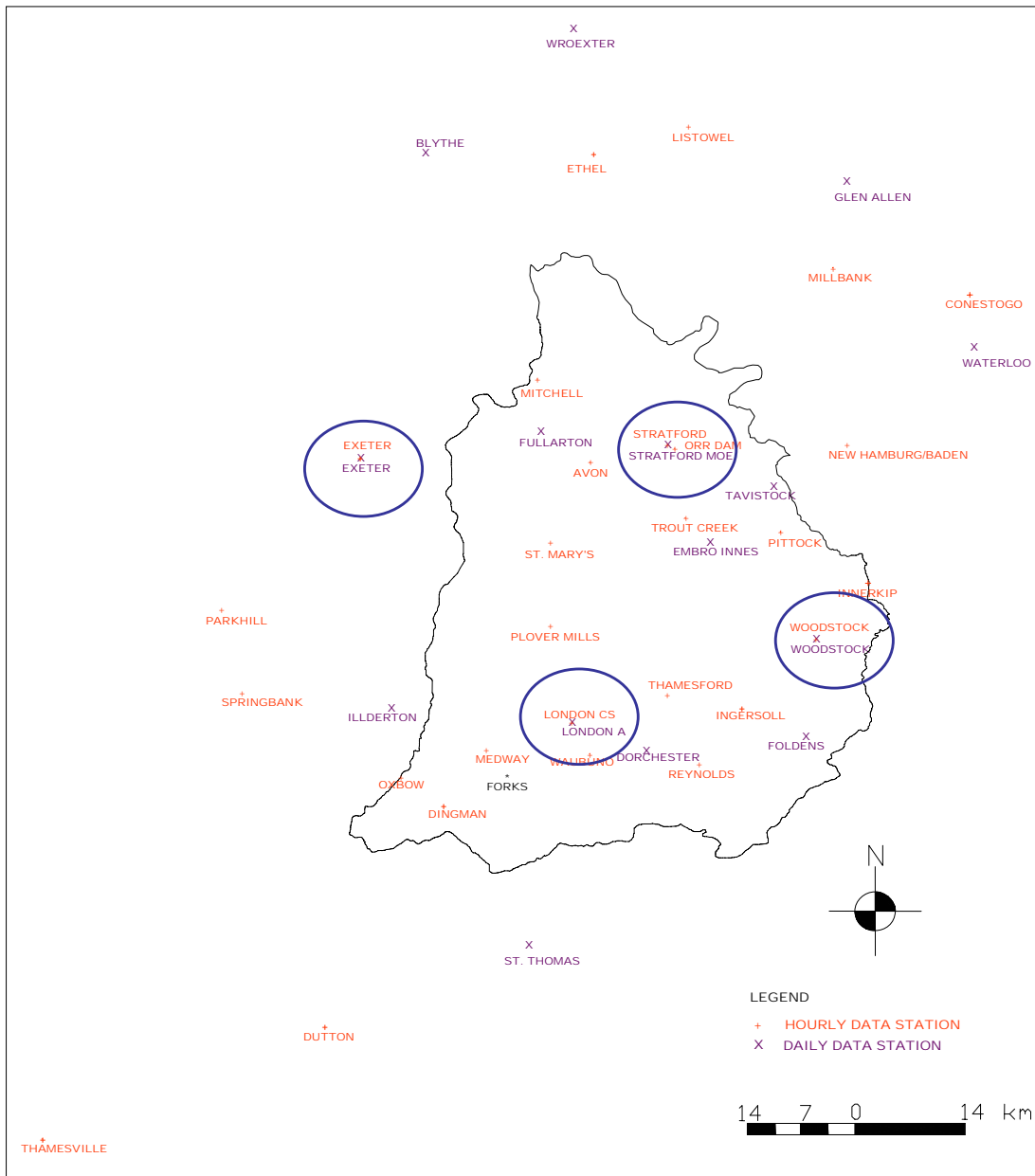
Figure 5-7: Watershed map showing rain gauges and key sites

5.3.2   Data Cleanup

For this research, missing data points were not filled in. The method used for spatial

interpolation used as many data points as were present for each time step. If a data

point was missing it was simply not used. However, outlying data were removed. Since the highest single-hour rainfall recorded by Ruhf and Cutrim (2003) in their study was 46mm (see Section 5.1.2), any data over 40mm was considered a potential outlier. Each point over 40mm was examined for evidence that the value was legitimate. It was assumed that a high hourly rainfall would show some evidence either in an adjacent hour and/or at an adjacent station. If the data point in question was not accompanied by either of these, it was considered to be an errant point and was removed. Although this method is highly subjective, there was no method for outlier removal in precipitation data found in the literature.

During the process of outlier removal, questions were raised regarding the gauge station at Plover Mills. This station had a high number of occurrences of outlying data accompanied by numerous negative values in this historical record. Due to the uncertainty produced by this, it was decided that it would be more appropriate to remove the entire record of this station from the study's data set rather than try to determine which portion of this record was usable.

5.4 Temporal Disaggregation Model

The key stations used for this study are identified in Figure 5-7. These stations were chosen because they all had both hourly and daily historical records so they were the stations used to calibrate the inverse distance method. They are expected to have the most accurate spatially interpolated data because of having both historical records.

Also, they are well spread out across the study region and so should give a good representation of the variation occurring in the entire watershed.

Table 5-7: Daily data recording times by station (Mortsch, 2006)

Station Name	Data Recoding Time
Blyth	7:00 AM
Dorchester	8:00 AM
Embro Innes	6:30 AM
Exeter	8:00 AM
Foldens	8:00 AM
Fullarton	N/A
Glen Allen	8:00 AM
Ilderton Bear Creek	8:00 AM
London A	1:00 AM
St. Thomas WPCP	10:00 AM
Stratford MOE	8:00 AM
Tavistock	N/A
Waterloo WPCP	N/A
Woodstock	7:30
Wroxeter	8:15 AM

N/A: Not Available

The actual daily recording times for the historical daily data are presented in Table 5-7. The nature of the method of fragments required all of the stations to have recording times on the hour. Changes to the given recording times were made in order to achieve the required times. Wroxeter's recording time was rounded to the closest hour, which was 8 a.m, other stations required more consideration because their actual recording time fell on the half hour. In Section 4.2 Woodstock was determined to correlate better with an 8 a.m. recording time than with a 7 a.m. recording time (see Figure 4-2). Therefore Woodstock's time was set to 8 a.m. Since Woodstock was rounded up to 8 a.m., Embro's recording time was rounded up as well, to 7 a.m. Stations with unknown

71

measurement times were filled in with 8 am as this was the most common. It should be

recognized that the majority of the stations have recording times in the morning hours.

The only station whose time differs significantly from the others is the station at London.

6　Analysis of Results

6.1　Spatial Interpolation

Spatial interpolation was completed as part of this study to generate hourly data at the same locations as the daily precipitation gauge sites. The inverse distance weighting method was used for spatial interpolation as described in Chapter 3. The outcome of the interpolation is provided below.

Although the correlations of the interpolated data could not be made to match the correlations of the historical data for the same region, an exponent value of six produced the best results from the inverse distance weighting method with hourly precipitation data. The use of this exponent value, which is higher than the exponent value used in the common inverse distance squared method, puts an increased weight on data from gauge sites that are closer to the location being interpolated. With this in mind, the need for a greater exponent value is logical because of the short time step involved. For instance, daily precipitation depths may be similar in two neighbouring cities while the hourly precipitation values in those same cities, perhaps even on a day with similar daily precipitation, could differ greatly. This is due to the relatively slow wind speeds, which are generally less than 25km/h in the region of study (Klock et al., 2002), that move weather systems (refer to Figure 5-5). Due to differences in timestep scale, inverse distance squared may be appropriate for other applications, including perhaps daily precipitation, but a larger exponent value of six is required for use with the inverse distance weighting method when applied to hourly precipitation data.

While the exponent value of six in the inverse distance weighting method produced acceptable results at four of the five stations tested, upon examination of Figure 3-2 it can be seen that the interpolated data for Stratford did not fall within the range of the 10% critical t-test value. In fact the data for Stratford did not fall within the range of the 10% critical t-test value unless the exponent had a value greater than seven; the reason for this is not known. However, it is recognized that the interpolated data at Stratford may be unduly influenced by the data at the Orr Dam gauge because of its close proximity to Stratford, which can be seen in Figure 5-7. This impact of closely neighbouring data sites is a known disadvantage of the inverse distance weighting method, as discussed in Section 2.3.2.

Along with the impact of closely neighbouring data stations, another characteristic of the inverse distance weighting method that affects the output is the tendency for peak values to be muted. Interpolation techniques create new data within the range of the original data; therefore, no interpolated point can be higher than the original maximum value or lower than the original minimum value. This is a positive trait of interpolation because the output data will always fall within the bounds of the original data and thus no unrealistic extreme values are created. However, the original maximum or minimum values of the data set may not be maintained, causing the new extremes to be closer together than in the original data set. This is a negative trait of interpolation techniques, especially because in studies such as this one the extreme events are of the most interest.

It was shown in Section 3.3 that the spatially interpolated data were more correlated, both spatially and temporally, than the original data. This occurred because inverse distance weighting tends to spread events out over multiple hours when perhaps they should have occurred in a single hour. An example of this is depicted in Figure 6-1, which is explained below.

3:00
+
NEW HAMBURG

?
X
TAVISTOCK

1:00
+
TROUT CREEK

Legend:
X   **Daily gauge station**
+   **Hourly gauge station**
1:00 **Time of rainfall**
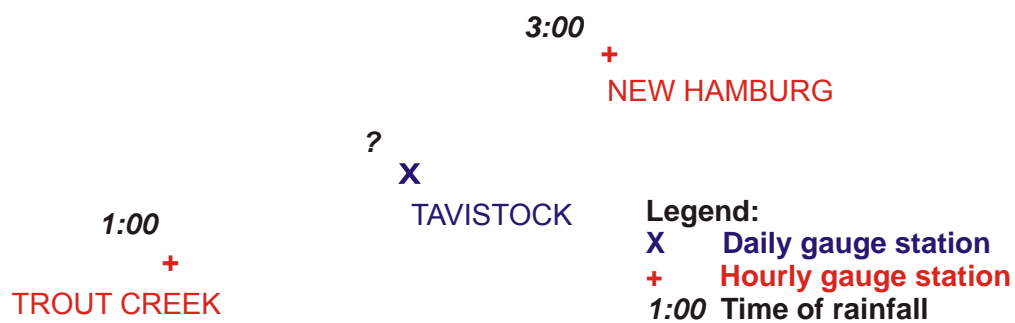
Figure 6-1: Spatial interpolation example

In the simplistic example given in Figure 6-1, interpolation is performed on Tavistock using the data from the Trout Creek and New Hamburg gauges. In this example, if it rained at Trout Creek at 1 o'clock and at New Hamburg at 3 o'clock one could assume that it rained at Tavistock at 2 o'clock. That is not how this situation would be modelled by inverse distance weighting however. With inverse distance weighting, precipitation values would be created at Tavistock at both 1 o'clock and 3 o'clock, but not at 2 o'clock, because there was no precipitation at the neighbouring stations at that time. Due to the precipitation data being simulated at 1 o'clock and 3 o'clock, both the autocorrelation and the spatial correlation values in the interpolated data of this example will be exaggerated. The autocorrelation will be inflated because there should have

75

been rain only once at Tavistock in the three-hour time span of the example. However, through inverse distance weighting, precipitation occurred in two of the three hours. Furthermore, from the example it can be seen that there will be a higher correlation between Trout Creek and Tavistock at 1 o'clock as well as a higher correlation between New Hamburg and Tavistock at 3 o'clock than there would have been if precipitation had been recorded at 2 o'clock in Tavistock. Because of this, the overall spatial correlation of the interpolated data will be higher than the spatial correlation of the original data. The exaggeration of these correlations, although always present, will be slightly reduced with the increase of the exponent value used in the formulae.

In Section 3.3.2 it was determined that the most appropriate method for calculating the distance in the inverse distance weighting formulae in the region of study is the absolute distance. The reason for this can be seen in Figure 5-5, which shows that weather systems in the region of study move in different directions based on the season. This seasonality in the wind tendencies was not worked into the testing for distance type, but if included could have resulted in a different optimal distance type. Since in each season the most common wind direction is neither latitudinal nor longitudinal, the absolute distance would likely remain the optimal distance type for use with the inverse distance weighting method even if seasonality was accounted for. This confirms the findings of Lapen and Hayhoe (2003) who determined that isotropy could be assumed when using the inverse distance weighting method.

6.2 Temporal Disaggregation

The main focus of this study was the temporal disaggregation model. Temporal disaggregation was performed on daily precipitation data to produce data at an hourly timescale for use in hydrologic models with the purpose of flood analysis. This disaggregation was completed through the method of fragments as described in Chapter 4. The results of the temporal disaggregation model are presented below.

6.2.1 Daily Data Measurement Time

To determine if the time of historical daily data measurement affected the disaggregation model, two runs were completed for the selected climate scenario CCSRNIES B21. The first run was completed assuming that all of the daily gauge stations took measurements at the same time of day, and the second run was completed using the actual times at which each station was measured (as given in Table 5-7). For the first run, the most common measurement time was used for all stations. The results of this test are shown in Figure 6-2 and Figure 6-3.

(a)

(b)
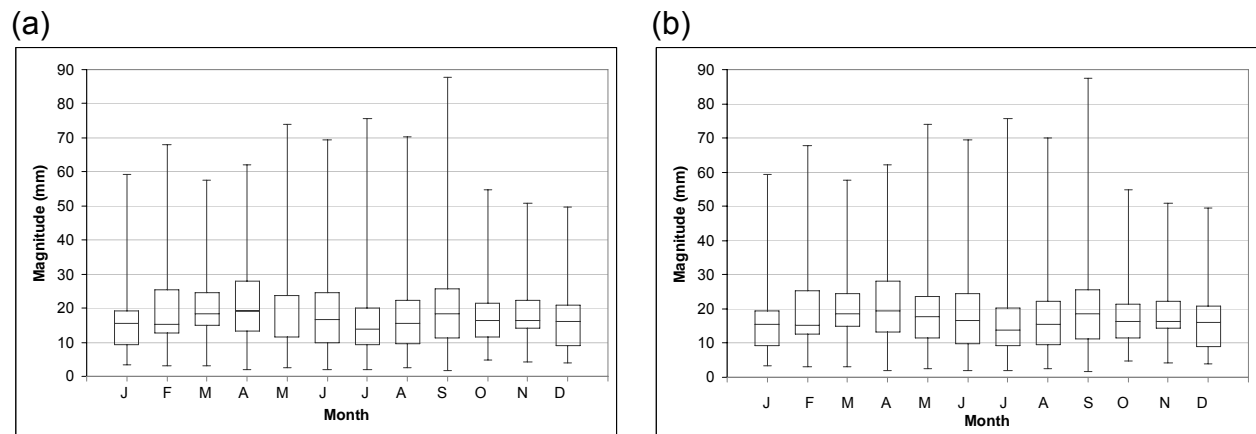
Figure 6-2: Average event magnitude by month for (a) common daily recording time and (b) actual varying daily recording time
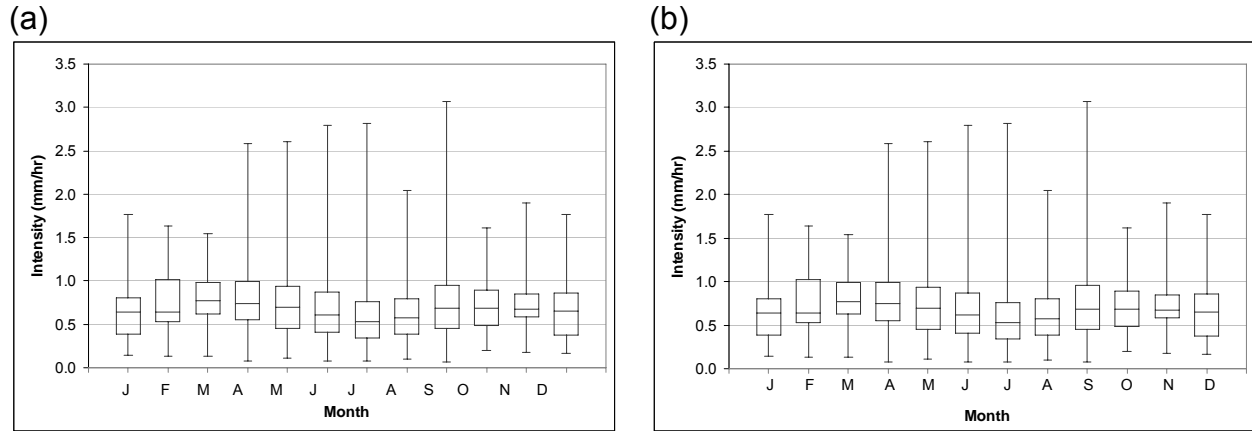
Figure 6-3: Average event intensity by month for (a) common daily recording time and (b) actual varying daily recording time

As can be seen from Figure 6-2 and Figure 6-3 the data output from the two runs of the model produced identical box plots. This suggests that because the daily data were produced by the weather generator the historical measurement times do not apply. Through further analysis, some advantages of each daily measurement method were discovered. With the use of the actual measurement times that vary from station to station, precipitation patterns were compromised because of an increase in the required use of the closest event model (refer to Section 6.2.3). However, with a common start time assumed for all stations, volumes were slightly compromised. This compromise was considered to be slight because no data were lost, however portions of it are potentially allotted to an adjacent day due to the potential error in the daily recording time.

6.2.2 Proposed Multisite Approach

The proposed multisite approach has been deemed a viable technique because it was able to complete disaggregation of multiple centuries of data at fifteen stations within a

reasonable amount of time. While doing this, it was also able to maintain the expected

variation across the watershed (see Section 6.2.4) and within each event (see Section

6.2.5).

6.2.3 Closest Precipitation Model

The closest precipitation model was introduced in this study to overcome difficulties

associated with the method of fragments in certain situations. The reasoning and

theory for this model are presented in Section 4.3.4.

The assumption that the closest precipitation model would be used infrequently was

determined to be correct. For the case using daily recording times common to all

stations this model was invoked only three times over a 100-year period. This was

considered to be an insignificant frequency and therefore was acceptable.

In the case where the actual daily recording times were used for each station, the

closest event model was utilized for 18 event days over the same 100-year period.

Some of these event days required the closest precipitation model to be run for multiple

stations. The total occurrences of the closest precipitation model for this disaggregation

run were 76. During some of these runs the model was not able to detect precipitation

in the daily period that was defined for that particular station. In this case the closest

precipitation model was forced to use the daily recording time of the neighbouring

station to determine the fragments to be transferred. In an extreme case, the same

fragments were used for the entire watershed because the only precipitation that

occurred in the chosen hourly series fell in an hour that was only considered part of that event day at one station. This complication was not desirable and reinforces the conclusion that a common daily recording time was the best option for use in the method of fragments.

6.2.4 Spatial Variation in Output Data

Along with the two selected GCM data sets produced by the weather generator, a data set was produced without any changes applied to the historical daily data's attributes. This data set is referred to as the historical generated data set. These data were created to determine the success of the disaggregation techniques; this will be determined through comparison of the disaggregated historical generated data to the spatially interpolated hourly data. Since the spatially interpolated data was generated from the historical daily data, but was not created through the use of temporal disaggregation, these two data sets should be similar.

As with the spatial interpolation model, the spatial correlation of hourly data was used as an assessment of the temporal disaggregation model's success. However, the autocorrelation was not used to assess the success of the temporal disaggregation model, since the output from this model was event based. Event data are not continuous, and therefore the autocorrelation would have no relevance. Figure 6-4 shows the spatial correlation of both the spatially interpolated event data and the historical generated event data. From Figure 6-4 it can be seen that spatial variation was maintained across the region of study through disaggregation. The spatial

80

correlation of the disaggregated historical generated data matched the spatial

correlation of the spatially interpolated data closely across the entire watershed. It

should be noted that Figure 6-4 cannot be directly compared to Figure 3-4 as the latter

was calculated using all data and the former was calculated using only data from within

event days.
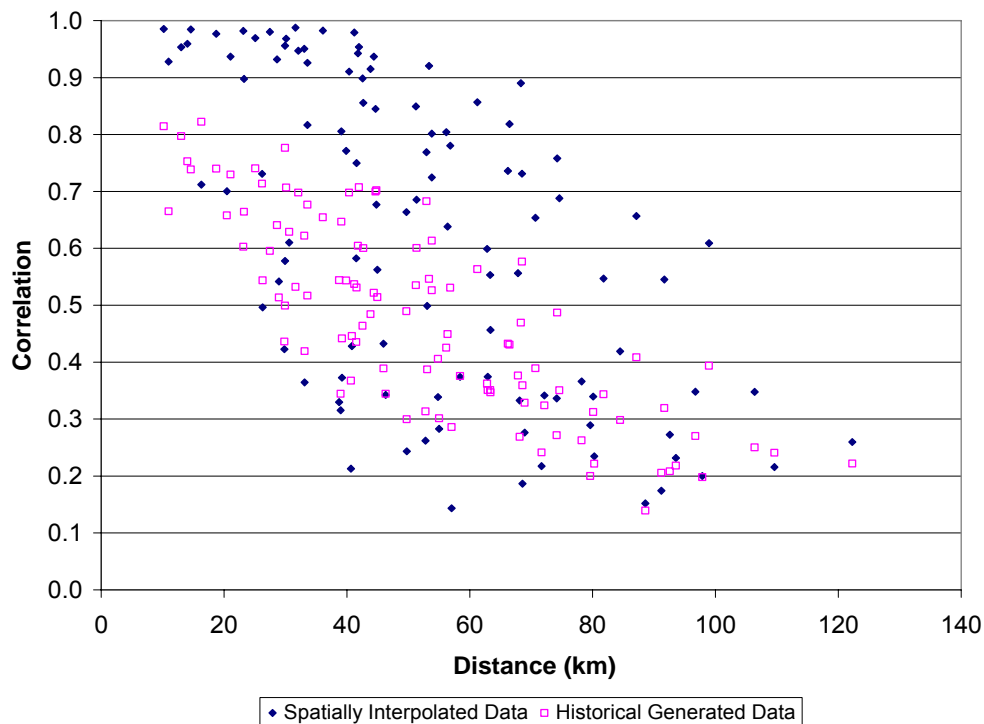
Figure 6-4: Spatial correlation of hourly event data from the historically generated scenario data and the spatially interpolated input data

Although Figure 6-4 is for the entire data set, it can be shown that spatial variation was

maintained within each event as well. Section 6.2.5 presents details of two example

events. From the isohyetal plots presented therein, it can be seen that plausible spatial

variation is obtained within events.

6.2.5 Event Statistics of Output Data

Some statistical properties of the events from the historical generated data are compared to the events of the spatially interpolated data here. This is done to examine the types and severity of events that were generated by the disaggregation in each season. In this portion of the study three properties of the event data were compared: event magnitude, event intensity and number of events. The outcomes of these comparisons at an example station, Woodstock, on a monthly basis are given in Figure 6-5, Figure 6-6 and Figure 6-7, respectively. The entire set of comparison results can be found in Appendix B.1.

In these graphs it can be seen that while the mean of the interpolated data falls within the range of the generated historical data for each parameter, the generated historical data does not simulate the spatially interpolated data very well. From these figures it can be seen that the spatially interpolated data has a higher average intensity and magnitude than the events in the historical scenario's data set. However, the spatially interpolated data has fewer events in every month. Therefore the spatially interpolated data set is composed of events of higher intensities and possibly higher durations than the events of the historical scenario's data set. It should be noted that while the historical scenario included 100 years of generated data, there were only 20 years of spatially interpolated data available for comparisons; this could cause some bias in the spatially interpolated data set. However, since this was the full set of historical data available, there was nothing that could be done in regards to this issue.
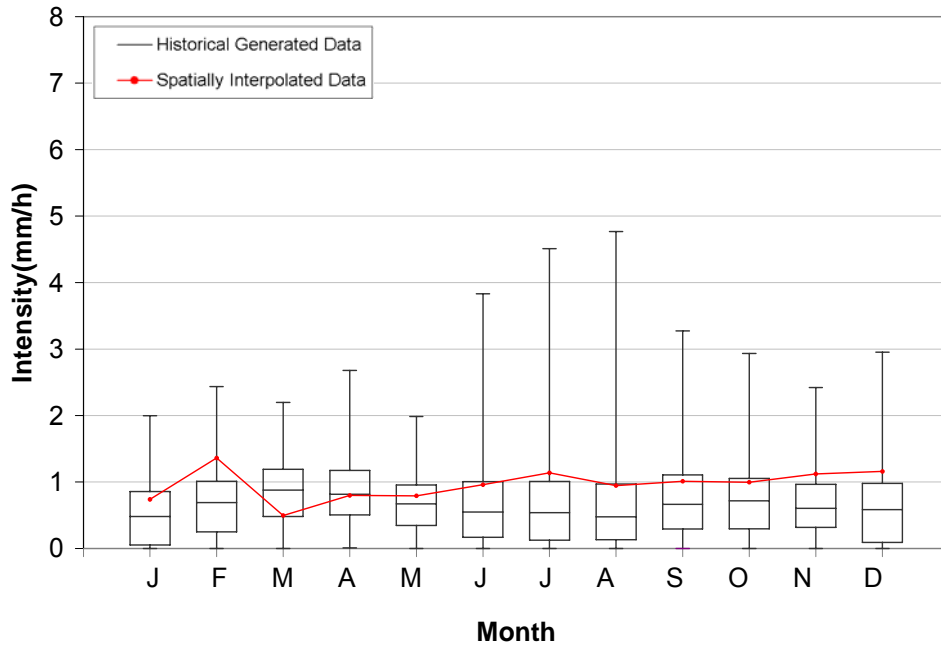
Figure 6-5: Box and whisker plot of generated historic event intensity versus mean of spatially interpolated event intensity, at Woodstock
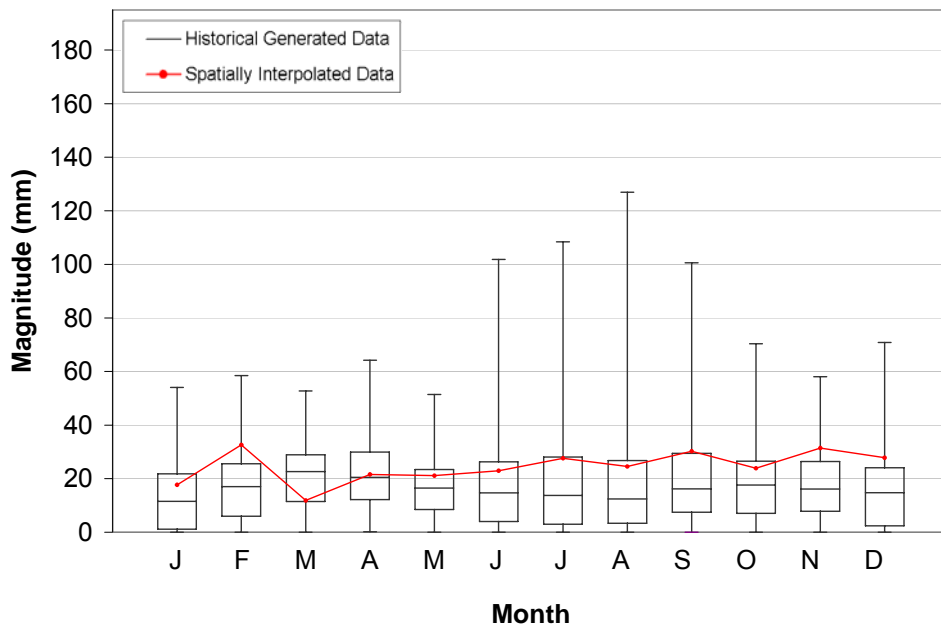
Figure 6-6: Box and whisker plot of generated historic event magnitude versus mean of spatially interpolated event magnitude, at Woodstock
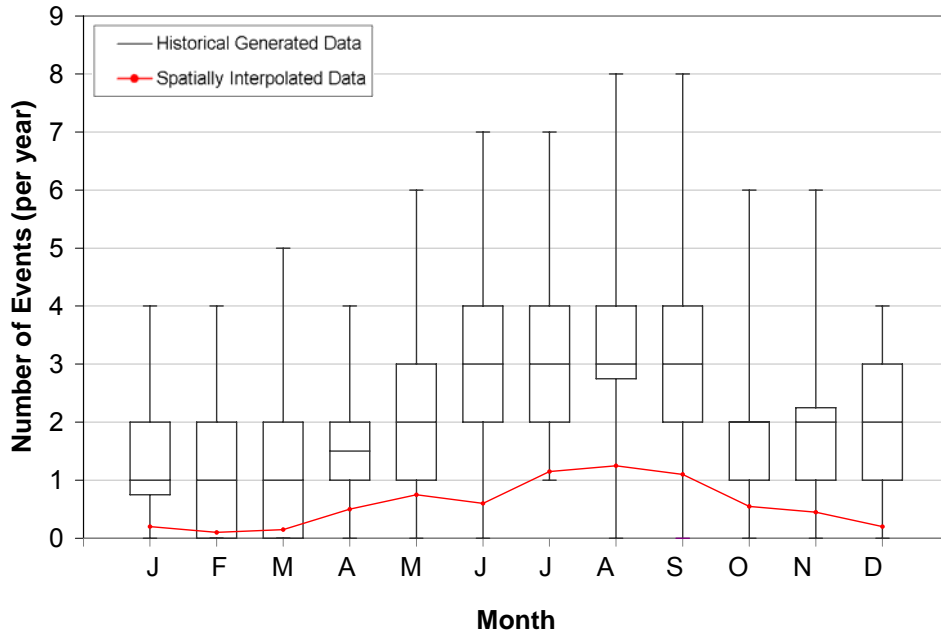
Figure 6-7: Number of generated historic events box and whisker plot versus mean number of spatially interpolated events

The discrepancy in these data sets is understandable because the historical daily data, from which the historical scenario was generated, were recorded over the period of 1964-2001, while the historical hourly data, from which the spatially interpolated data were created, were recorded over the period of 1984-2003. This means that the spatially interpolated data already contains a bias towards certain trends because weather patterns differed greatly between those two periods. As can be seen in Figure 6-8, climate change is already occurring as the average temperature from 1984-2003 is significantly higher than that of 1964-2001. Since a change in precipitation can be assumed to accompany this change in temperature, the discrepancy in the above graphs does not necessarily indicate that the disaggregation was unsuccessful, but it could be a result of climate change that has already occurred.
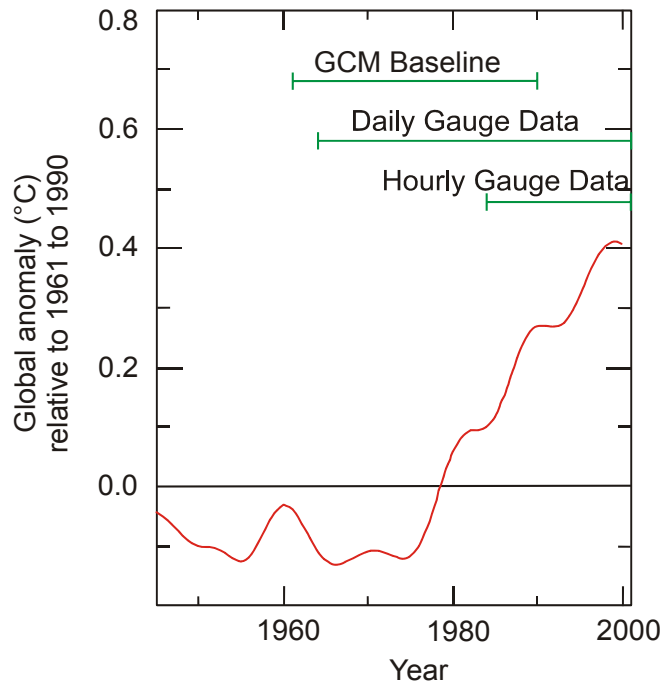
**Figure 6-8: Historical land surface air temperature trends
(adapted from Intergovernmental Panel on Climate Change, 2001, p. 113)**

6.3   Potential Impacts of Climate Change on Precipitation

in the Study Area

This section consists of two parts, a comparison of the future scenarios to the historical

scenario and a contrast between the two future scenarios. The intent of this section is

to determine the extent to which climate change will affect precipitation in the region of

study.

6.3.1 Future Scenario Data versus Historical Scenario Data

Analysis was completed comparing both the CSIROM2kb B11 data set and the

CCSRNIES B21 data set (the future scenarios) to the historical generated data set (the

historical scenario). Since it was determined that climate change has already affected

the spatially interpolated data, this data set was not used in any further comparisons. The same parameters as in the previous section (i.e., event intensity, event magnitude and number of events) were used in the comparisons of these data sets. The results of these comparisons for Woodstock, the selected example station, can be seen in Figure 6-9 through Figure 6-11. Results for each station in the study can be found in Appendix B.2 and Appendix B.3, for CSIROM2kb B11 and CCSRNIES B21, respectively.

It can be seen from Figure 6-9 that the event intensities produced through both of the future scenarios are similar to those produced through the historical scenario over the majority of the months. However, it appears that both of the future scenarios produced slightly lower event intensities in the summer than the historical scenario did. From Figure 6-10 it can be determined that the event magnitudes of the future scenarios are similar, but slightly lower than the historical scenario event magnitudes. Figure 6-11 shows that the future scenarios produced more events in the summer and fewer events in the spring than the historical scenario did.
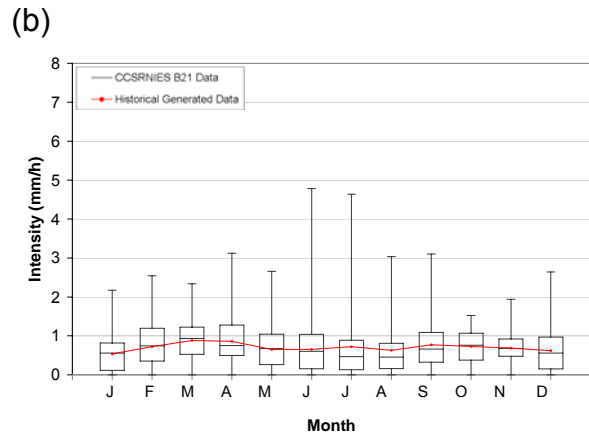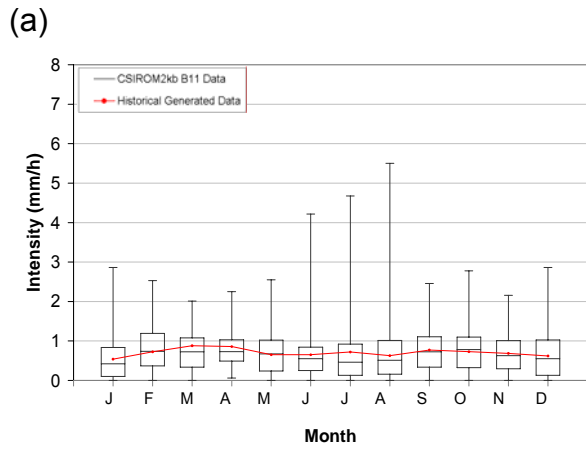
Figure 6-9: Box and whisker plot of generated (a) CSIROM2kb B11 and (b) CCSRNIES B21 event intensity versus mean of generated historic event intensity, at Woodstock
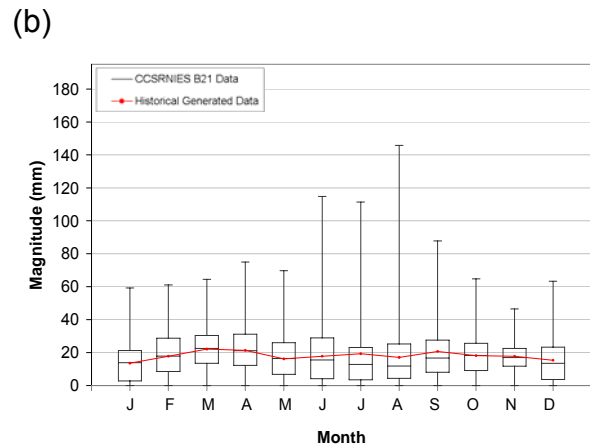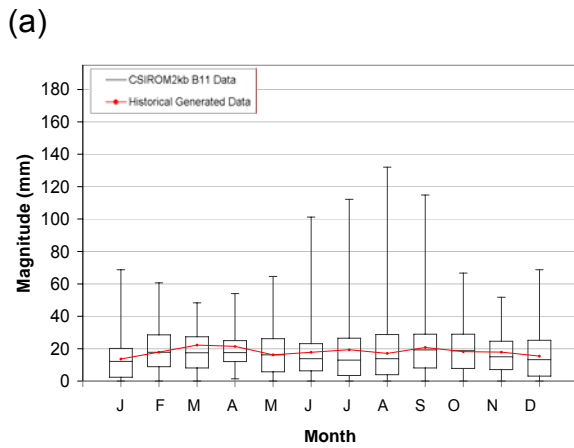
Figure 6-10: Box and whisker plot of generated (a) CSIROM2kb B11 and (b) CCSRNIES B21 event magnitude versus mean of generated historic event magnitude, at Woodstock
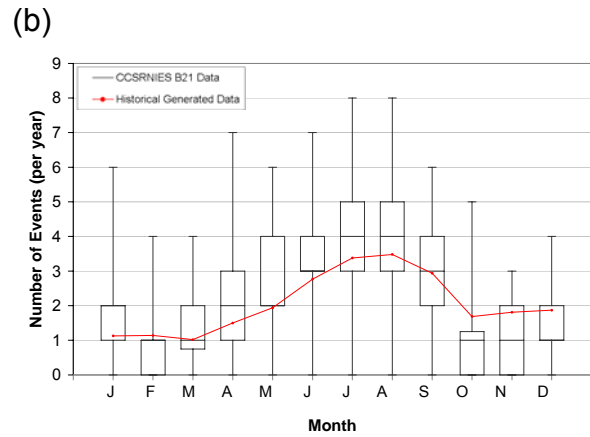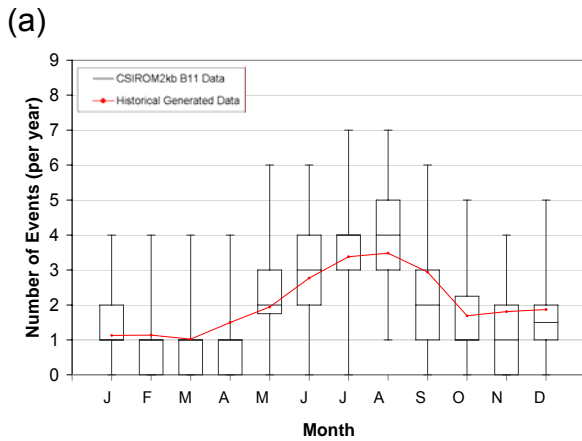
Figure 6-11: Number of generated (a) CSIROM2kb B11 and (b) CCSRNIES B21 events box and whisker plot versus mean number of generated historic events

Referring again to Figure 6-8, it can be seen that the GCM baseline, from which the change fields given in Table 5-3 and Table 5-4 were calculated, are the normals from 1961-1990. However, the historical data set was generated from data recorded over the years 1964-2001. As stated earlier, this means that some climate change is already represented in the historical data generated set. Therefore some of the climate change that should be seen in the CSIROM2kb B11 and CCSRNIES B21 generated data sets is masked by the historical scenario's data set. This could explain why the differences between the future scenarios and the historical scenario are not as visible as may have been expected. Since the historical data generated set was generated in a previous portion of this project (i.e. data generation was not within the scope of the current thesis), generation of a data set from data recorded over the years 1961-1990 was not feasible.

The overall trends that were expected based on the change fields presented in Table 5-3 and Table 5-4 for CSIROM2kb B11 and CCSRNIES B21, respectively are seen in the output data. These trends include more events in the summer and fewer in the spring and autumn, with the summer events resulting in a lower average magnitude of precipitation than the spring and autumn events, even though there are higher extreme events in the summer. Therefore the historical trends of lake-effect induced autumn precipitation and convection induced summer precipitation as noted in the literature (see Section 5.1.2) have been maintained through the climate change and through disaggregation.

6.3.2 Contrast between Two Future Scenarios

Comparisons were made between the two future scenarios in order to determine which of the scenarios has the potential to produce the most flooding in the region of study. Again the event intensity, event magnitude and number of events were used to compare the scenarios. For the sake of clarity only the mean of each data set was plotted. The results of these comparisons at Woodstock can be found in Figure 6-12. The entire set of results is presented in Appendix B.4. Comparisons of the variation in the future scenario's data can be made from the box plots presented in the previous section.

It can be seen from Figure 6-12 that CSIROM2kb B11 has higher precipitation values than CCSRNIES B21 in autumn, particularly in October. However, CCSRNIES B21 produced higher values for all three parameters in winter, spring and summer, with the exception being the month of May. In the winter months the event intensities and magnitudes produced by the two scenarios were very similar.

As noted in Section 5.1.1, the majority of floods in the region of study occur due to intense rainfall events, such as those experienced by summer weather patterns, or during spring snowmelt. Due to this, it is assumed that the CCSRNIES B21 presents the worst case scenario for flooding in the study region. As can be seen in Figure 6-12, CCSRNIES B21 has higher values than CSIROM2kb B11 in the spring and summer for all of the event parameters that were tested. This result is logical based on a comparison of the change fields presented in Table 5-3 and Table 5-4 for CSIROM2kb B11 and CCSRNIES B21, respectively, as larger precipitation increases are given by

the change fields for CCSRNIES B21 during these months. Therefore the

disaggregation process did not disrupt the trends that were applied to the data by the

GCMs through the change fields.

(a)

(b)

(c)
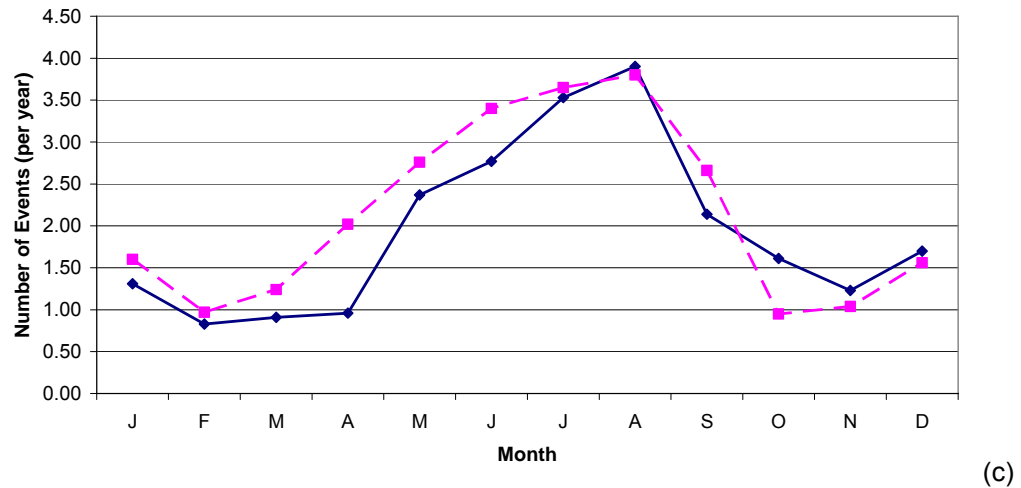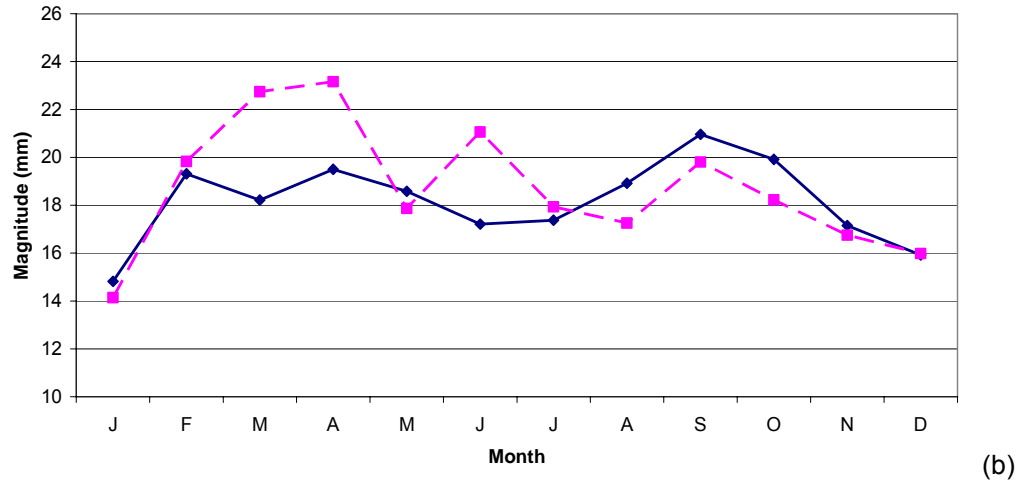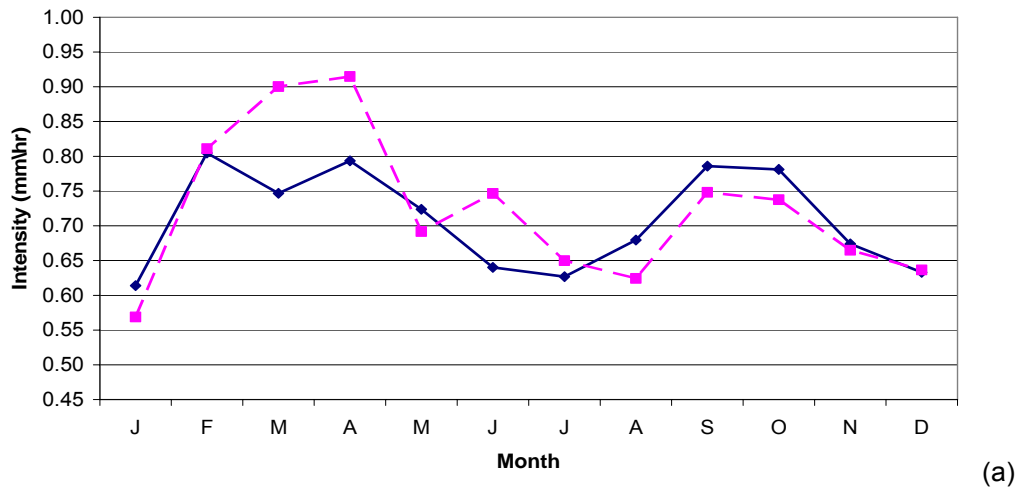
CSIROM2kb B11   CCSRNIES B21

Figure 6-12: Comparisons between CSIROM2kb B11 and CCSRNIES B21 (a) mean event intensity at Woodstock, (b) mean event magnitude at Woodstock, (c) mean number of events per year

Upon examination of Figure 6-9 through Figure 6-11 it was determined that CCSRNIES B21 produced data with greater variance of each parameter than CSIROM2kb B11 did for the majority of months. Therefore there would be a greater occurrence of extreme events in the CCSRNIES B21 scenario. This reinforces the conclusion that CCSRNIES B21 produces the worst case scenario for potential flooding in the region of study.

6.4 Extreme Events

A required outcome of this research was to determine potential extreme precipitation events for the region of study. This section provides details of two events which were selected from the temporal disaggregation model output for further analysis using hyetographs and isohyets. These two events are intended to give a representation of extreme precipitation events which may be experienced in the study area due to climate change. One event was chosen from each of the two future scenarios studied here

6.4.1 CSIROM2kb B11 Simulated Event #1403

From the CSIROM2kb B11 scenario event number 1403 was selected for analysis. This event was chosen because of its high intensity. This event possessed the traits characteristic of a convective summer event. It had high intensities and tended to be localized, with some stations receiving a lot of rain while others received very little. This event occurred on July 15 in the 60th year of the simulation and lasted for one event day.

The hyetograph of this event at Woodstock is presented in Figure 6-13. From this hyetograph it can be seen that high intensities were experienced for short durations multiple times throughout the event. The set of hyetographs for the entire watershed can be found in Appendix C.1.1.
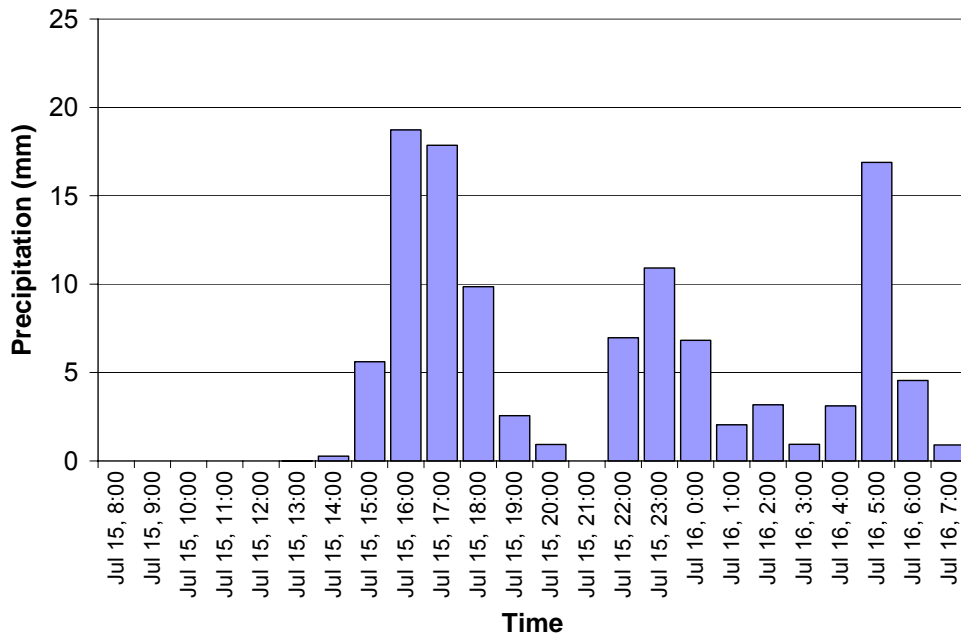
Figure 6-13: Hyetograph of CSIROM2kb B11 Event #1403 at Woodstock

Figure 6-14 is an isohyetal plot for the study area at 4 p.m. on July 15th of this event. This figure clearly shows the highly localized nature of this event, as only a portion of the watershed is receiving heavy rainfall during this hour. Isohyetal plots for each hour of this event can be found in Appendix C.2.1.
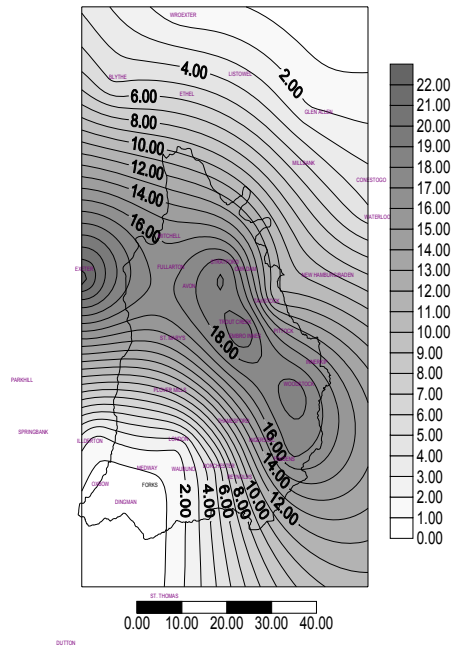
Figure 6-14: Isohyetal plot of CSIROM2kb B11 Event #1403 on July 15 at 16:00

6.4.2 CCSRNIES B21 Simulated Event #1197

Event number 1197 was chosen for analysis from the output of the CCSRNIES B21 scenario because of its severe magnitude. This event displays traits characteristic of a spring or autumn event with lake-effect influences. Unlike the convective summer event presented above, this event was not localized. While containing pockets of high intensity, the precipitation in this event was generally well spread out over the region of study. This event occurred starting on September 6 in the 47th year of the simulation and lasted for two event days. Therefore CCSRNIES B21 event 1197 implemented the smoothing methods which were presented in Section 4.3.3.

Figure 6-15 shows the hyetograph for this event at Woodstock, the example station. A set of hyetographs for the entire study area can be found in Appendix C.1.2. From Figure 6-15 it can be seen that while there was one hour with high intensities, the majority of this event consisted of low intensity precipitation. The isohyetal plot for this event at 1 a.m. on September 7th is given in Figure 6-16. This figure shows a precipitation front moving through the entire width of the watershed. Isohyetal plots for each hour of this event can be found in Appendix C.2.2. This event achieves its large magnitude through low intensity precipitation spread widely both spatially and temporally.
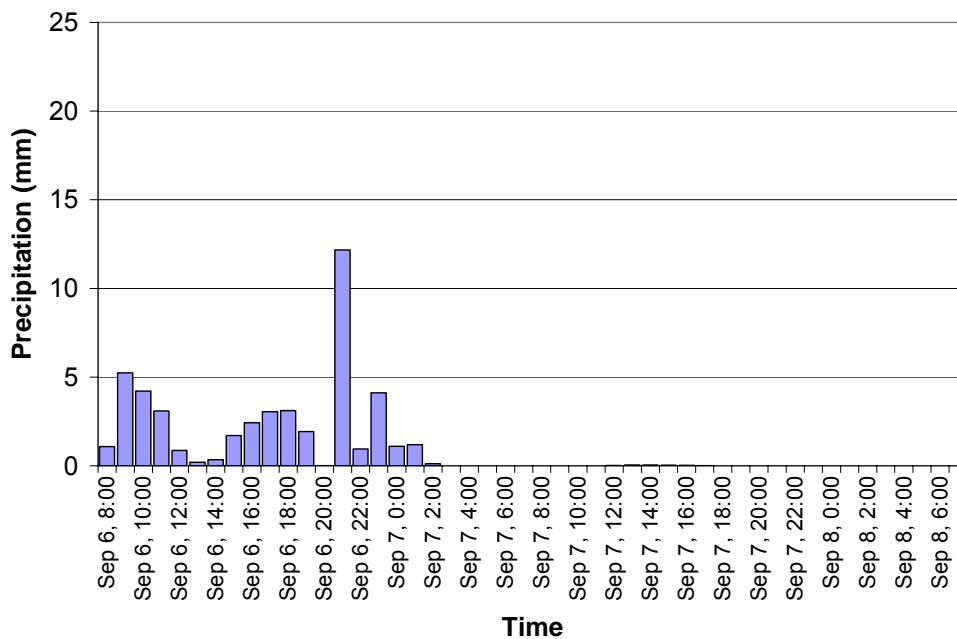
Figure 6-15: Hyetograph of CCSRNIES B21 Event #1197 at Woodstock

Figure 6-16: Isohyetal plot of CCSRNIES B21 Event #1197on September 7 at 01:00

From the isohyetal plots in Appendix C.1.2 it can be seen that there was very little precipitation occurring at the end of the first event day. Consequently there was very little precipitation at the beginning of the second event day. This demonstrates that the fragment selection process for subsequent event days was successful.

7   Conclusions and Recommendations

7.1   Conclusions

7.1.1 Spatial Interpolation Model

In this study it was determined that use of the basic inverse distance squared method was not acceptable for interpolation of hourly precipitation data, however, the more general inverse distance weighting method is acceptable for this application. An exponent value of six should be used to achieve viable results when interpolating hourly precipitation data. This greater exponent value was required because of the high variability, both spatially and temporally, of hourly precipitation data. This study also showed that isotropy can be assumed when using the inverse distance weighting method for hourly precipitation data in the region of study. Inverse distance weighting of hourly precipitation data is a robust method requiring only five gauge stations to accurately interpolate data at the watershed scale.

7.1.2 Temporal Disaggregation Model

The method of fragments appears to be an acceptable approach for disaggregation of daily precipitation data. This study implemented some new variations to the method of fragments to overcome some deficiencies that hindered its use in previous studies which were presented in the literature.

Testing was completed to determine the effect of daily recording time of the input data on the disaggregation model's output. It was determined that a common recording time

was required for all stations in the multisite scenario such that a 'day' was well defined. However, the assumption of a common daily recording time was found to be acceptable, if one did not exist.

The multiple key sites tactic used in this study for choosing fragment sets in a multisite study was shown to be effective. This tactic allowed the model to disaggregate data in a reasonable amount of time while maintaining spatial variation across the region of study. As well, the smoothing methods used in the selection of fragments for subsequent event days produced acceptable results.

The 61-day seasonality window appears to have been a success because the disaggregated data show well defined seasonal variation, including the types of events present in each season. The data output from the temporal disaggregation model shows evidence that summer precipitation events will continue to be the result of convective thunderstorms and autumn events will continue to be influenced by lake-effects.

The closest precipitation model introduced in this study rectified the deficiency previously experienced by multisite models. This new method allowed for the fragments of one station to be used at another when the fragments originally selected for that station proved insufficient.

The events output by the temporal disaggregation model acceptably reproduced the spatial correlation of the input data. Furthermore, the trends applied to the data through the GCM change fields were not disrupted by the disaggregation process.

7.1.3 Case Study Conclusions

From the case study of the Thames River basin in Ontario, Canada, it was determined that the future scenarios produce results which are quite similar to those of the historic scenario. It was also determined that in the region studied the CCSRNIES B21 scenario presents a higher potential for flooding than the CSIROM2kb B11 does. While the CSIROM2kb B11 has higher precipitation values than CCSRNIES B21 in autumn, the CCSRNIES B21 produced higher values for all three event parameters tested in both spring and summer. Since the majority of floods in this region occur in the spring and summer, the CCSRNIES B21 creates the worst case scenario.

7.2   Recommendations

7.2.1 Previous Work

A few recommendations are put forth here in regards to the data that were used as inputs in this study. Implementation of these recommendations would improve the output of the temporal disaggregation model.

The weather generator, which was developed in a previous portion of this project, should be run using data from the period of 1961-1990 only, instead of from the period

1964-2001. By doing this, the data generated would match the properties of the GCM baseline and would provide a better basis for comparison. Furthermore, scenarios generated from the data recorded during the period of the GSM baseline would facilitate better estimations of the effects of various climate change scenarios.

A second recommendation is that the precipitation gauge systems should record data at the same time of day at each station. It is assumed that this is becoming increasingly feasible as more gauge stations become automated and do not require human interaction at each reading. By synchronizing the gauge stations in this way, the temporal disaggregation model would not need to make assumptions regarding the effect of data recording time on simulated data.

7.2.2 Spatial Interpolation Model

Although an exponent value of six was determined to produce acceptable results based on t-test comparisons, the correlations of the interpolated data could not be made to match the correlations of the historical data for the same region. Therefore a better method for interpolation of precipitation data at this time scale is needed. It is recognized that a mean square error test is an appropriate alternative approach to the t-test for the testing done in this section.

7.2.3 Temporal Disaggregation Model

Recommendations for future work in disaggregation by the method of fragments include the use of the synthetic method of fragments. This would increase the number of

potential fragments for each period being disaggregated. Along with this, the stochastic k-nn method, presented by Wòjcik and Buishand (2003), for choosing fragments should be tested to determine its viability. Both of these methods would aid in decreasing the repetition of event patterns known to adversely affect output from the method of fragments.

References

Anhalt, M. (2004). "Thiessen-Polygone." http://www.portiko.de/portiko/modules/portiko/kataloge/module/a2/thiessen/thiessen.htm#, Portiko, ed., Accessed: May 17, 2006, Webpage.

Brown, D. M., McKay, G. A., and Chapman, L. J. (1980). *The Climate of Southern Ontario (3rd ed.)*, Environment Canada: Atmospheric Environment Service, Toronto.

Canadian Heritage Rivers System. (2006). "Thames River." http://www.chrs.ca/Rivers/Thames/Thames-F_e.htm, Accessed: May 25, 2006, Webpage.

Canadian Institute for Climate Studies (2005). "Canadian Climate Impacts Scenarios." http://www.cics.uvic.ca/scenarios/, University of Victoria, ed., Accessed: June 29, 2006, Webpage.

City of London. (2006). "City of London Sewage Treatment." http://www.london.ca/PollutionControl/Sewagetreatment_index.htm, Accessed: July 19, 2006, Webpage.

Dingman, S. L. (2002). *Physical Hydrology*, Prentice-Hall, Upper Saddle River, New Jersey.

Gutierrez-Magness, A. L., and McCuen, R. H. (2004). "Accuracy Evaluation of Rainfall Disaggregation Methods." *Journal of Hydrologic Engineering*, 9(2), 71-78.

Helsten, M. (2006). Upper Thames River Conservation Authority, Personal Communication.

Hornberger, G. M., Raffensperger, J. P., Wiberg, P. L., and Eshleman, K. N. (1998). *Elements of Physical Hydrology*, Johns Hopkins University Press, Baltimore.

Intergovernmental Panel on Climate Change. (2000). *Special Report on Emissions Scenarios*, Cambrige University Press, Cambridge, United Kingdom.

Intergovernmental Panel on Climate Change. (2001). *Climate Change 2001: The Scientific Basis*, Cambridge University Press, Cambridge, United Kingdom.

Klock, R., Simard, G., and Mullock, J. (2002). *The Weather of Ontario and Quebec: Graphic Area Forecast 33*, NAV CANADA, Ottawa, Ontario.

Kottegoda, N. T., Natale, L., and Raiteri, E. (2003). "A Parsiomonious Approach to Stochastic Multisite Modelling and Disaggregation of Daily Rainfall." *Journal of Hydrology*, 274, 47-61.

Lane, W. L. (1983). *Applied Stochastic Techniques (LAST Computer Package), User Manual*, Division of Planning Technical Services, Engineering and Research Center, Bureau of Reclamation, U.S. Department of the Interior

Lapen, D. R., and Hayhoe, H. N. (2003). "Spatial Analysis of Seasonal and Annual Temperature and Precipitation Normals in Southern Ontario, Canada." *Journal of Great Lakes Research*, 29(4), 529-544.

Maheepala, S., and Perera, B. J. C. (1996). "Monthly Hydrologic Data Generation by Disaggregation." *Journal of Hydrology*, 178, 277-291.

Masters, G. M. (1998). *Introduction to Environmental Engineering and Science*, Prentice Hall, New Jersey.

McMahon, T. A., and Mein, R. G. (1986). *River and Reservoir Yield*, Water Resources Publications, Littleton, Colorado.

Mejia, J. M., and Rouselle, J. (1976). "Disaggregation Models in Hydrology Revisited." *Water Resources Research,* 12(2), 185-186.

Montgomery, D. C. (2001). *Design and Analysis of Experiments*, John Wiley and Sons, Arizona.

Mortsch, L. (2005). "Data for Climate Scenario Development." Waterloo ON, Personal Communication.

Mortsch, L. (2006). "Daily Data Recording Times." Waterloo ON, Personal Communication.

Olsson, J., and Berndtsson, R. (1998). "Temporal Rainfall Disaggregation Based on Scaling Properties." *Water Science and Technology*, 37(11), 73-79.

Porter, J. W., and Pink, B. J. "A Method of Synthetic Fragments for Disaggregation in Stochastic Data Generation." *International Hydrology and Water Resources Symposium*, Perth, Austrailia, 781-786.

Richardson, C. W. (1981). "Stochastic Simulation of Daily Precipitation, Temperature and Solar Radiation." *Water Resources Research*, 17(1), 182-190.

Ruhf, R. J., and Cutrim, E. M. C. (2003). "Time Series Analysis of 20 Years of Hourly Precipitation in Southwest Michigan." *Journal of Great Lakes Research*, 29(2), 256-267.

Salas, J. D., Delleur, J. W., Yevjevich, V., and Lane, W. L. (1980). *Applied Modeling of Hydrologic Time Series*, Water Resources Publications, Littleton, Colorado.

Sharif, M., and Burn, D. H. (2004). *Development and Application of K-Nearest Neighbour Weather Generating Model*, 57th Canadian Water Resources Association Annual Congress, Montreal, Quebec.

Sharif, M., and Burn, D. H. (2006). "Simulating Climate Change Scenarios Using an Improved K-nearest Neighbor Model." *Journal of Hydrology*, 325, 179-196.

Socolofsky, S., Adams, E. E., and Entekhabi, D. (2001). "Disaggregation of Daily Rainfall for Continuous Watershed Modeling." *Journal of Hydrologic Engineering*, 6(4), 300-309.

Srikanthan, R., and McMahon, T. A. (1982). "Stochastic Generation of Monthly Streamflows." *Proceedings of the American Society of Civil Engineers. Journal of the Hydraulics Division*, 108(3), 419-441.

Svanidze, G. G. (1977). *Mathematical Modeling of Hydrologic Series*, T. Guerchon, translator, Water Resources Publications, Littleton, Colorado.

Tabios, G. Q., and Salas, J. D. (1985). "A Comparative Analysis of Techniques for Spatial Interpolation of Precipitation." *Water Resources Bulletin*, 21(3), 365-380.

Thames River Background Study Research Team. (1998). "The Thames River Watershed: A Background Study for Nomination under the Canadian Heritage Rivers System."

The Weather Network. (2006). "Statistics: London, ON, Canada." http://theweathernetwork.ca/weather/stats/pages/C02016.htm, Accessed: July 11, 2006, Webpage.

United Nations Environment Programme. (1996). "Precipitation changes: trend over land from 1900 to 1994 - Climate Change." http://www.grida.no/climate/vital/18.htm, Accessed: July 30, 2006.

Upper Thames River Conservation Authority. (1995). "Watershed Map." London Ontario.

Valencia, D., and Schaake, J. C. (1973). "Disaggregation Processes in Stochastic Hydrology." *Water Resources Research*, 9(3), 580-585.

Watt, W. E., Lathem, K. W., Neill, C. R., Richards, T. L., and Rousselle, J. (1989). "Hydrology of Floods in Canada: A Guide to Planning and Design." National Research Council of Canada, Associate Committee on Hydrology, Ottawa.

Wilks, D. S. (1998). "Multisite Generation of a Daily Stochastic Precipitation Generation Model." *Journal of Hydrology*, 210, 178-191.

Wilks, D. S. (1999). "Multisite Downscaling of Daily Precipitation with a Stochastic Weather Genereator." *Climate Research*, 11, 125-136.

Wójcik, J., and Buishand, T. A. (2003). "Simulation of 6-hourly Rainfall and Temperature by Two Resampling Schemes." *Journal of Hydrology*, 273, 69-80.

Yates, D., Gangopadhyay, S., Rajagopalan, B., and Strzepek, K. (2003). "A Technique for Generating Regional Climate Scenarios Using a Nearest-Neighbour Algorithm." *Water Resources Research*, 39(7), 2-15.

Appendix A.   Flowchart of Temporal Disaggregation Model

Start of a function

Call a function

Calculation

Decision

Parameters from calling function

Return to calling function

Input or output (generally from a file)

File function (open, close, rewind etc.)

On page reference

Off page reference

End of a function

Figure A-1: Legend of flow chart symbols

Main

Main

Page 1

Is there rain in the basin?

No → All hours = 0 → Print to Output → B

Yes → Is there rain at any key sites?

No → Set alternate key sites to all sites with rain

Yes → Choose Series

Choose Series → Open hourly file → Method of Fragments → Close hourly file → B

For all stations

B → Has any day file ended?

No → A

Yes → Close all files → End Main

Calculate Standard Deviation (Daily)

Calculate Standard Deviation (Daily)

Given: data file of a station

Read a line from the file

sum= sum+data

count= count+1

For entire file

Mean=sum/count

Rewind the file

sum=0

A

A

Read a Line from the file

Sum= sum+ $\frac{(data-mean)^2}{(count-1)}$

For entire file

st. dev= sqrt(sum)

Rewind the file

Return st. dev

End of Calculate Standard Dev.

Calculate Standard Deviation (Hourly)

```
┌─────────────────┐
│  Calculate      │
│  Standard       │
│  Deviation      │
│  (Hourly)       │
└────────┬────────┘
         │
┌────────▼────────┐
│  Given: data    │
│  file of station│
│  & hour of      │
│  intrest (ie last│
│  hour of day)   │
└────────┬────────┘
         │
┌────────▼────────┐
│  Read a line    │
│  from the file  │
└────────┬────────┘
         │
      ◇ Does ◇
      time
      read =       ── No ──►
      given
      hour?
         │
        Yes
         │
┌────────▼────────┐
│  sum= sum+data  │
│                 │
│  count= count+1 │
└────────┬────────┘
         │
┌────────▼────────┐
│  Mean=sum/count │
└────────┬────────┘
         │
┌────────▼────────┐
│  Rewind the file│
└────────┬────────┘
         │
┌────────▼────────┐
│  sum=0          │
└────────┬────────┘
         │
        (A)
```

For entire file

```
        (A)
         │
┌────────▼────────┐
│  Read a Line    │
│  from the file  │
└────────┬────────┘
         │
      ◇ Does ◇
      time
      read =       ── No ──►
      given
      hour?
         │
        Yes
         │
┌────────▼────────┐
│  Sum= sum+      │
│  (data-mean)²   │
│  (count-1)      │
└────────┬────────┘
         │
┌────────▼────────┐
│  st. dev= sqrt(sum)│
└────────┬────────┘
         │
┌────────▼────────┐
│  Rewind the file│
└────────┬────────┘
         │
┌────────▼────────┐
│  Return st. dev │
└────────┬────────┘
         │
┌────────▼────────┐
│  End of Calculate│
│  Standard Dev.  │
└─────────────────┘
```

For entire file

$$Sum = sum + \frac{(data-mean)^2}{(count-1)}$$

$$st.\ dev = sqrt(sum)$$

Choose Series

Given: date
(daily)

Open files for all
key stations

Read 24 lines
from each file

Seasonality

Is data
from file
in
season? — Yes

No

Compare Day

Have
any files
ended? — No

Yes

A

A

Close all opened
files

Return best
date

End Choose
Series

Seasonality

Seasonality

Given: hourly and daily dates & variation for season

Begin= daily day-variation

End= daily day+ variation

Is hourly year a leap year?

No ← → Yes

Is End >365?

No

Is End >366?

No

Yes

Yes

End= End-365

End= End-366

Year crossover = true

Year crossover = false

Year crossover = true

Page 2

Seasonality

Is previous year a leap year?

No ─── Yes

Is Begin <1? ─── No ─── No ─── **Is Begin <1?**

Yes ─── Yes

Begin= Begin+365

Begin= Begin+366

Year crossover = true

Year crossover = false

Year crossover = true

Year cross over

false ─── true

Hourly day >Begin **AND** Hourly day <End? ─── No ─── No ─── Hourly day >Begin **OR** Hourly day <End?

Yes ─── Yes

Season = true

Season = false

Season = true

Return Season

End Seasonality

Compare Day

```
Compare Day
```

Given: best day, data (hourly & daily), st devs

Sum the hourly data

$a = a + \dfrac{(day\text{-}sum)^2}{(day\ stdev)}$

For all key stations

$\text{ß} = \text{ß} + \dfrac{(day's\ last\ hour\text{-}proposed\ last\ hour)^2}{(hour\ stdev)}$

$a + \text{ß} <$ best date value?

Yes

Replace best date

No

Return best date

End Compare Day

Method of Fragments

```
  ┌─────────────┐
 (│  Method of  │)
  │  Fragments  │
  └─────────────┘
         │
         ▼
  ┌─────────────┐
  │  Given: day │
  │  data, day  │
  │    date     │
  └─────────────┘
         │
         ▼
  ┌─┬───────────┬─┐
  │ │ Get Series│ │
  └─┴───────────┴─┘
         │
         ▼
  ┌─────────────┐
  │             │
  │ Sum hourly  │
  │    data     │
  └─────────────┘
         │
         ▼
     ╱╲ Does ╲
    ╱  sum=0?  ╲
    ╲          ╱
     ╲_____╱
   No │      │ Yes
      ▼
    (A)
```

```
        ╱╲ Does ╲
       ╱   day    ╲
       ╲  data=0  ╱──── Yes ────┐
        ╲_____╱               │
          │ No                   ▼
          ▼              ┌─────────────┐
   ┌─┬─────────┬─┐       │  All new    │
   │ │ Closest │ │       │  hours =0   │
   │ │Precipita│ │       └─────────────┘
   │ │  tion   │ │              │
   └─┴─────────┴─┘              ▼
          │                    (B)
          ▼
   ┌─────────────┐
   │ Sum hourly  │
   │    data     │
   └─────────────┘
          │
          ▼
        (A)
```

```
        (A)
         │
         ▼
  ┌─────────────┐
  │ Calculate 24│
  │   weights:  │
  │w=hour data/sum│
  └─────────────┘
         │
         ▼
  ┌─────────────┐
  │ Calculate new│
  │    hours:   │
  │new=w*day data│
  └─────────────┘
         │
         ▼
  ┌─┬─────────┬─┐
(B)─│ │Print to │ │
  │ │ Output  │ │
  └─┴─────────┴─┘
         │
         ▼
  (  End Method of  )
  (   Fragments     )
```

Get Series

Get Series

Given: date and file

Read a line from file

No

Is line read the line prior to given date?

Yes

Read and store 24 hours of data

Return data

End Get Series

Closest Precipitation

```
            ┌──────────────┐
            │   Closest    │
            │ Precipitation│
            └──────────────┘
                   │
            ┌──────────────┐
            │ Given: date, │
            │   station    │
            │  locations,  │
            │   current    │
            │   station    │
            └──────────────┘
                   │
            ┌──────────────┐
            │ Calculate the│
            │distance to each│
            │   station    │
            └──────────────┘
                   │
            ┌──────────────┐
            │ Find closest │
            │unchecked station│
            └──────────────┘
                   │
            ┌──────────────┐
            │ Open file for│
            │ closest station│
            └──────────────┘
                   │
            ┌──────────────┐
            │  Get Series  │
            └──────────────┘
                   │
            ┌──────────────┐
            │ Close file for│
            │ closest station│
            └──────────────┘
                   │
            ╱──────────────╲
            │  Is there    │
   ┌─────────┤   rainfall   │
   │   No    │   in this    │
   │         │    data?     │
   │         ╲──────────────╱
┌──────────────┐     │
│This station has│   Yes
│ been checked │     │
└──────────────┘ ┌──────────────┐
                 │  Return data │
                 └──────────────┘
                       │
                 ┌──────────────┐
                 │ End Closest  │
                 │ Precipitation│
                 └──────────────┘
```

Print to Output

Print to
Output

Given: year,
day, data,
output file

Day=given day

Year=given year

8am to Midnight

Is day
Dec 31?

No — Yes

Day=given day+1

Year=given year

Day=1

Year=given year+1

1am to 7am

1am to 7am

Print "year
day time
data" to file

8am to 7am

End of Print to
Output

Appendix B.   Output Data for All Stations

B.1   Historical Generated versus Spatially Interpolated

(a)

(b)

Figure B-1: Box and whisker plot of generated historic event data compared to spatially interpolated event data at Blyth; (a) intensity and (b) magnitude

(a)

(b)
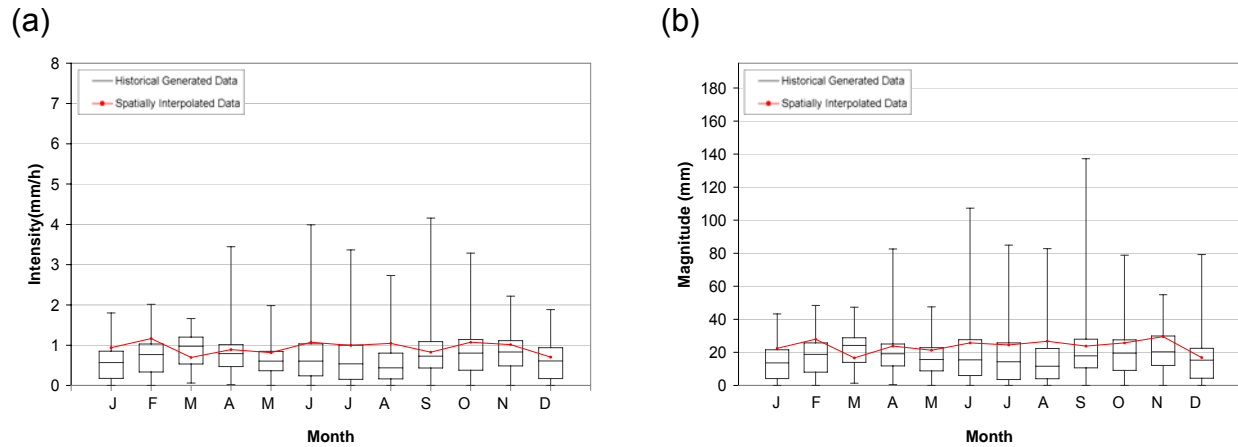
Figure B-2: Box and whisker plot of generated historic event data compared to spatially interpolated event data at Dorchester; (a) intensity and (b) magnitude

(a)

(b)
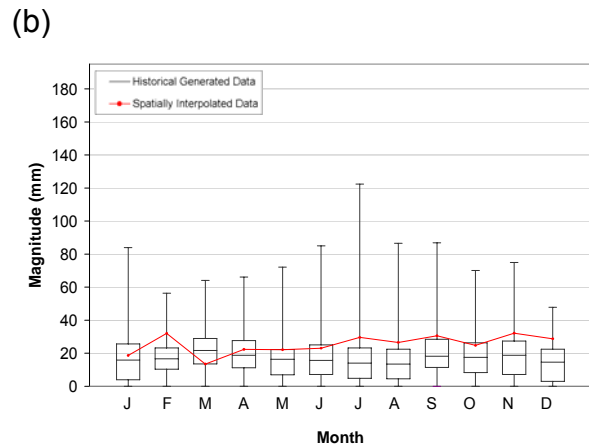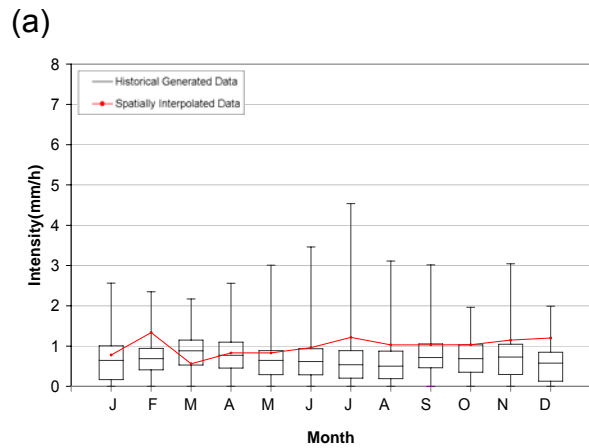
Figure B-3: Box and whisker plot of generated historic event data compared to spatially interpolated event data at Embro; (a) intensity and (b) magnitude

(a)

(b)
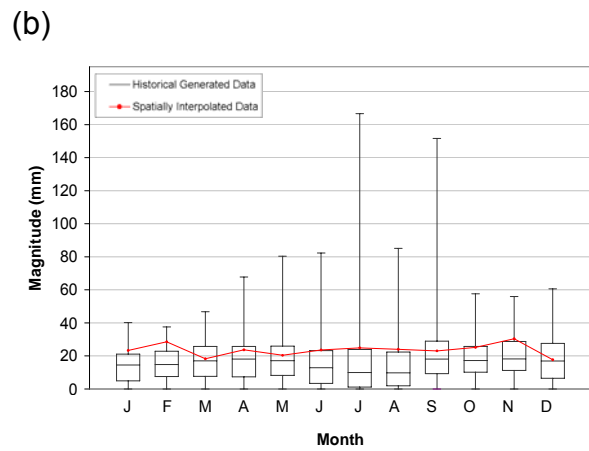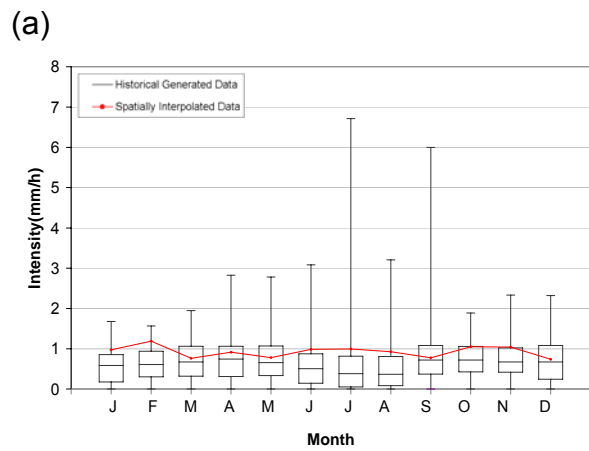
Figure B-4: Box and whisker plot of generated historic event data compared to spatially interpolated event data at Exeter; (a) intensity and (b) magnitude

(a)

(b)
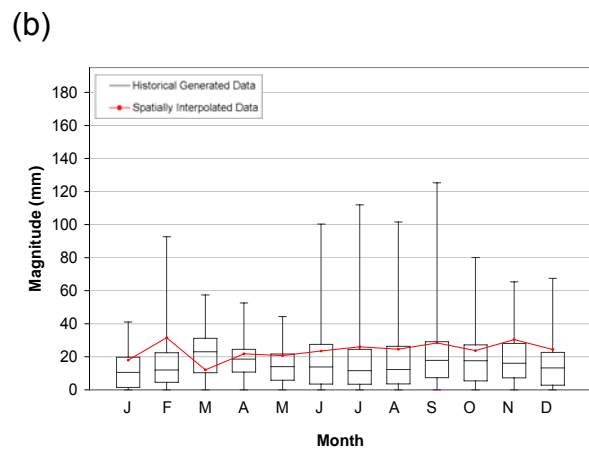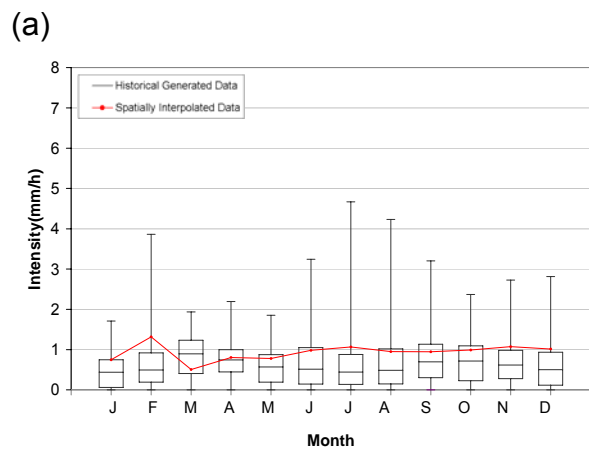
Figure B-5: Box and whisker plot of generated historic event data compared to spatially interpolated event data at Foldens; (a) intensity and (b) magnitude

119

(a)   (b)
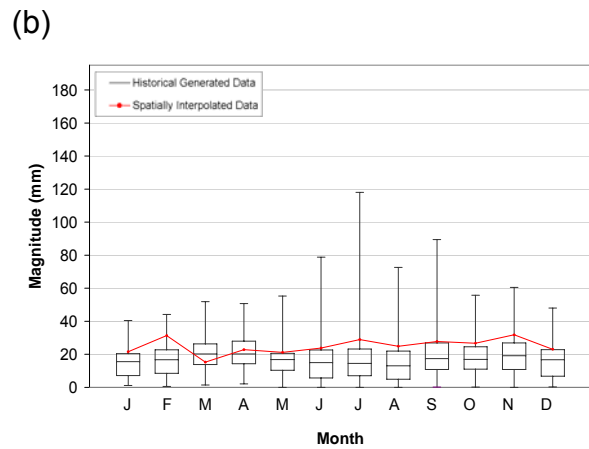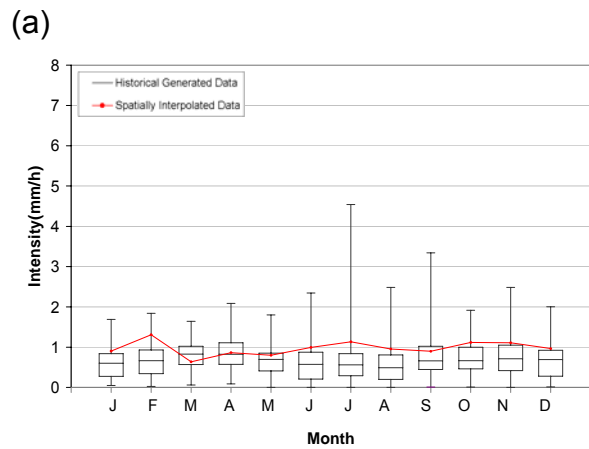
Figure B-6: Box and whisker plot of generated historic event data compared to spatially interpolated event data at Fullarton; (a) intensity and (b) magnitude

(a)   (b)
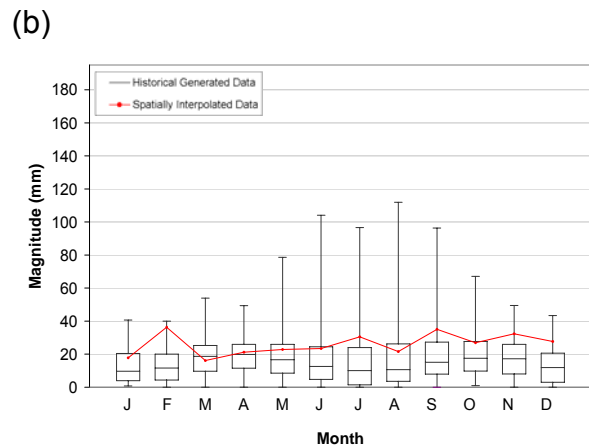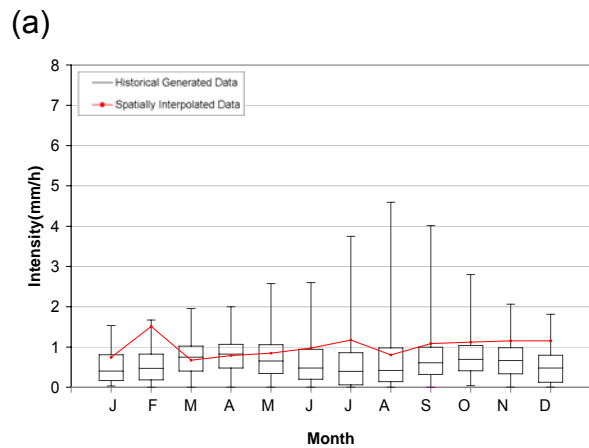
Figure B-7: Box and whisker plot of generated historic event data compared to spatially interpolated event data at Glen Allan; (a) intensity and (b) magnitude

(a)   (b)
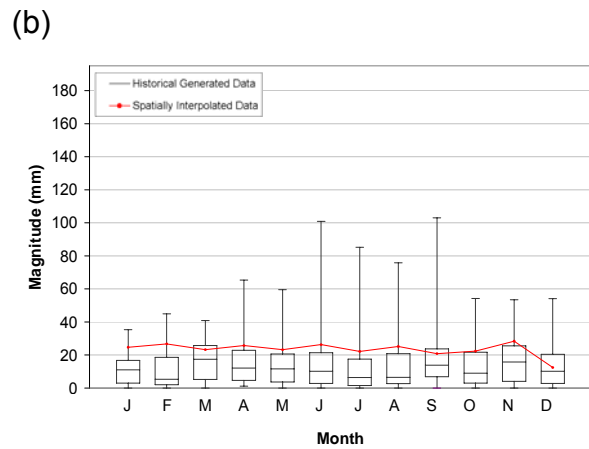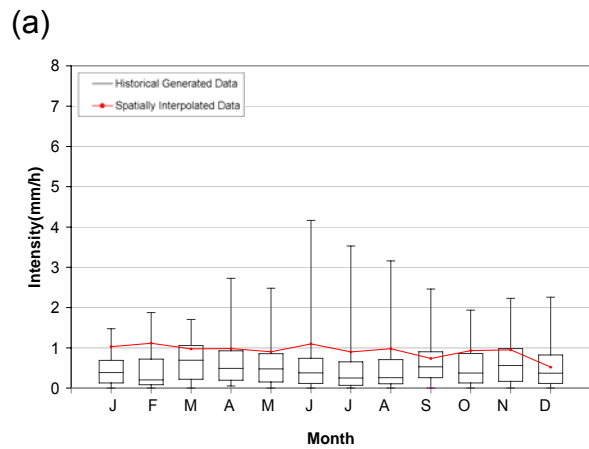
Figure B-8: Box and whisker plot of generated historic event data compared to spatially interpolated event data at Ilderton; (a) intensity and (b) magnitude

120
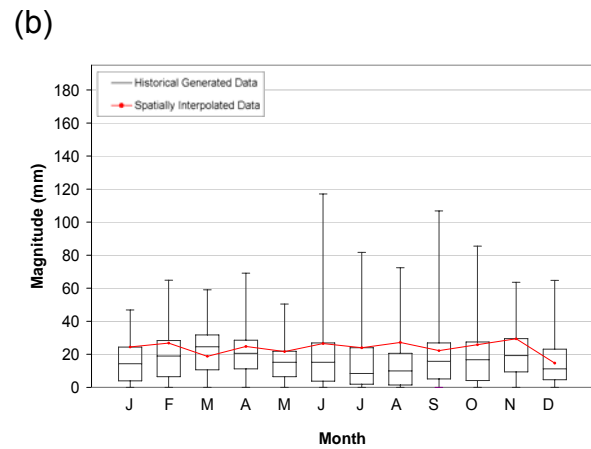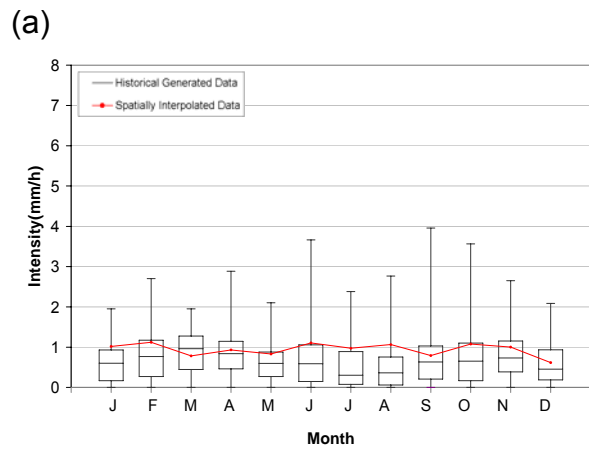
Figure B-9: Box and whisker plot of generated historic event data compared to spatially interpolated event data at London; (a) intensity and (b) magnitude
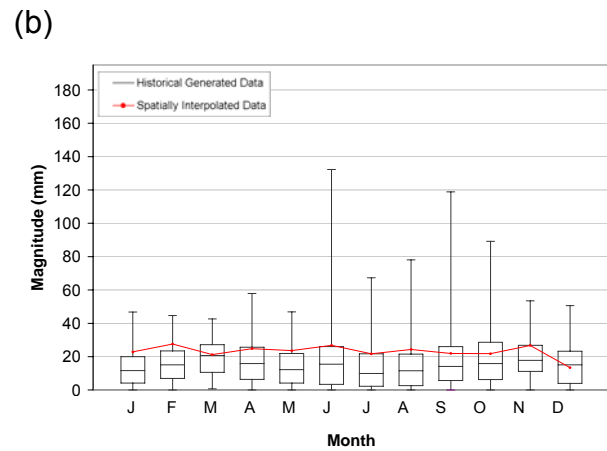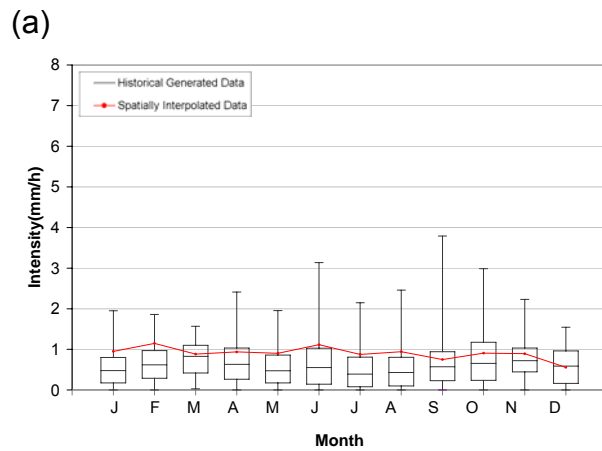
Figure B-10: Box and whisker plot of generated historic event data compared to spatially interpolated event data at St. Thomas; (a) intensity and (b) magnitude
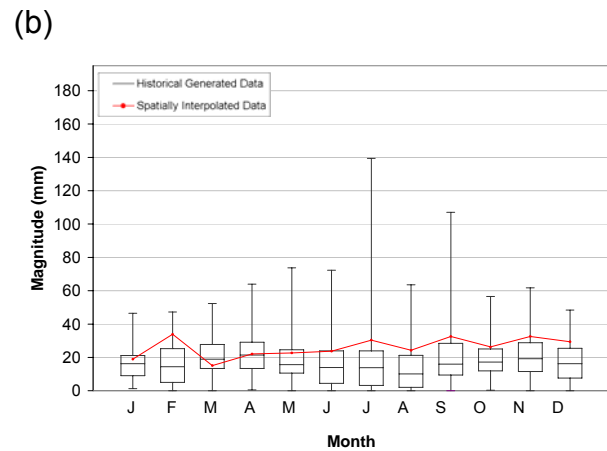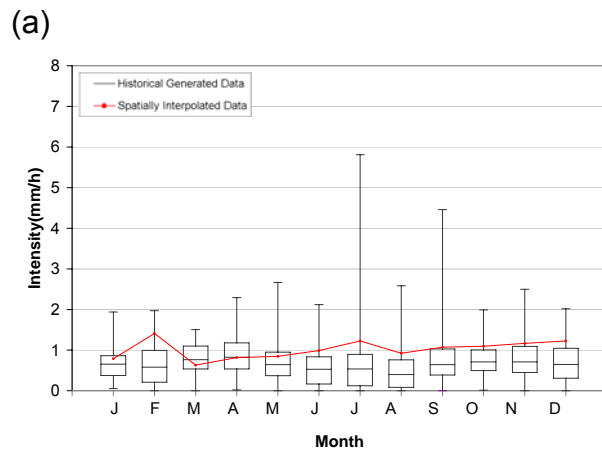
Figure B-11: Box and whisker plot of generated historic event data compared to spatially interpolated event data at Stratford; (a) intensity and (b) magnitude

(a)

(b)
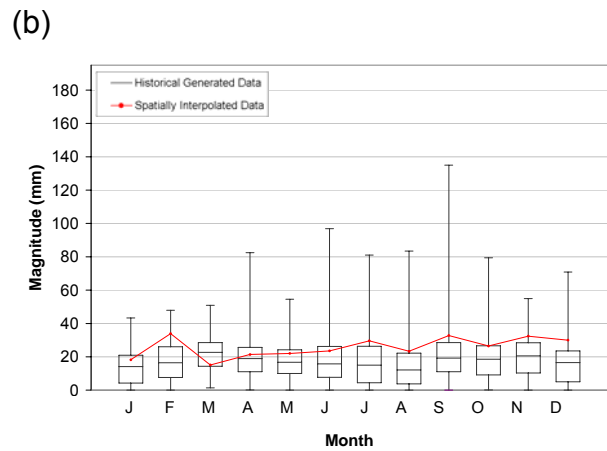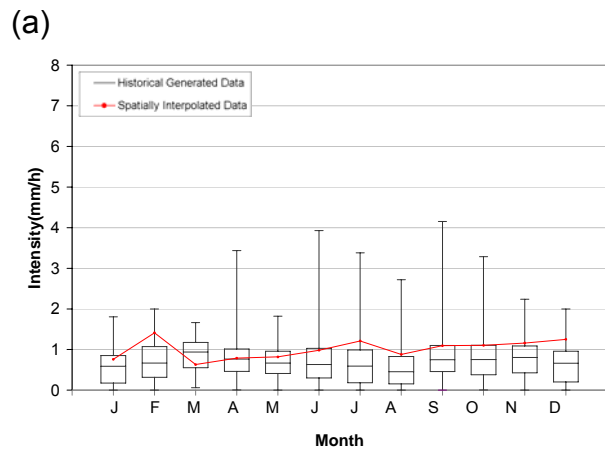
Figure B-12: Box and whisker plot of generated historic event data compared to spatially interpolated event data at Tavistock; (a) intensity and (b) magnitude

(a)

(b)
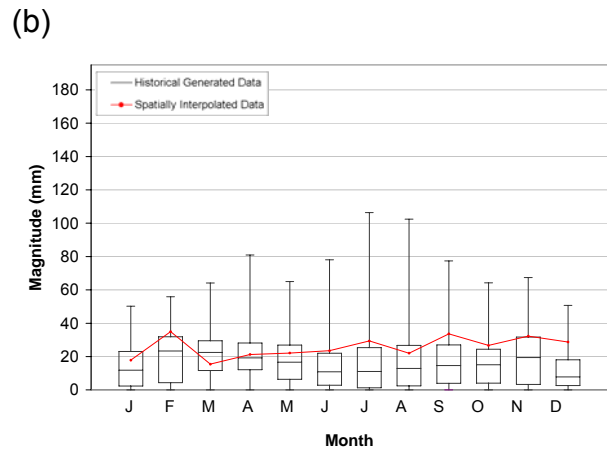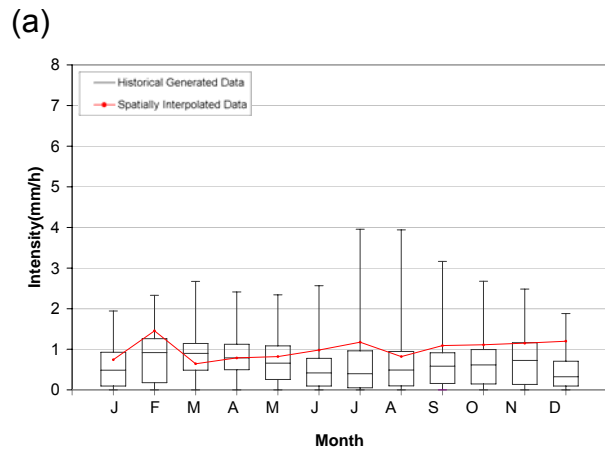
Figure B-13: Box and whisker plot of generated historic event data compared to spatially interpolated event data at Waterloo; (a) intensity and (b) magnitude

(a)

(b)
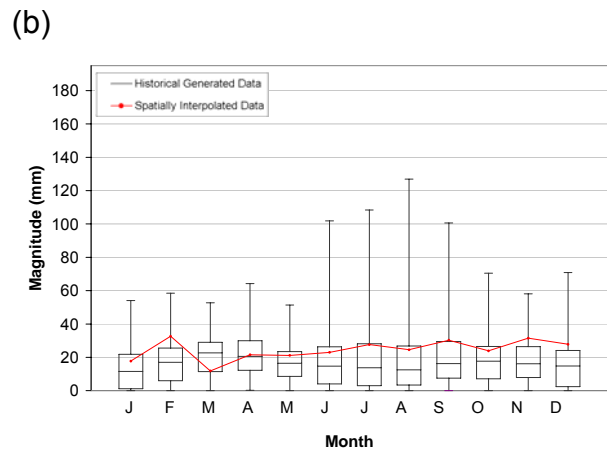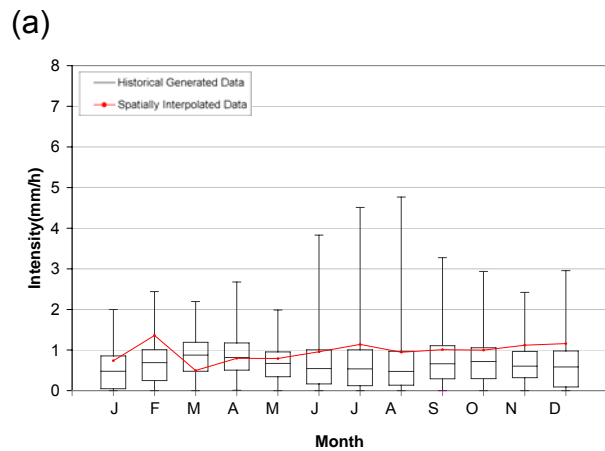
Figure B-14: Box and whisker plot of generated historic event data compared to spatially interpolated event data at Woodstock; (a) intensity and (b) magnitude

122

(a)
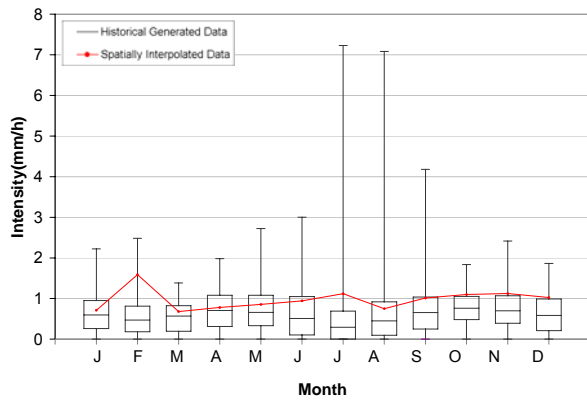
(b)
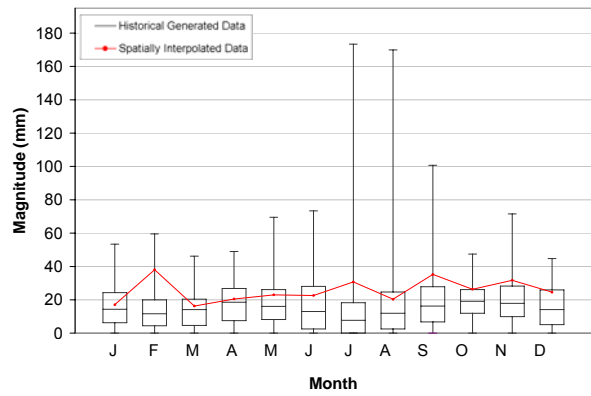
Figure B-15: Box and whisker plot of generated historic event data compared to spatially interpolated event data at Wroxeter; (a) intensity and (b) magnitude

B.2 CSIROM2kb B11 versus Historical Generated

(a)
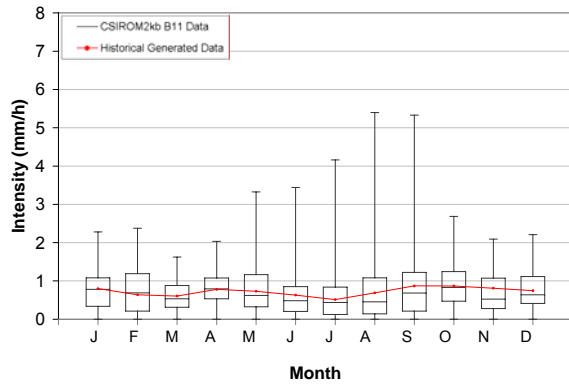
(b)
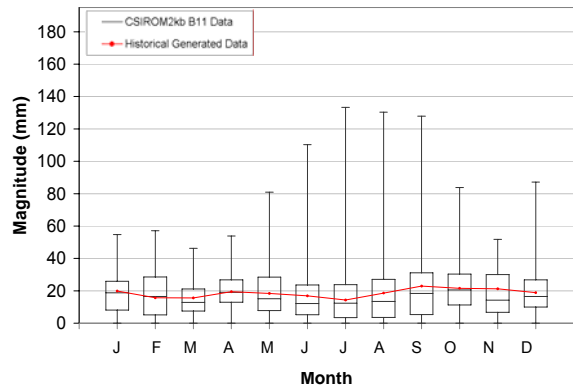
Figure B-16: Box and whisker plot of CSIROM2kb B11 event data compared to generated historical event data at Blyth; (a) intensity and (b) magnitude

(a)
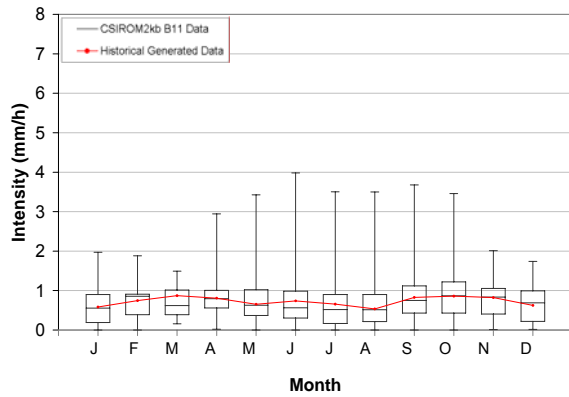
(b)
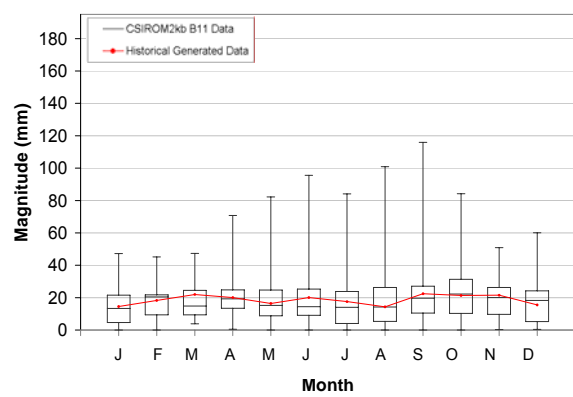
Figure B-17: Box and whisker plot of CSIROM2kb B11 event data compared to generated historical event data at Dorchester; (a) intensity and (b) magnitude

(a)
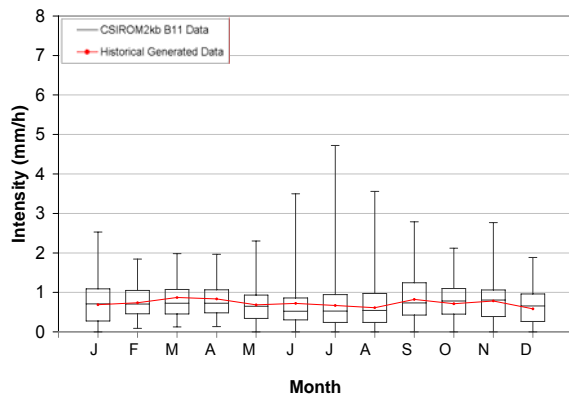
(b)
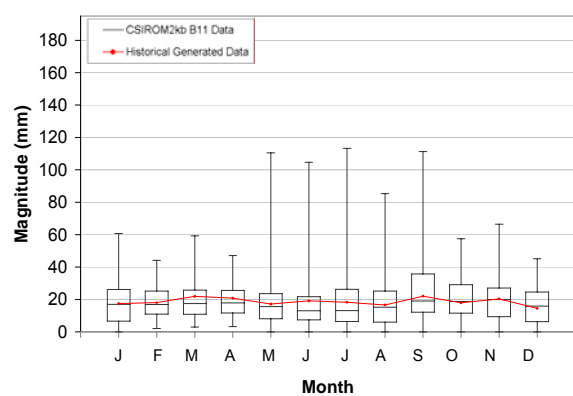
Figure B-18: Box and whisker plot of CSIROM2kb B11 event data compared to generated historical event data at Embro; (a) intensity and (b) magnitude
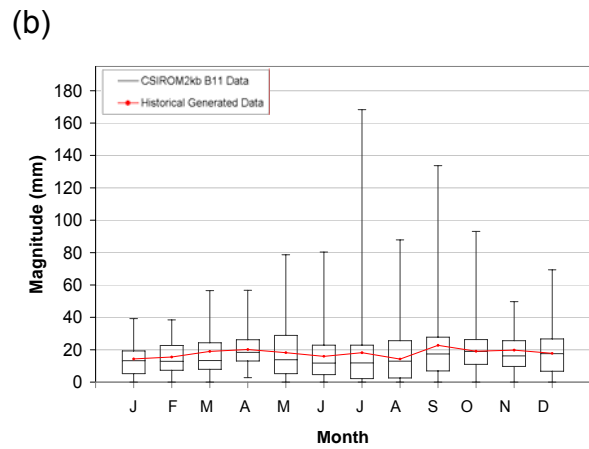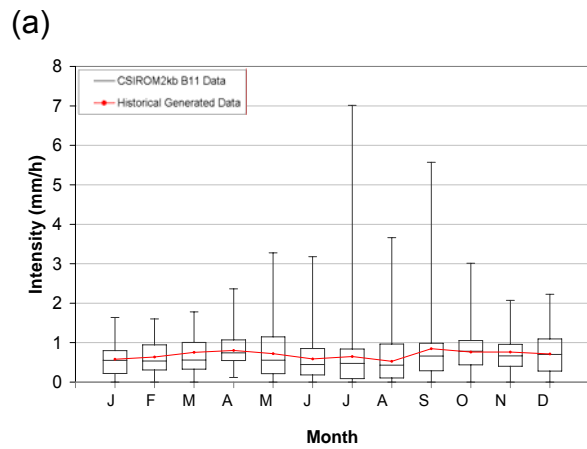
Figure B-19: Box and whisker plot of g CSIROM2kb B11 event data compared to generated historical event data at Exeter; (a) intensity and (b) magnitude
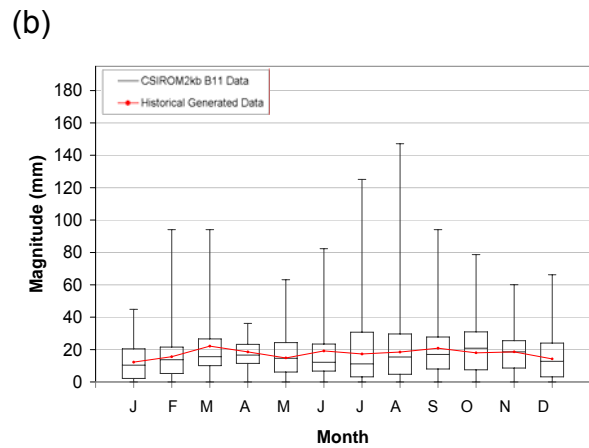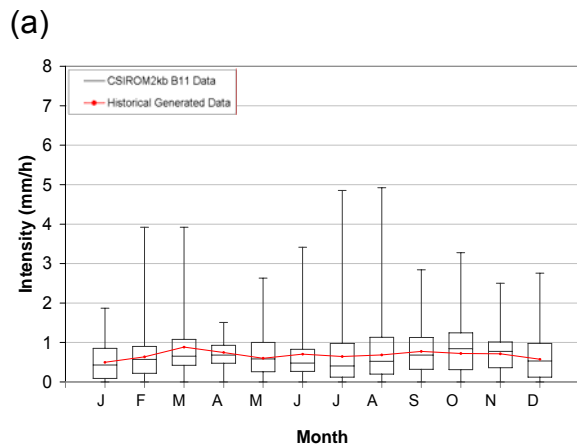
Figure B-20: Box and whisker plot of CSIROM2kb B11 event data compared to generated historical event data at Foldens; (a) intensity and (b) magnitude
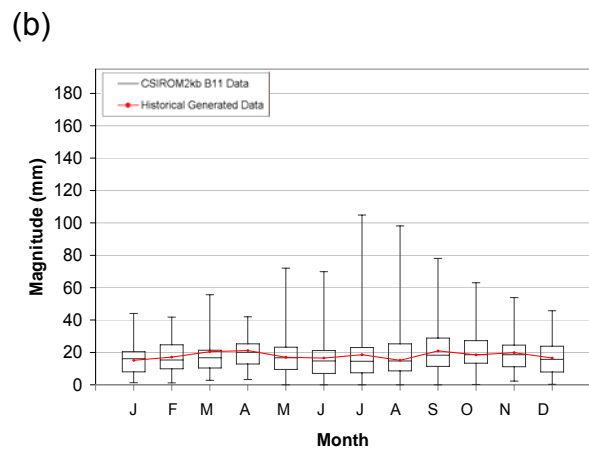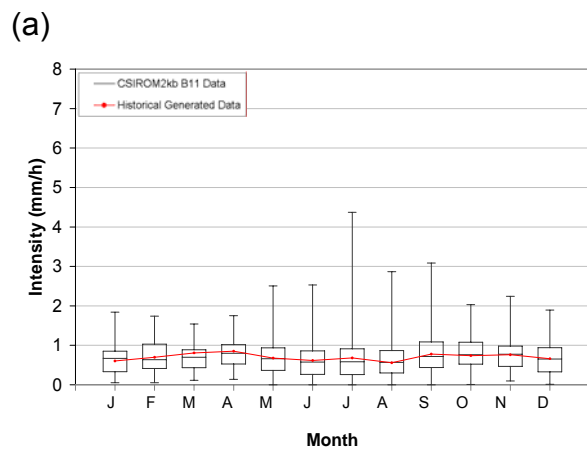
Figure B-21: Box and whisker plot of CSIROM2kb B11 event data compared to generated historical event data at Fullarton; (a) intensity and (b) magnitude
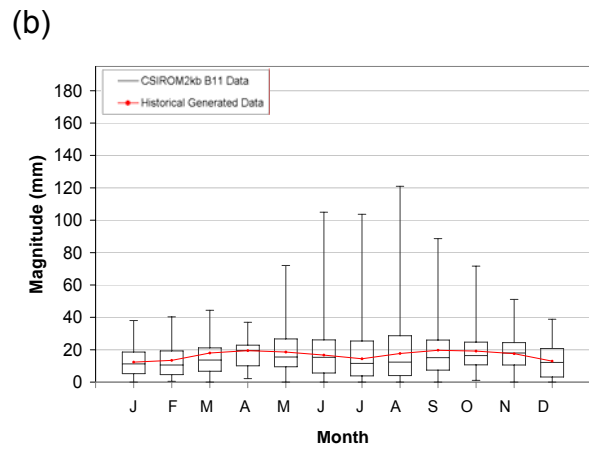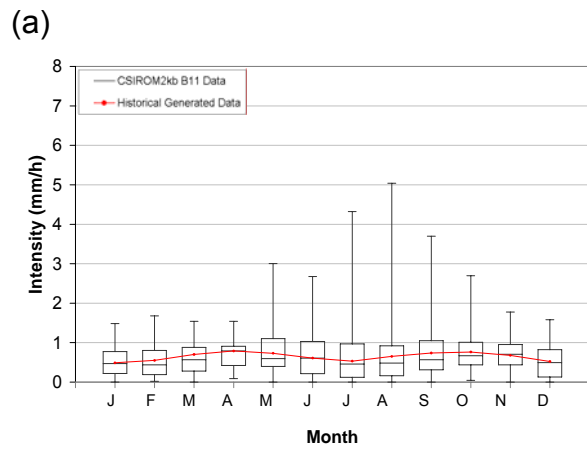
Figure B-22: Box and whisker plot of CSIROM2kb B11 event data compared to generated historical event data at Glen Allan; (a) intensity and (b) magnitude
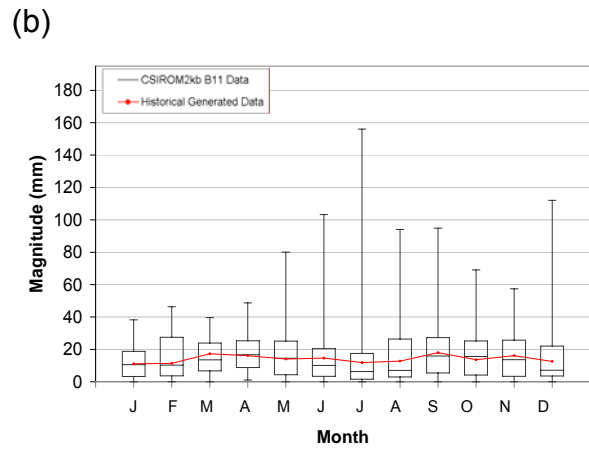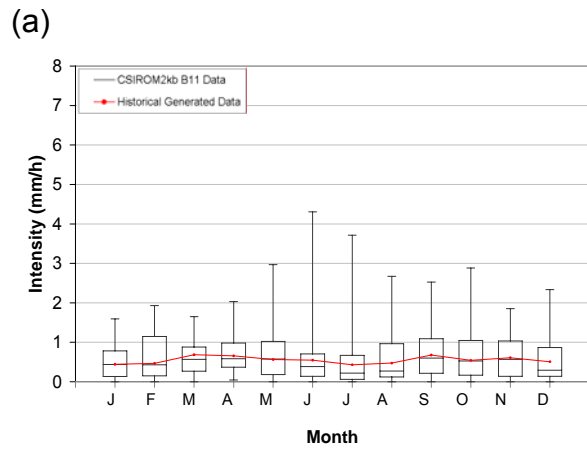
Figure B-23: Box and whisker plot of CSIROM2kb B11 event data compared to generated historical event data at Ilderton; (a) intensity and (b) magnitude
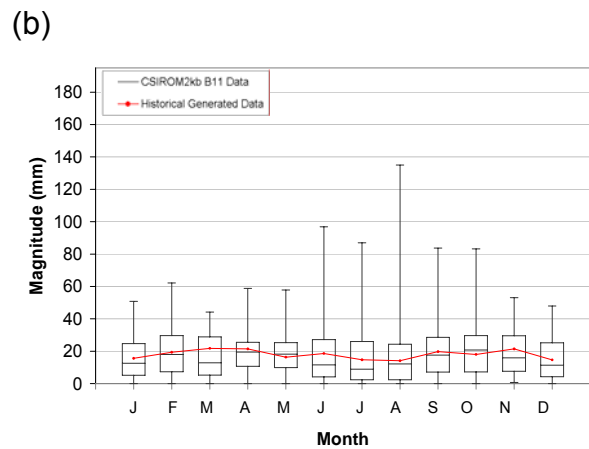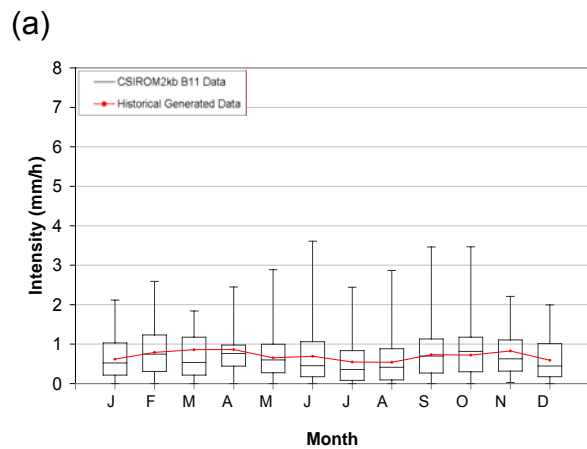
Figure B-24: Box and whisker plot of CSIROM2kb B11 event data compared to generated historical event data at London; (a) intensity and (b) magnitude

126
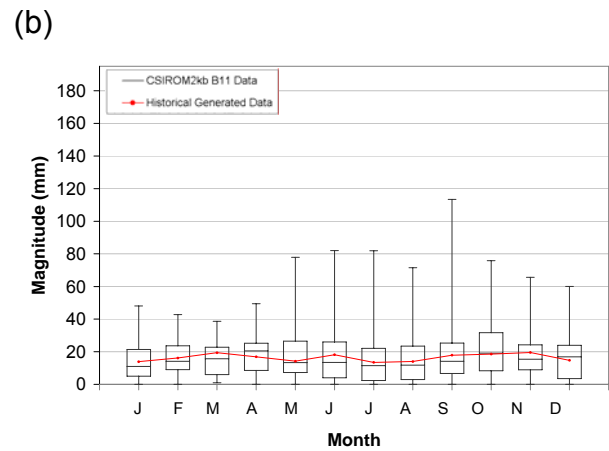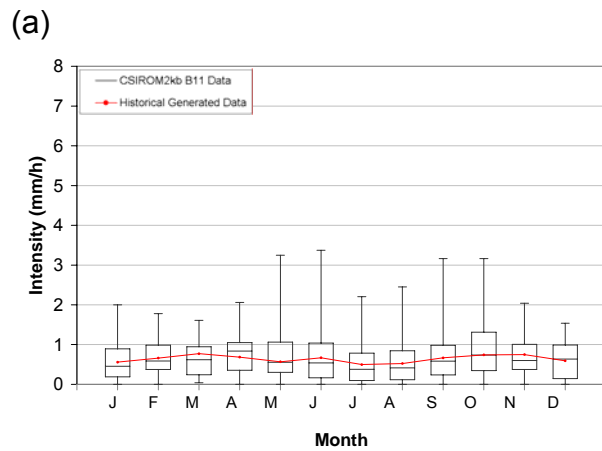
Figure B-25: Box and whisker plot of CSIROM2kb B11 event data compared to generated historical event data at St. Thomas; (a) intensity and (b) magnitude
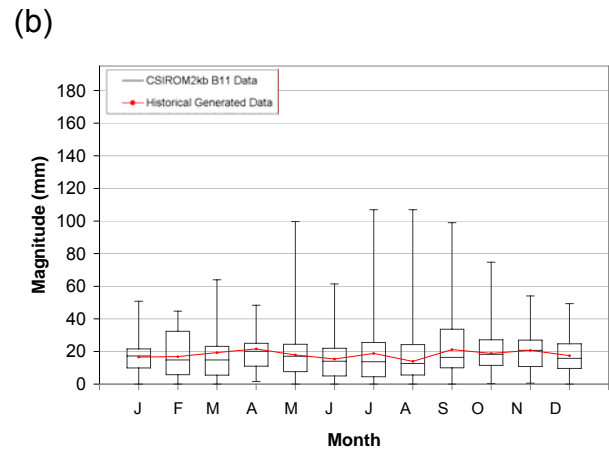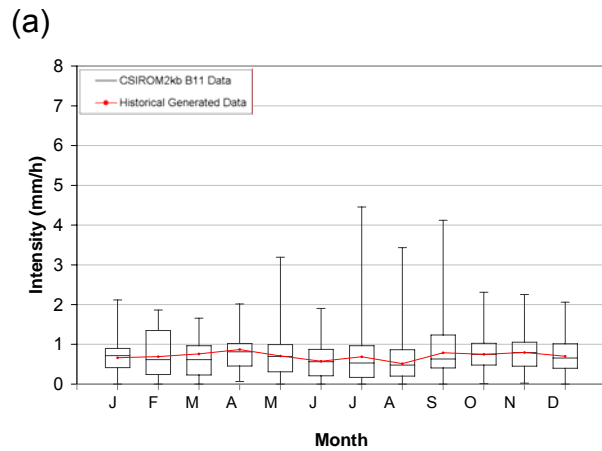
Figure B-26: Box and whisker plot of CSIROM2kb B11 event data compared to generated historical event data at Stratford; (a) intensity and (b) magnitude
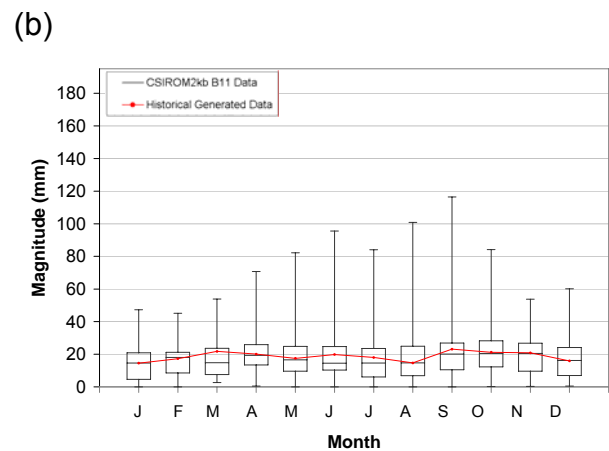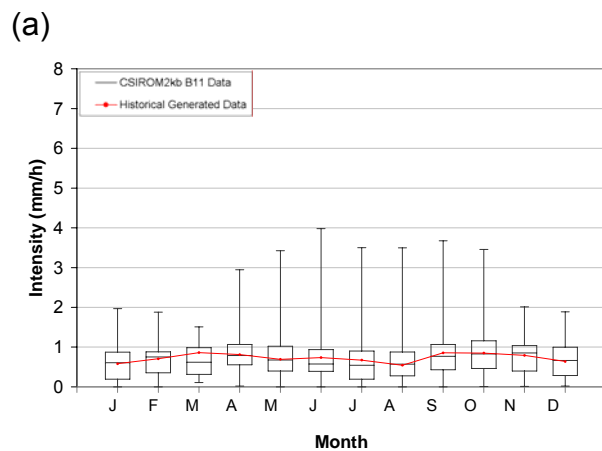
Figure B-27: Box and whisker plot of CSIROM2kb B11 event data compared to generated historical event data at Tavistock; (a) intensity and (b) magnitude

(a)   (b)
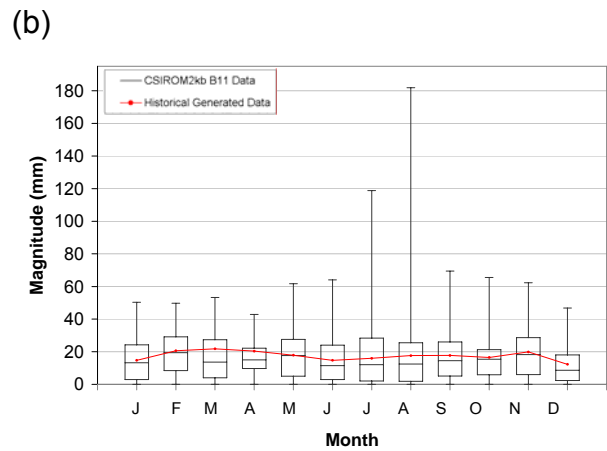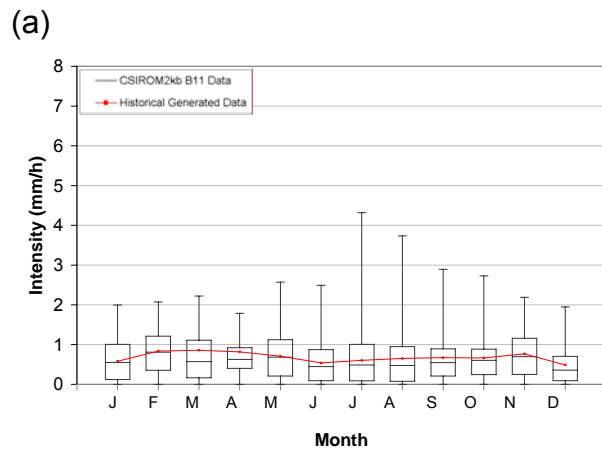
Figure B-28: Box and whisker plot of CSIROM2kb B11 event data compared to generated historical event data at Waterloo; (a) intensity and (b) magnitude

(a)   (b)
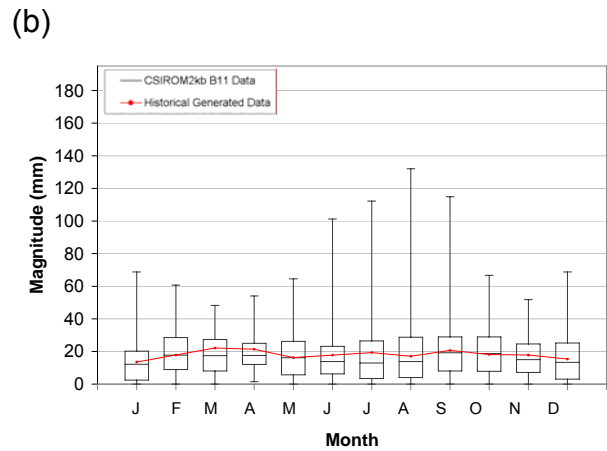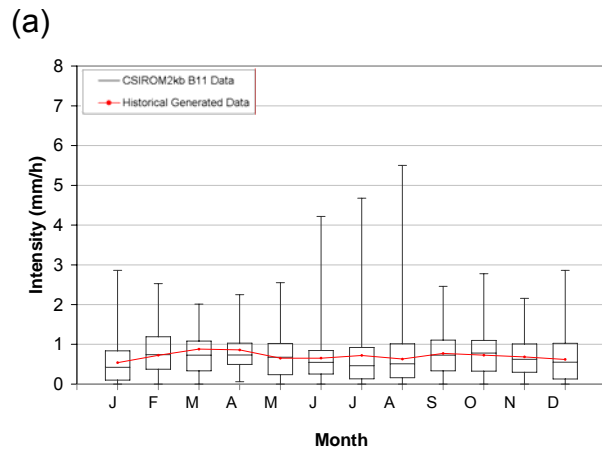
Figure B-29: Box and whisker plot of CSIROM2kb B11 event data compared to generated historical event data at Woodstock; (a) intensity and (b) magnitude

(a)   (b)
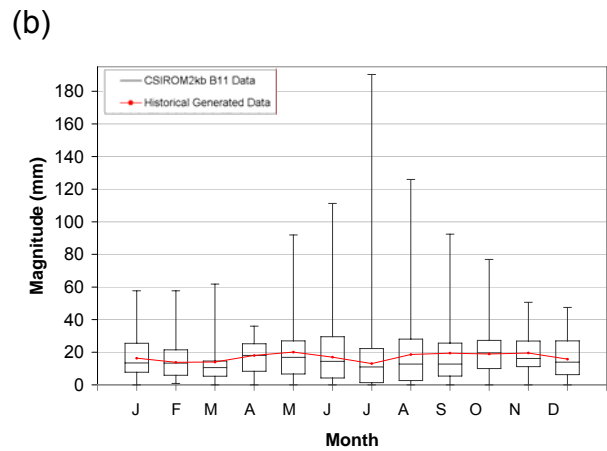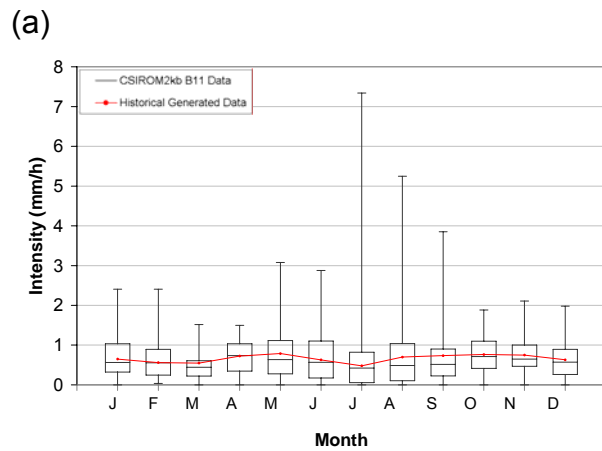
Figure B-30: Box and whisker plot of CSIROM2kb B11 event data compared to generated historical event data at Wroxeter; (a) intensity and (b) magnitude

128

B.3   CCSRNIES B21 versus Historical Generated

(a)
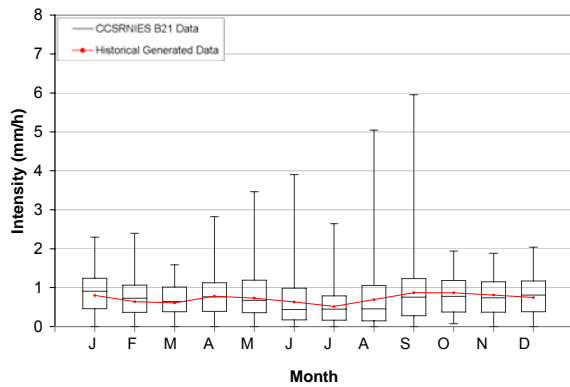
(b)
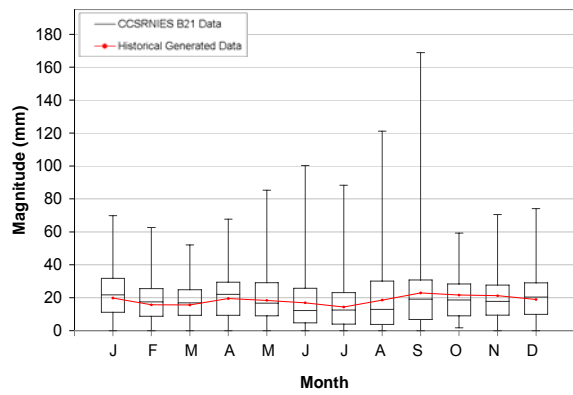
Figure B-31: Box and whisker plot of CCSRNIES B21 event data compared to generated historical event data at Blyth; (a) intensity and (b) magnitude

(a)
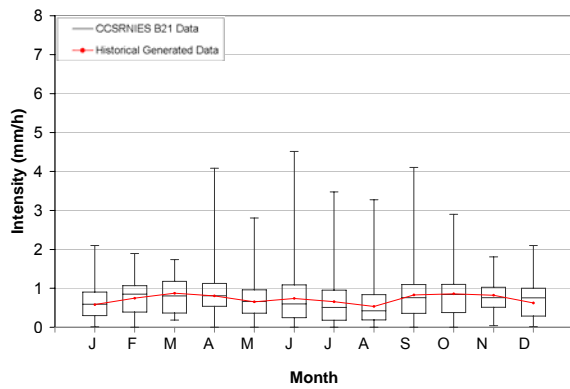
(b)
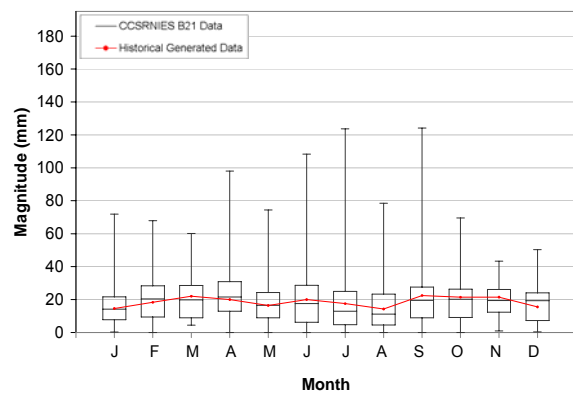
Figure B-32: Box and whisker plot of CCSRNIES B21 event data compared to generated historical event data at Dorchester; (a) intensity and (b) magnitude

(a)
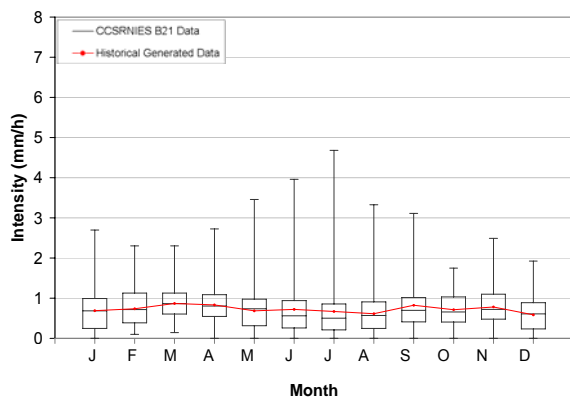
(b)
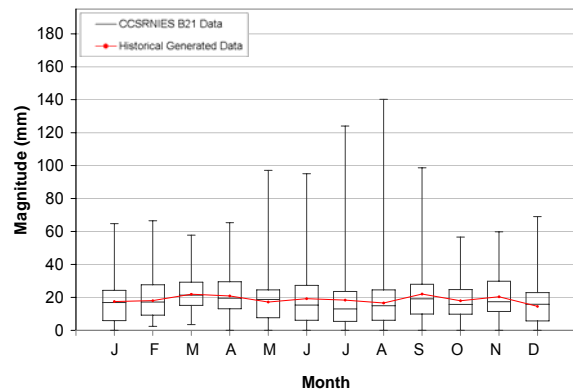
Figure B-33: Box and whisker plot of CCSRNIES B21 event data compared to generated historical event data at Embro; (a) intensity and (b) magnitude

(a)

(b)
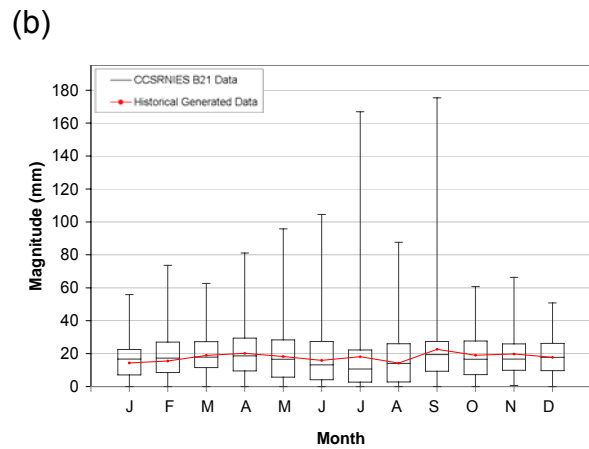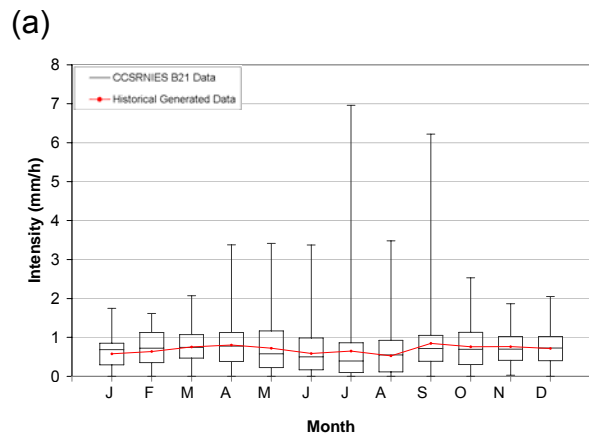
Figure B-34: Box and whisker plot of g CCSRNIES B21 event data compared to generated historical event data at Exeter; (a) intensity and (b) magnitude

(a)

(b)
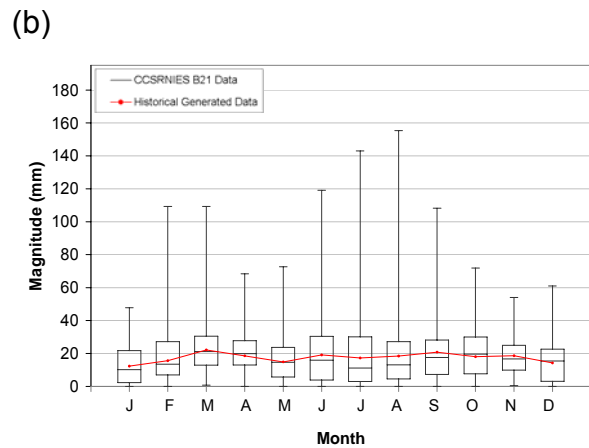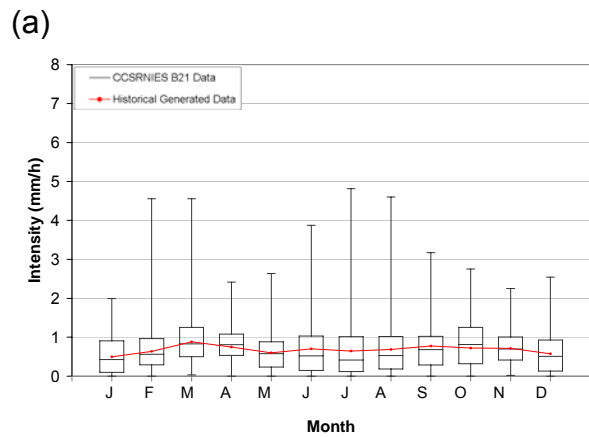
Figure B-35: Box and whisker plot of CCSRNIES B21 event data compared to generated historical event data at Foldens; (a) intensity and (b) magnitude

(a)

(b)
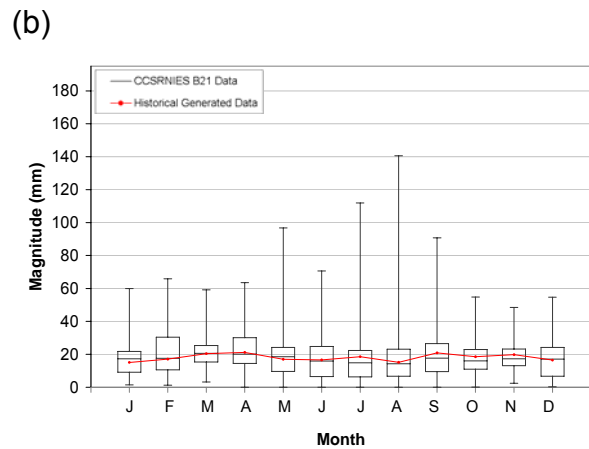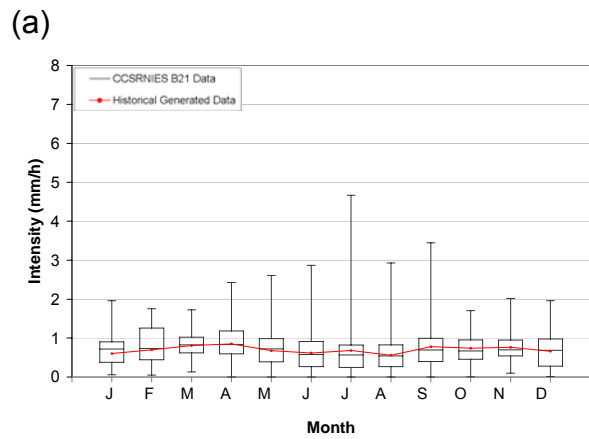
Figure B-36: Box and whisker plot of CCSRNIES B21 event data compared to generated historical event data at Fullarton; (a) intensity and (b) magnitude
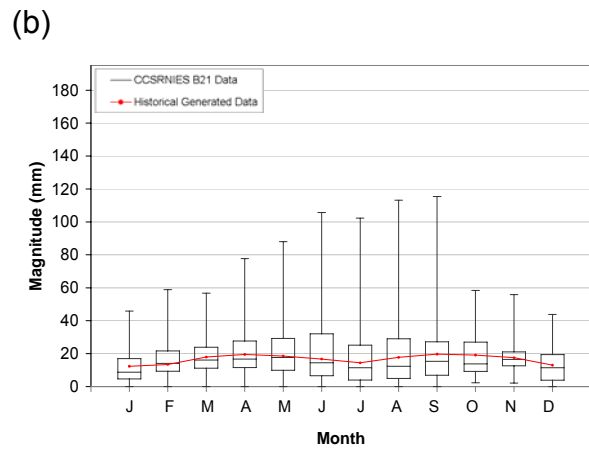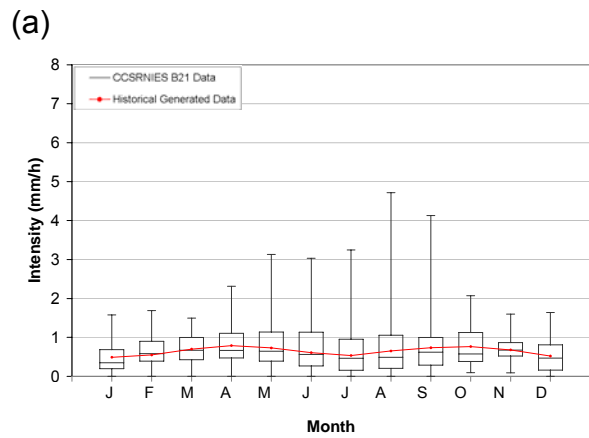
Figure B-37: Box and whisker plot of CCSRNIES B21 event data compared to generated historical event data at Glen Allan; (a) intensity and (b) magnitude
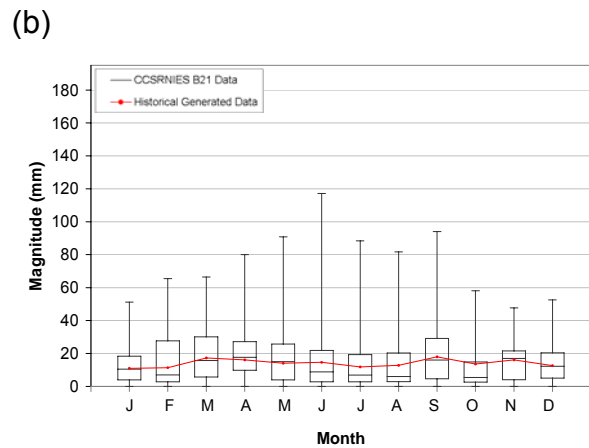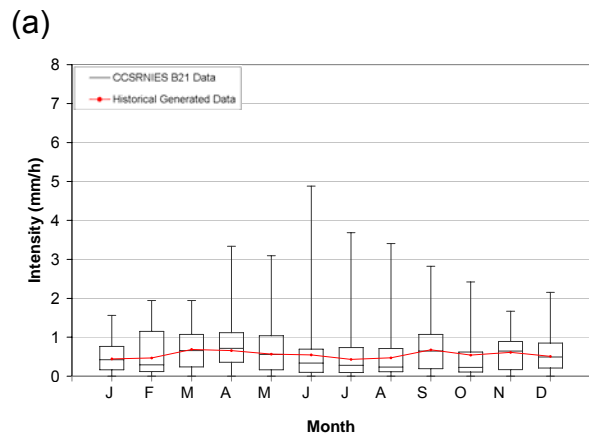
Figure B-38: Box and whisker plot of CCSRNIES B21 event data compared to generated historical event data at Ilderton; (a) intensity and (b) magnitude
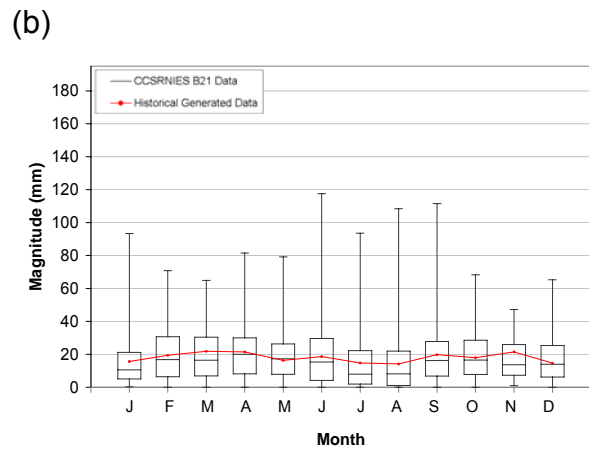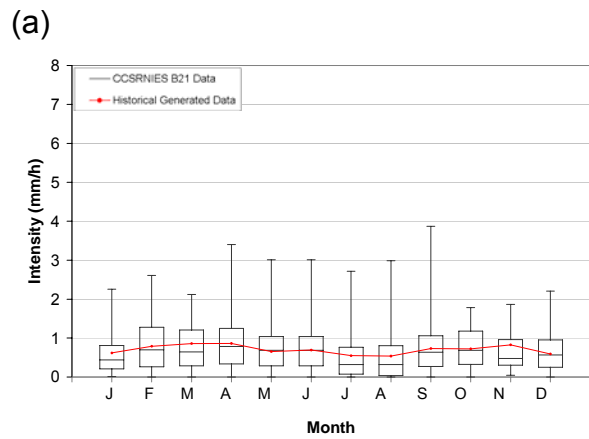
Figure B-39: Box and whisker plot of CCSRNIES B21 event data compared to generated historical event data at London; (a) intensity and (b) magnitude

131
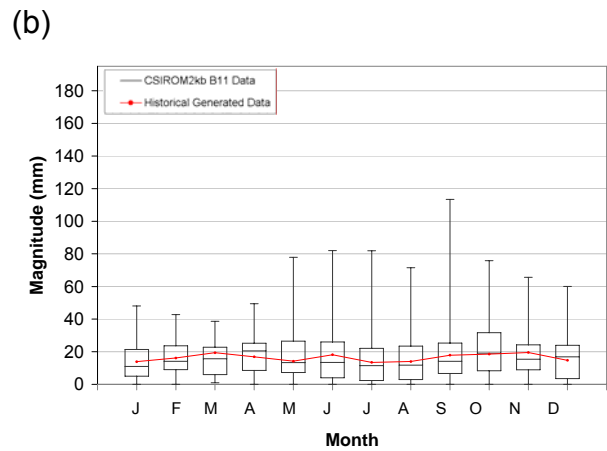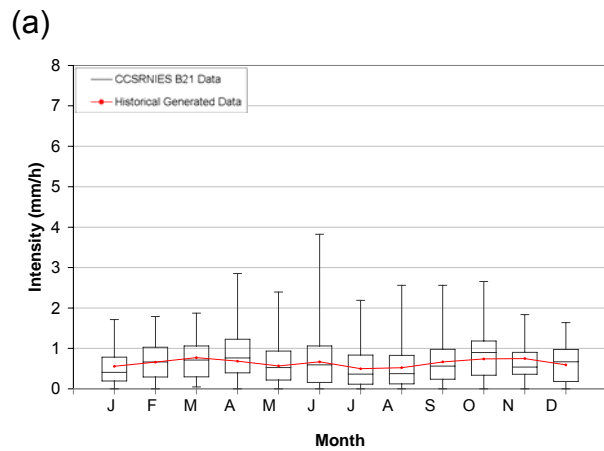
Figure B-40: Box and whisker plot of CCSRNIES B21 event data compared to generated historical event data at St. Thomas; (a) intensity and (b) magnitude
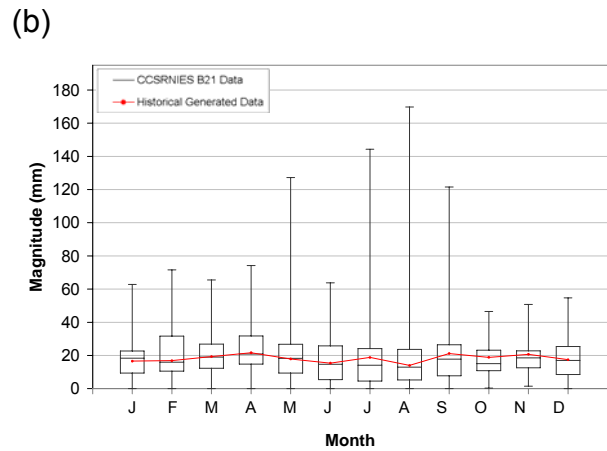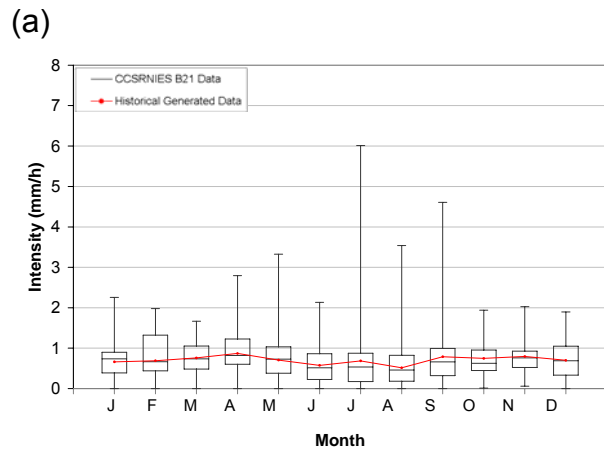
Figure B-41: Box and whisker plot of CCSRNIES B21 event data compared to generated historical event data at Stratford; (a) intensity and (b) magnitude
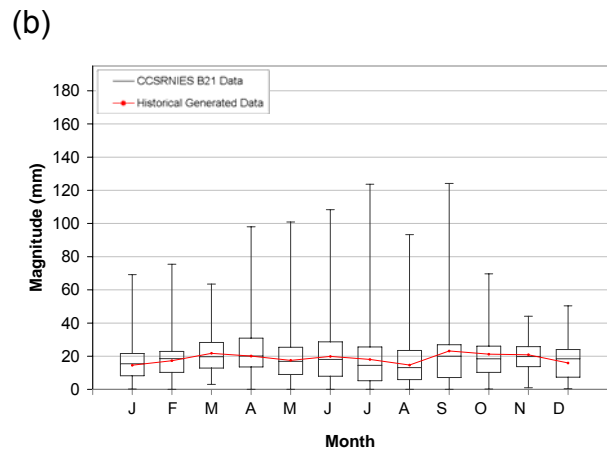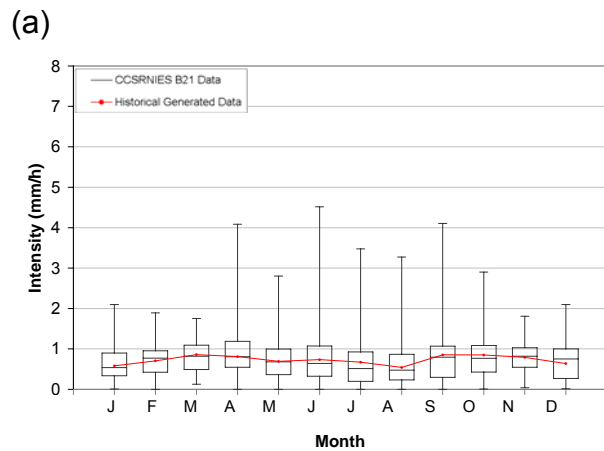
Figure B-42: Box and whisker plot of CCSRNIES B21 event data compared to generated historical event data at Tavistock; (a) intensity and (b) magnitude

(a)

(b)
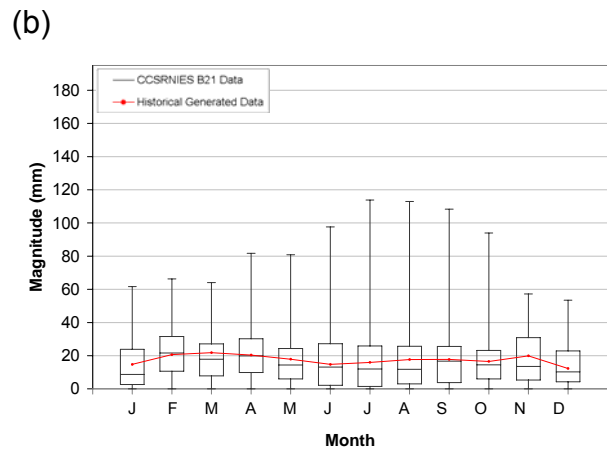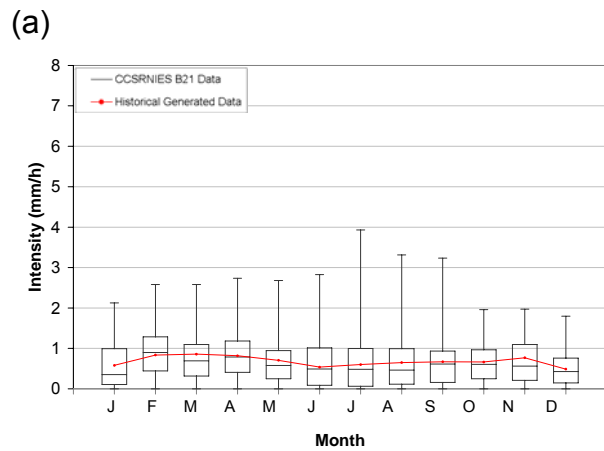
Figure B-43: Box and whisker plot of CCSRNIES B21 event data compared to generated historical event data at Waterloo; (a) intensity and (b) magnitude

(a)

(b)
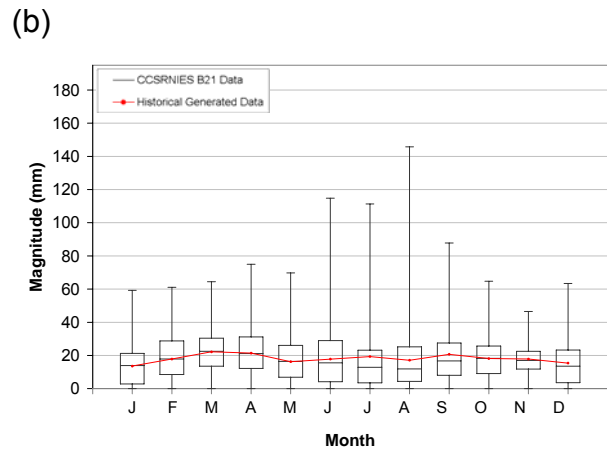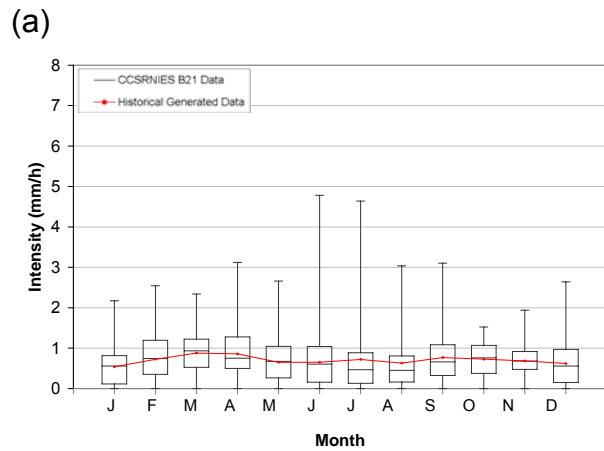
Figure B-44: Box and whisker plot of CCSRNIES B21 event data compared to generated historical event data at Woodstock; (a) intensity and (b) magnitude

(a)

(b)
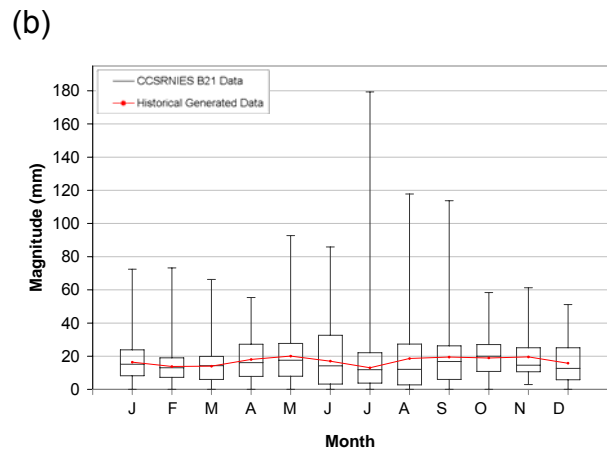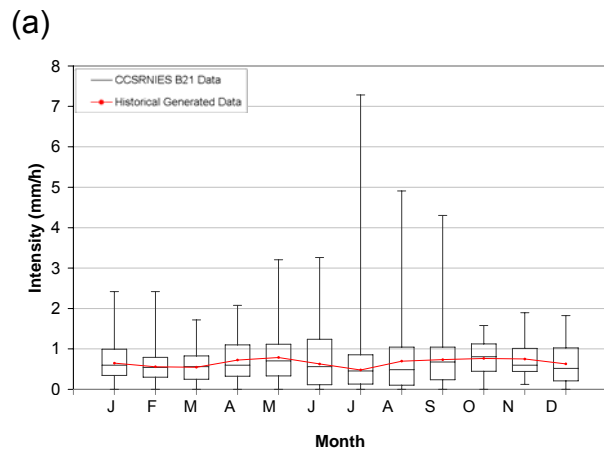
Figure B-45: Box and whisker plot of CCSRNIES B21 event data compared to generated historical event data at Wroxeter; (a) intensity and (b) magnitude

B.4 CSIROM2kb B11 versus CCSRNIES B21

(a)
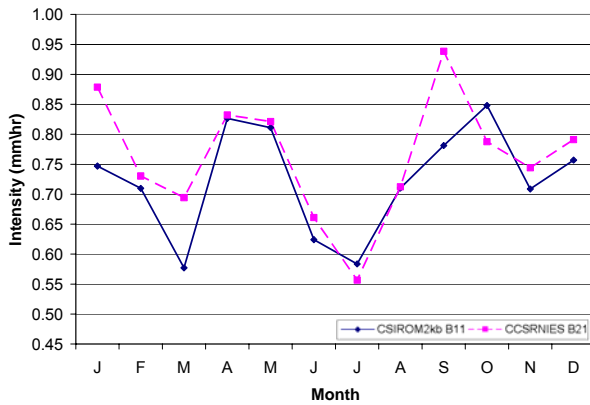
(b)
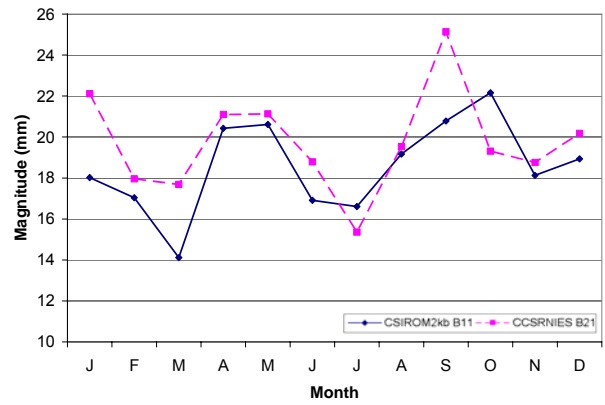
Figure B-46: Mean of CSIROM2kb B11 event data compared to mean of CCSRNIES B21 event data at Blyth; (a) intensity and (b) magnitude

(a)
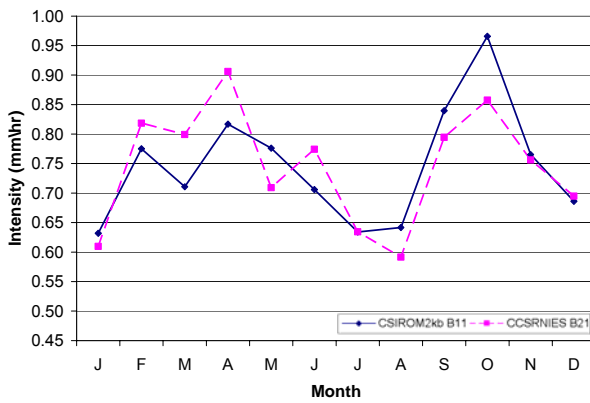
(b)
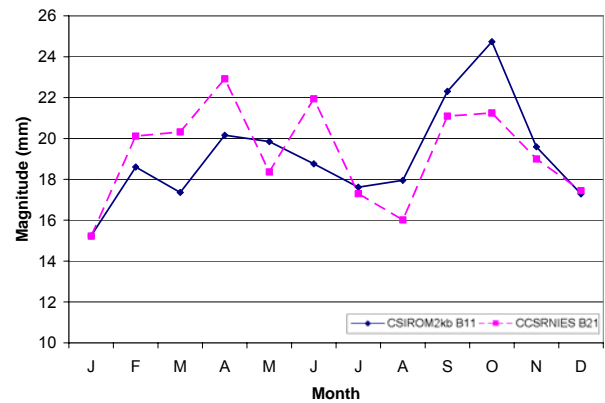
Figure B-47: Mean of CSIROM2kb B11 event data compared to mean of CCSRNIES B21 event data at Dorchester; (a) intensity and (b) magnitude

(a)
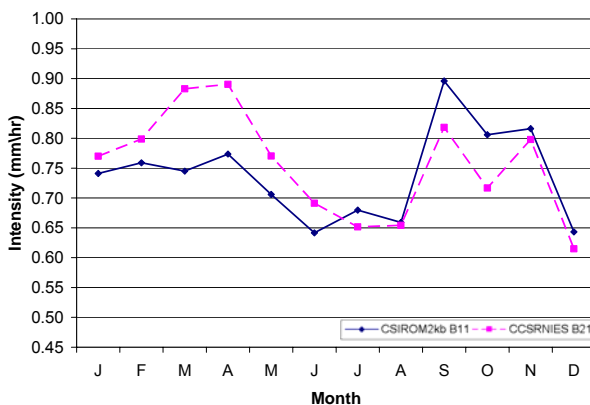
(b)
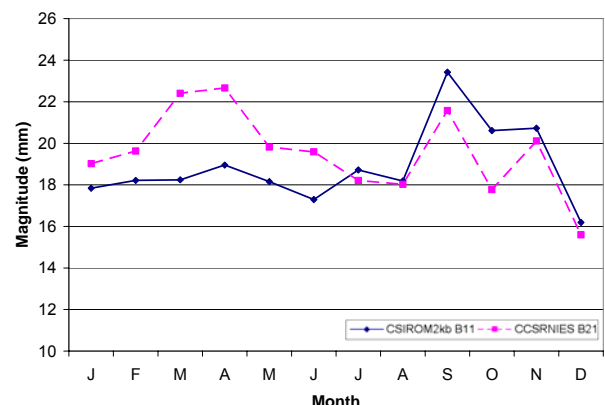
Figure B-48: Mean of CSIROM2kb B11 event data compared to mean of CCSRNIES B21 event data at Embro; (a) intensity and (b) magnitude

134

(a)

(b)
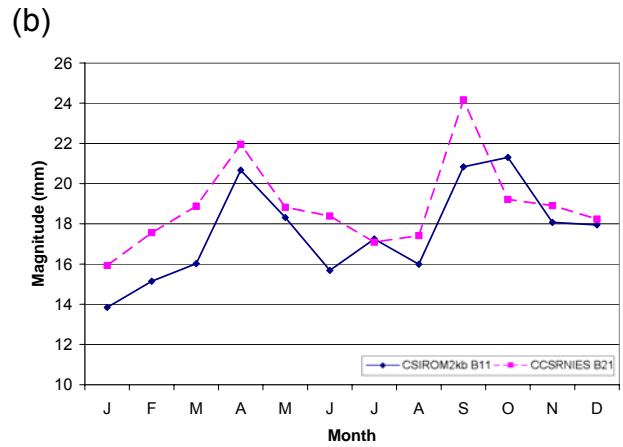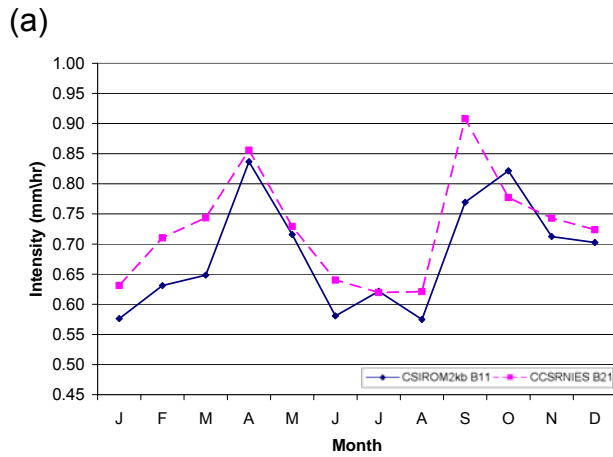
Figure B-49: Mean of CSIROM2kb B11 event data compared to mean of CCSRNIES B21 event data at Exeter; (a) intensity and (b) magnitude

(a)

(b)
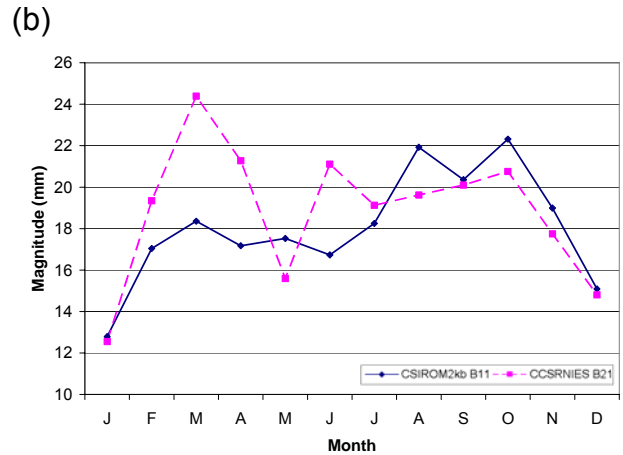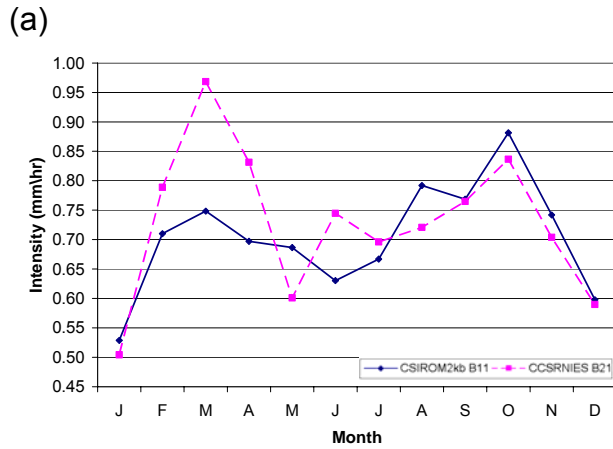
Figure B-50: Mean of CSIROM2kb B11 event data compared to mean of CCSRNIES B21 event data at Foldens; (a) intensity and (b) magnitude

(a)

(b)
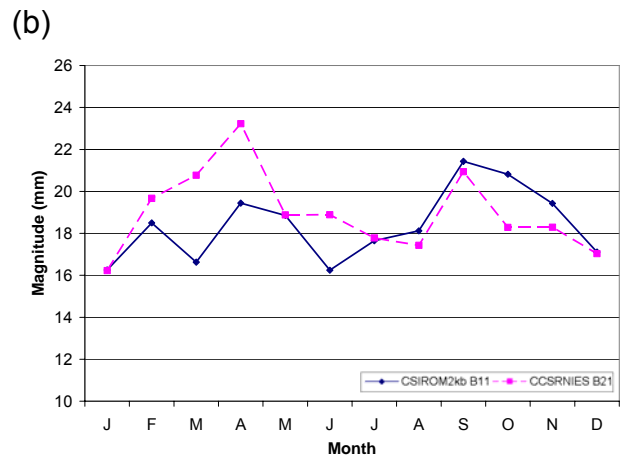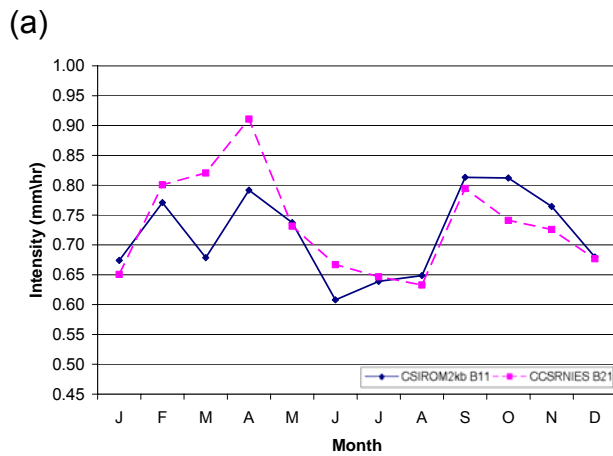
Figure B-51: Mean of CSIROM2kb B11 event data compared to mean of CCSRNIES B21 event data at Fullarton; (a) intensity and (b) magnitude

(a)

(b)
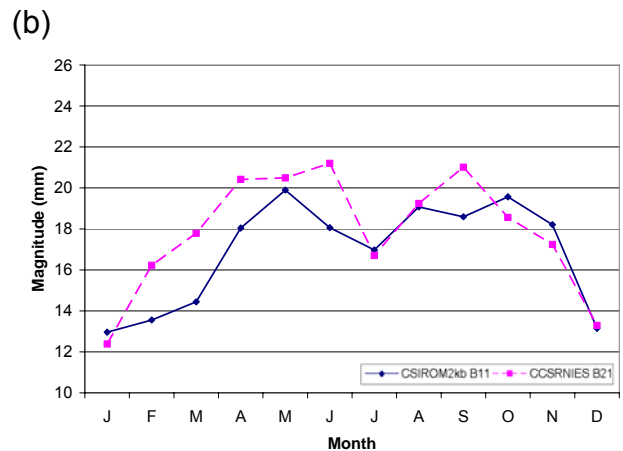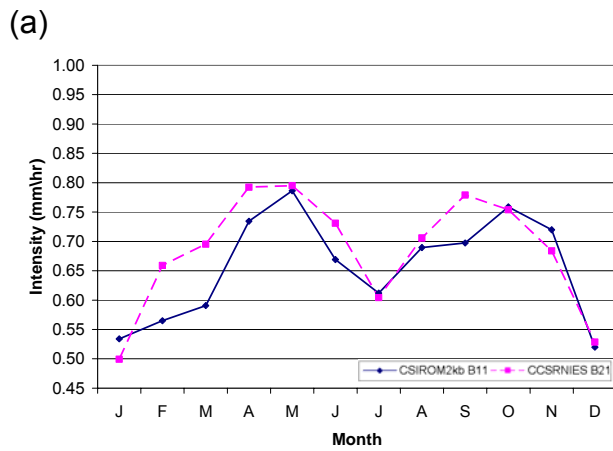
Figure B-52: Box and whisker plot of CCSRNIES B21 event data compared to generated historical event data at Glen Allan; (a) intensity and (b) magnitude

(a)

(b)
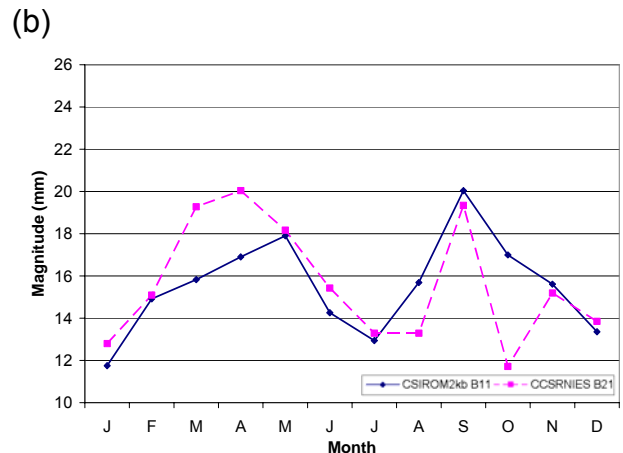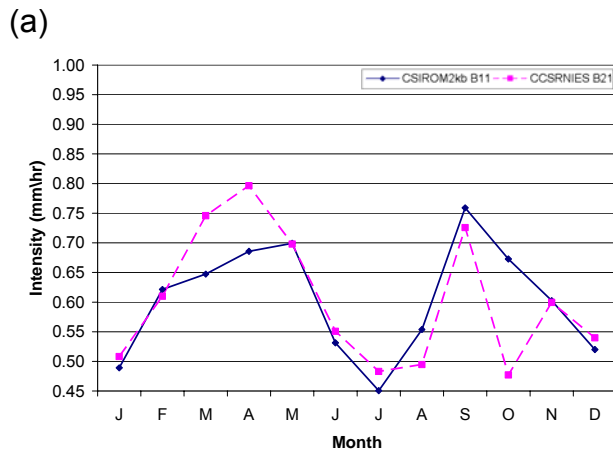
Figure B-53: Mean of CSIROM2kb B11 event data compared to mean of CCSRNIES B21 event data at Ilderton; (a) intensity and (b) magnitude

(a)

(b)
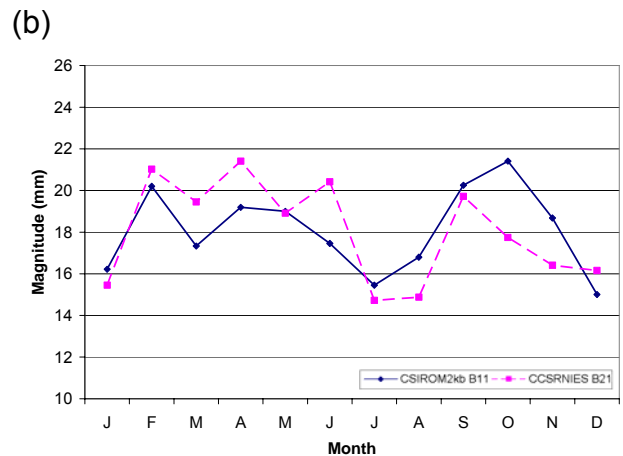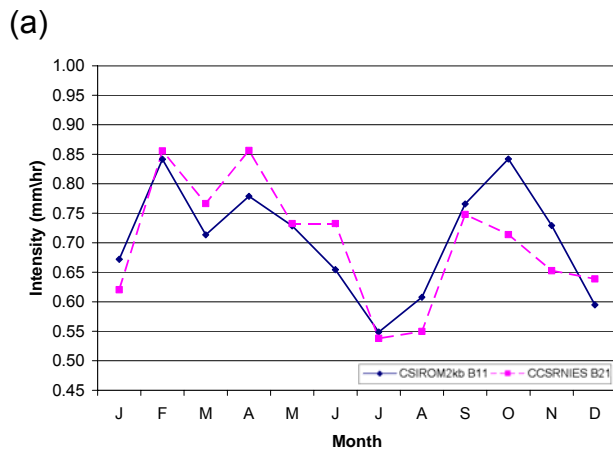
Figure B-54: Mean of CSIROM2kb B11 event data compared to mean of CCSRNIES B21 event data at London; (a) intensity and (b) magnitude

136

(a)

(b)
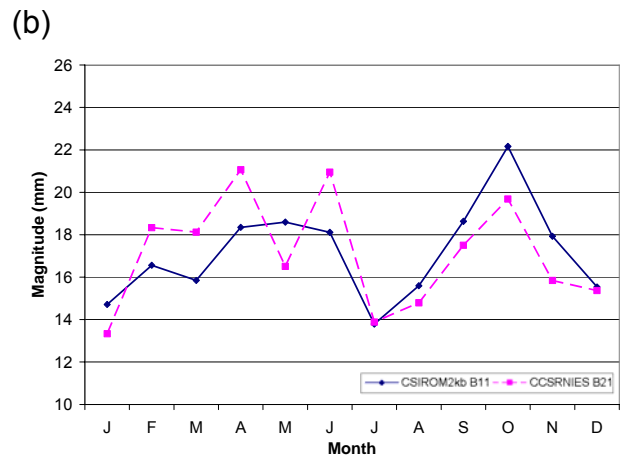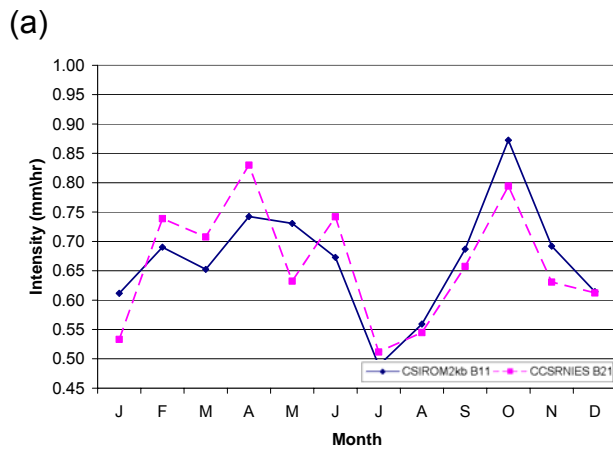
Figure B-55: Mean of CSIROM2kb B11 event data compared to mean of CCSRNIES B21 event data at St. Thomas; (a) intensity and (b) magnitude

(a)

(b)
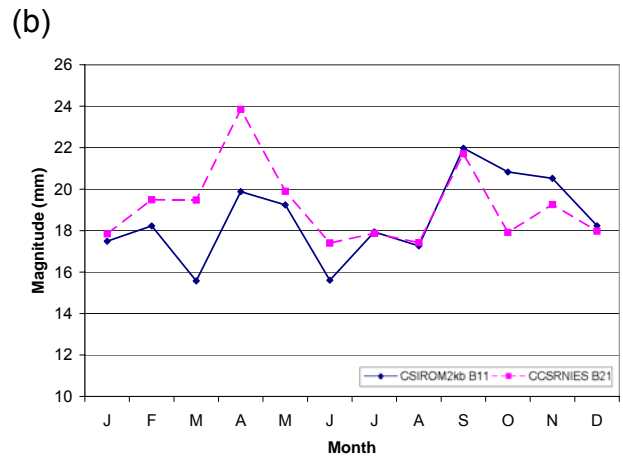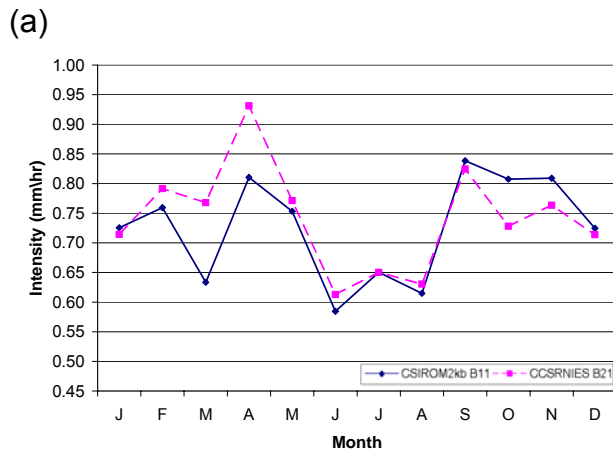
Figure B-56: Mean of CSIROM2kb B11 event data compared to mean of CCSRNIES B21 event data at Stratford; (a) intensity and (b) magnitude

(a)

(b)
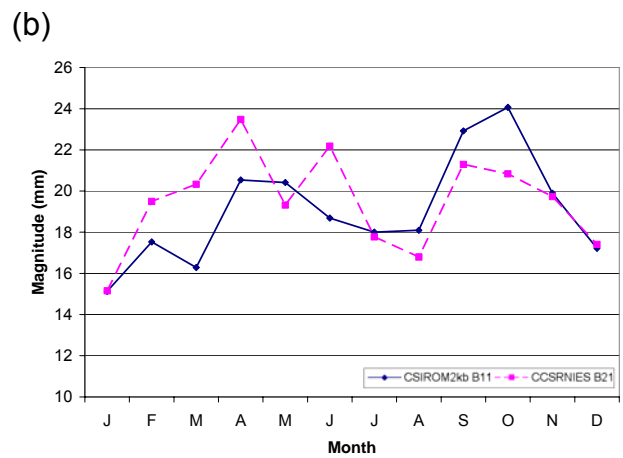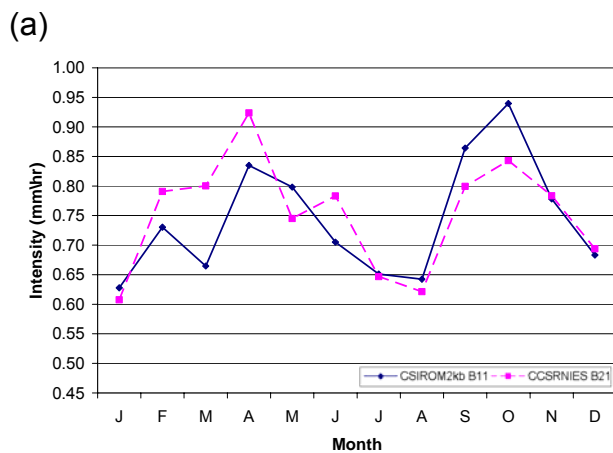
Figure B-57: Mean of CSIROM2kb B11 event data compared to mean of CCSRNIES B21 event data at Tavistock; (a) intensity and (b) magnitude

137
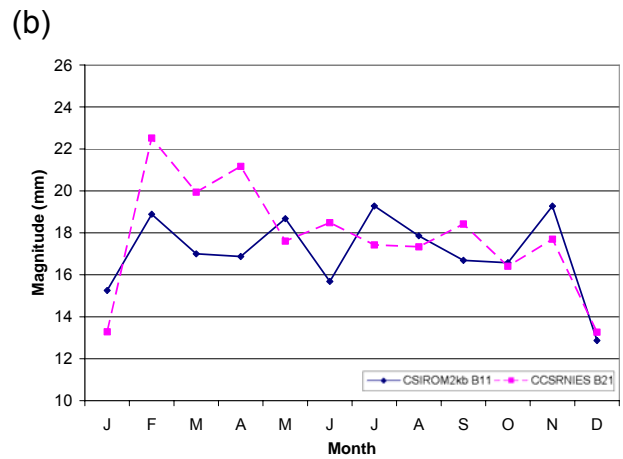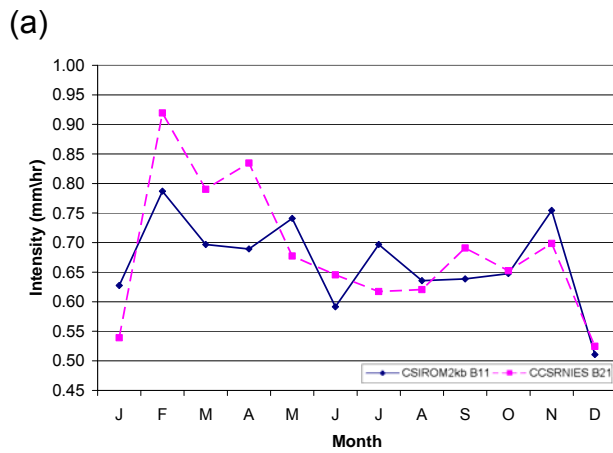
Figure B-58: Mean of CSIROM2kb B11 event data compared to mean of CCSRNIES B21 event data at Waterloo; (a) intensity and (b) magnitude
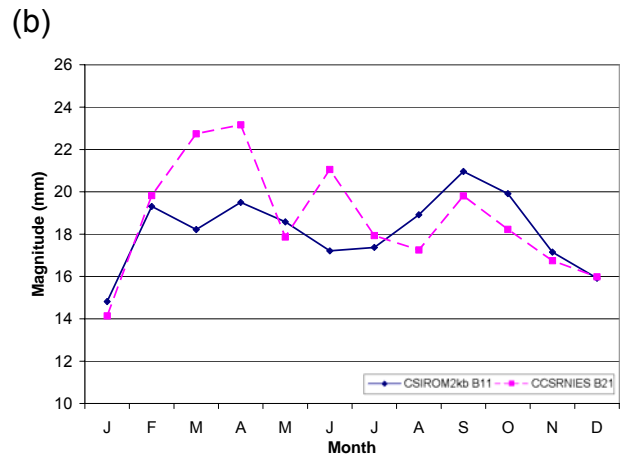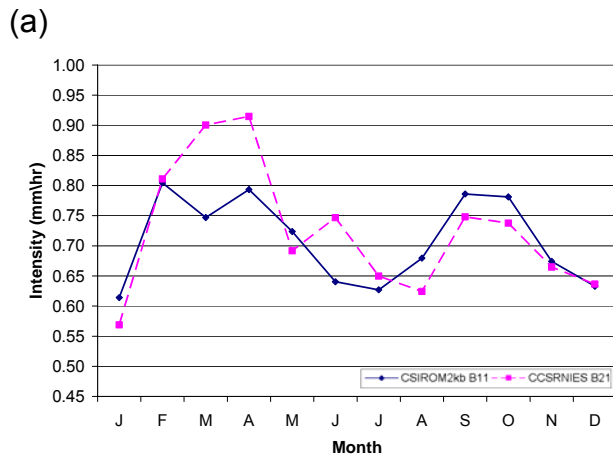
Figure B-59: Mean of CSIROM2kb B11 event data compared to mean of CCSRNIES B21 event data at Woodstock; (a) intensity and (b) magnitude
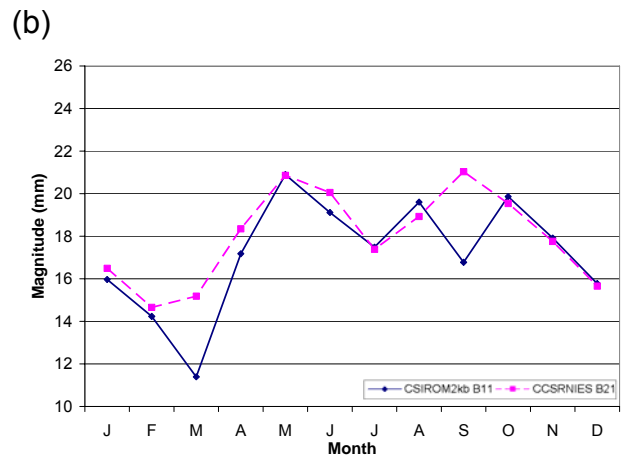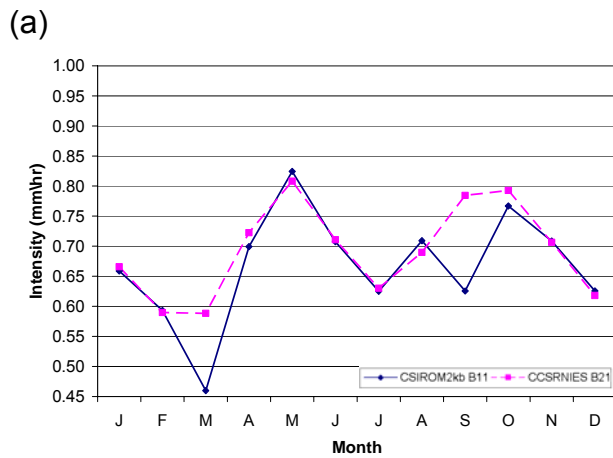
Figure B-60: Mean of CSIROM2kb B11 event data compared to mean of CCSRNIES B21 event data at Wroxeter; (a) intensity and (b) magnitude

Appendix C.   Data for Selected Extreme Events

C.1   Hyetographs

C.1.1 CSIROM2kb B11 Simulated Event #1403
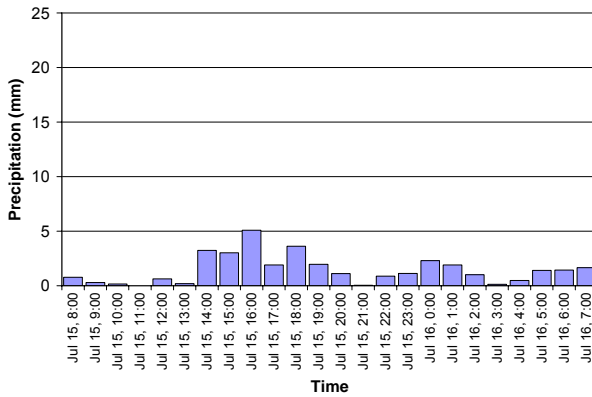
Figure C-1: Hyetograph of CSIROM2kb B11 Event #1403 at Blyth
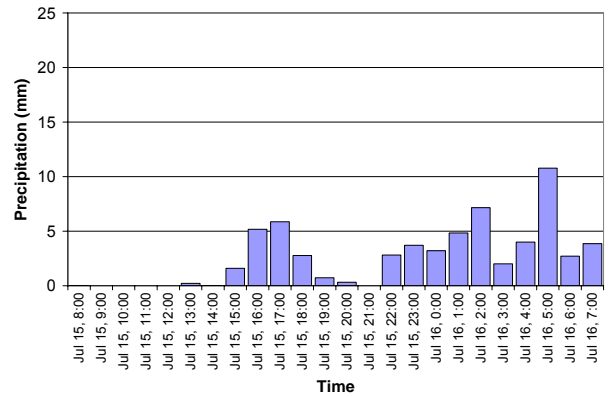
Figure C-2: Hyetograph of CSIROM2kb B11 Event #1403 at Dorchester
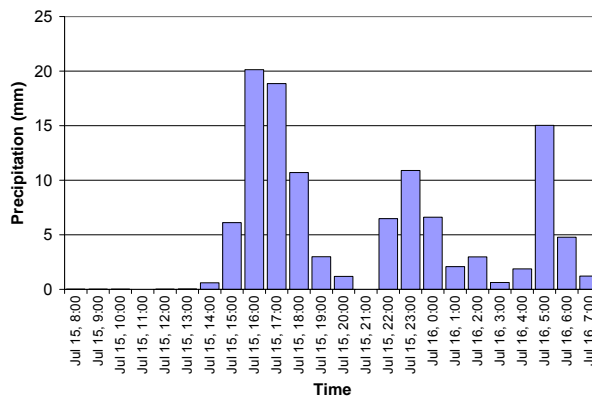
Figure C-3: Hyetograph of CSIROM2kb B11 Event #1403 at Embro
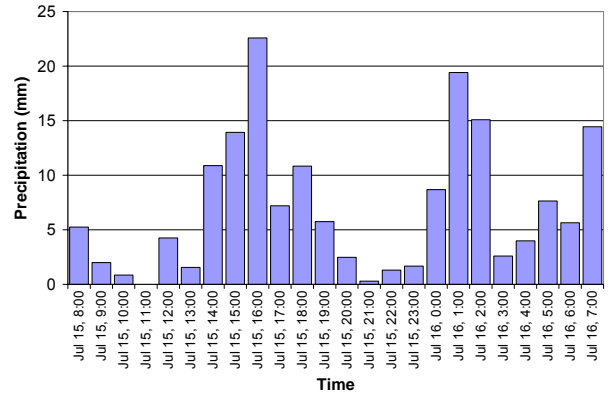
Figure C-4: Hyetograph of CSIROM2kb B11 Event #1403 at Exeter
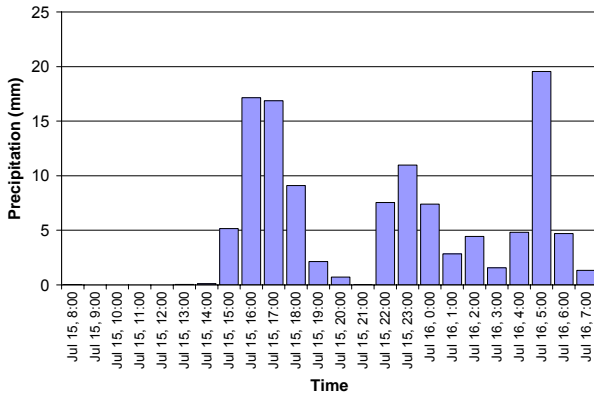
Figure C-5: Hyetograph of CSIROM2kb B11 Event #1403 at Foldens
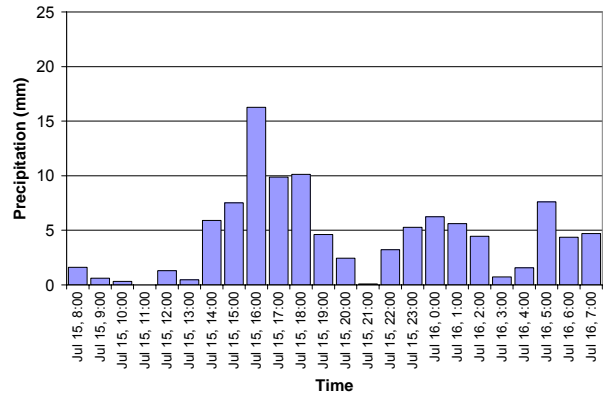
Figure C-6: Hyetograph of CSIROM2kb B11 Event #1403 at Fullarton
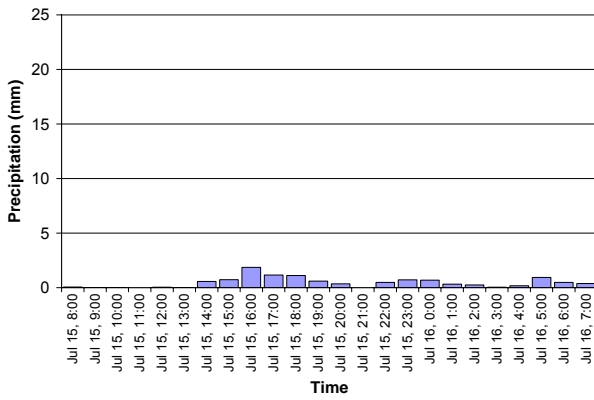
Figure C-7: Hyetograph of CSIROM2kb B11 Event #1403 at Glen Allan
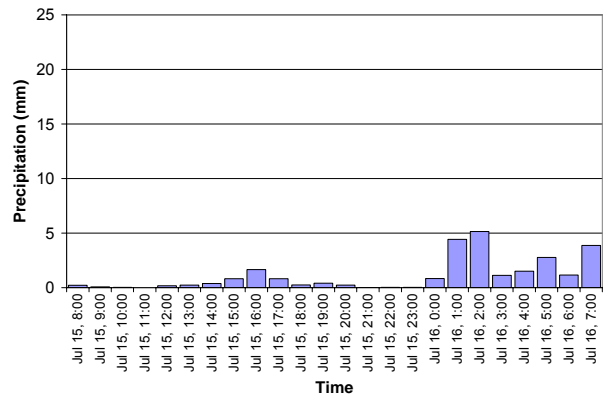
Figure C-8: Hyetograph of CSIROM2kb B11 Event #1403 at Ilderton
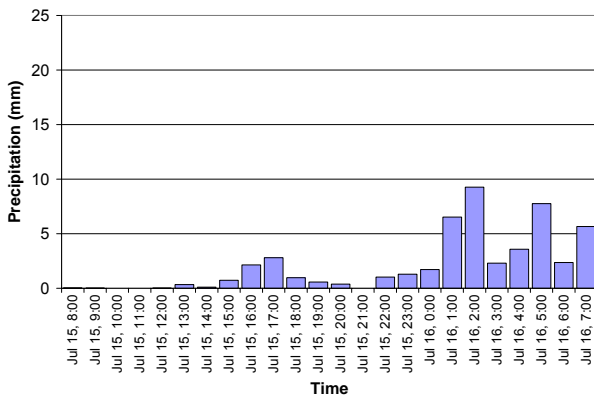
Figure C-9: Hyetograph of CSIROM2kb B11 Event #1403 at London
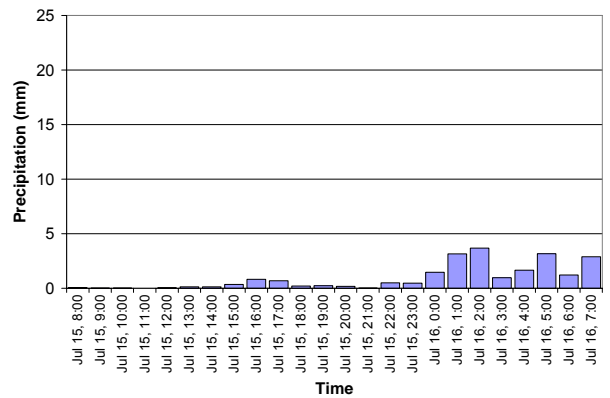
Figure C-10: Hyetograph of CSIROM2kb B11 Event #1403 at St. Thomas
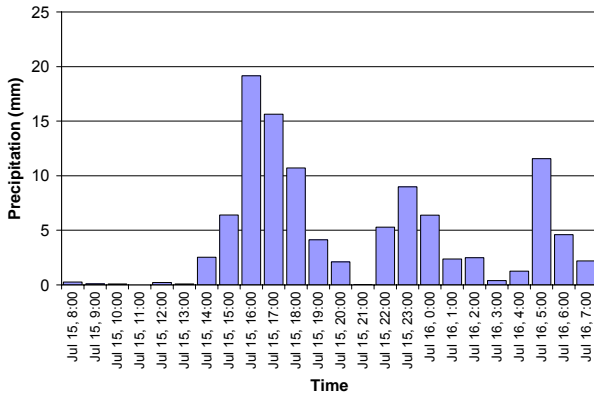
Figure C-11: Hyetograph of CSIROM2kb B11 Event #1403 at Stratford
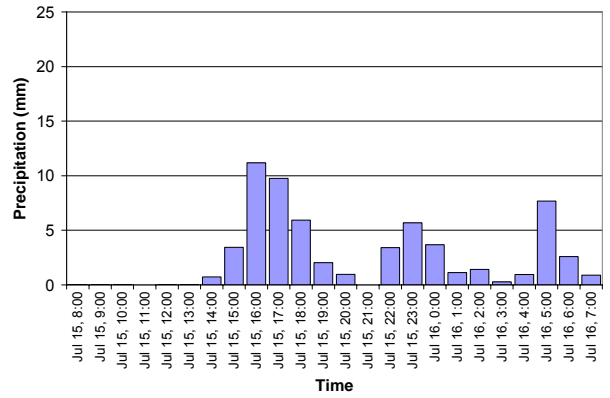
Figure C-12: Hyetograph of CSIROM2kb B11 Event #1403 at Tavistock
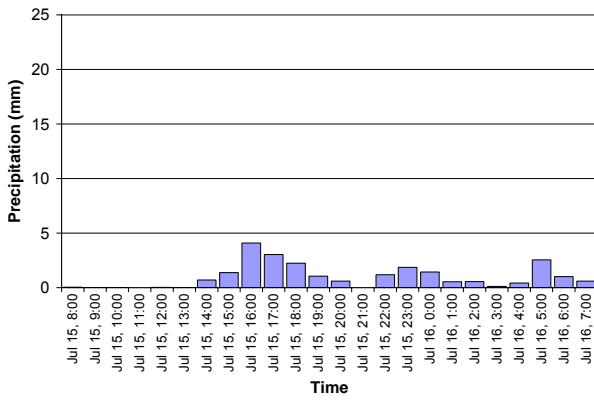
Figure C-13: Hyetograph of CSIROM2kb B11 Event #1403 at Waterloo
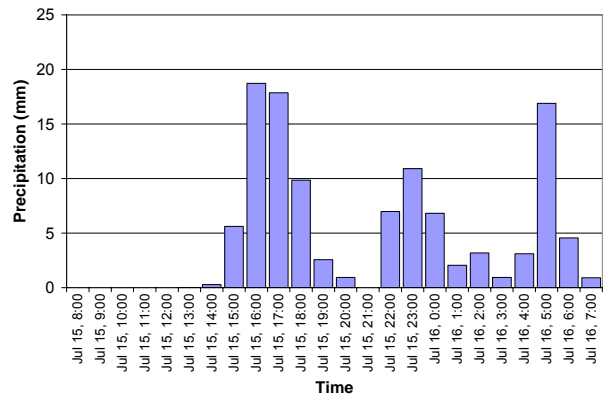
Figure C-14: Hyetograph of CSIROM2kb B11 Event #1403 at Woodstock
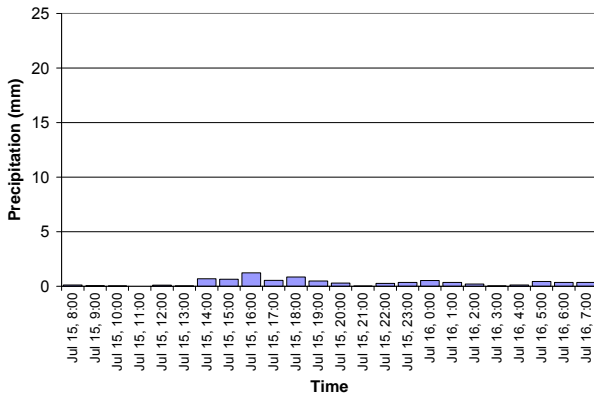
Figure C-15: Hyetograph of CSIROM2kb B11 Event #1403 at Wroxeter

141

C.1.2 CCSRNIES B21 Simulated Event #1197
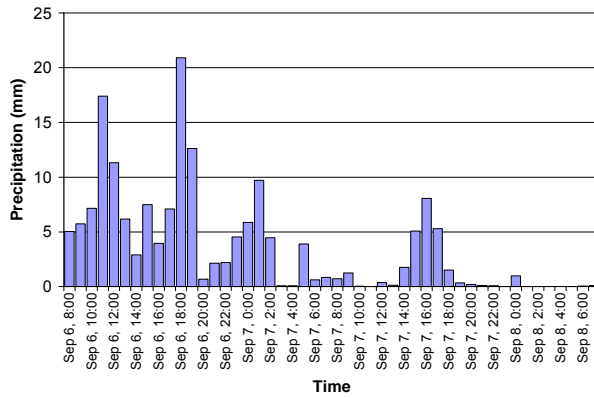
Figure C-16: Hyetograph of CCSRNIES B21 Event #1197 at Blyth
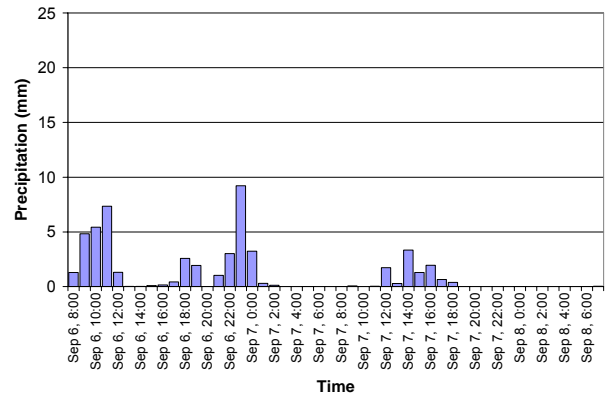
Figure C-17: Hyetograph of CCSRNIES B21 Event #1197 at Dorchester
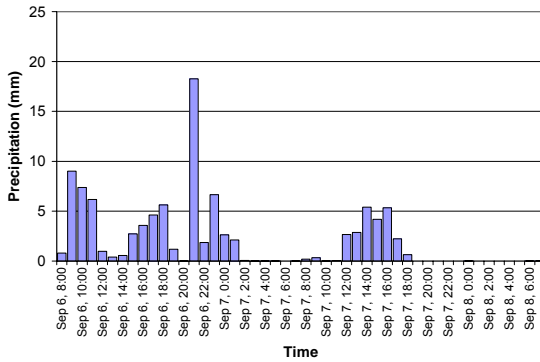
Figure C-18: Hyetograph of CCSRNIES B21 Event #1197 at Embro
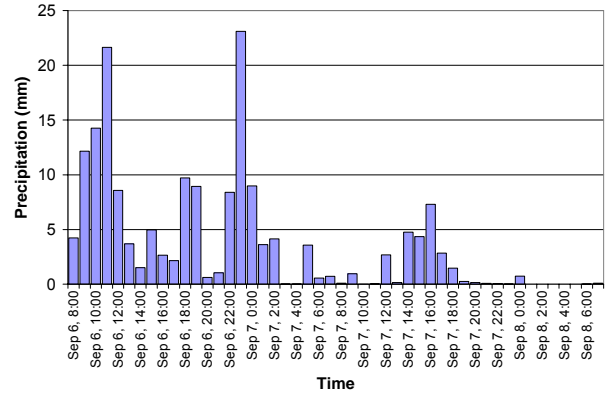
Figure C-19: Hyetograph of CCSRNIES B21 Event #1197 at Exeter
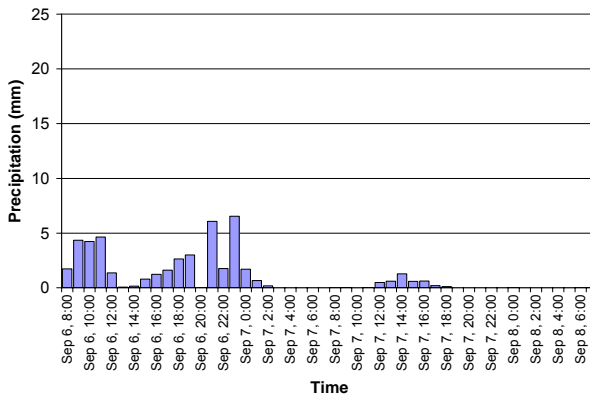
Figure C-20: Hyetograph of CCSRNIES B21 Event #1197 at Foldens
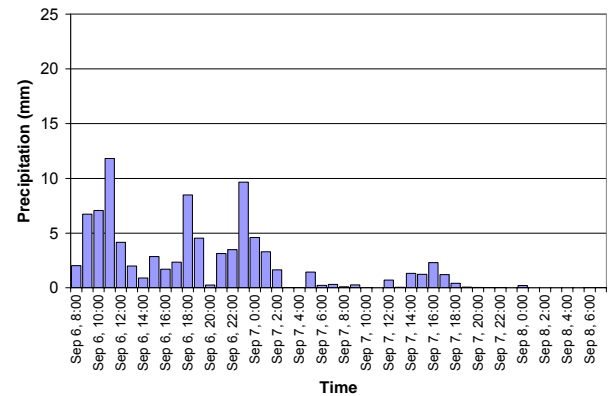
Figure C-21: Hyetograph of CCSRNIES B21 Event #1197 at Fullarton

142
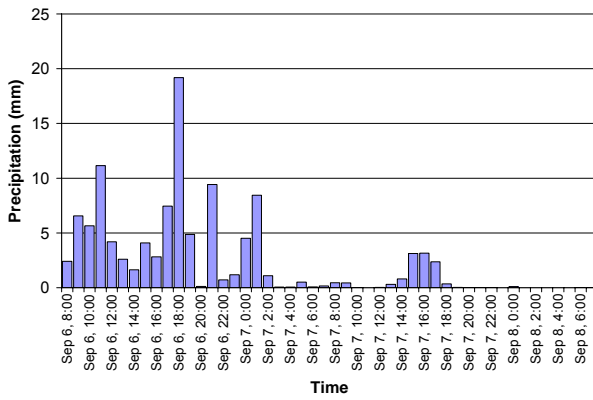
Figure C-22: Hyetograph of CCSRNIES B21 Event #1197 at Glen Allan
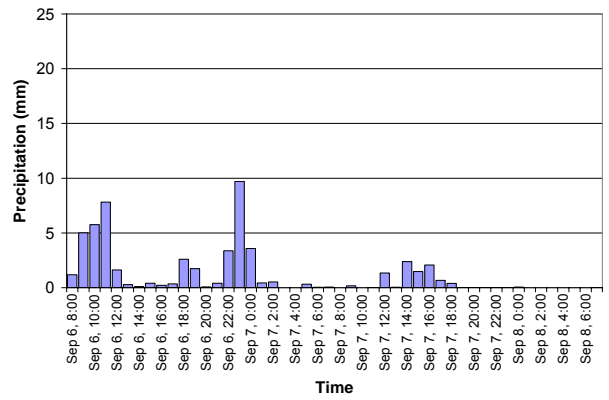
Figure C-23: Hyetograph of CCSRNIES B21 Event #1197 at Ilderton
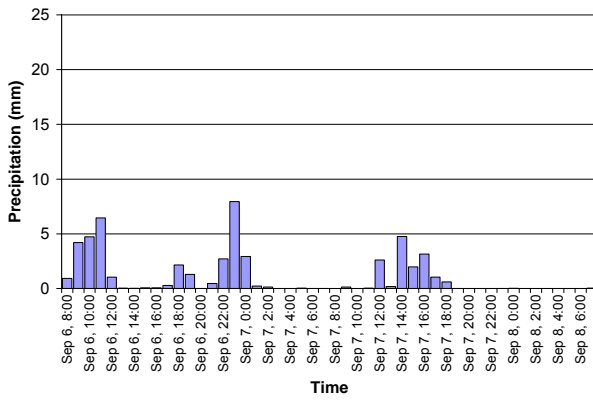
Figure C-24: Hyetograph of CCSRNIES B21 Event #1197 at London
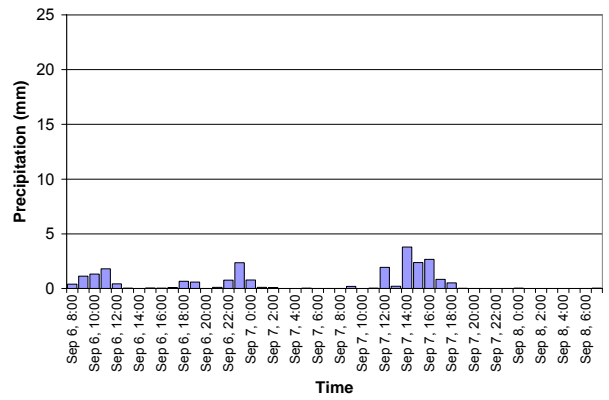
Figure C-25: Hyetograph of CCSRNIES B21 Event #1197 at St. Thomas
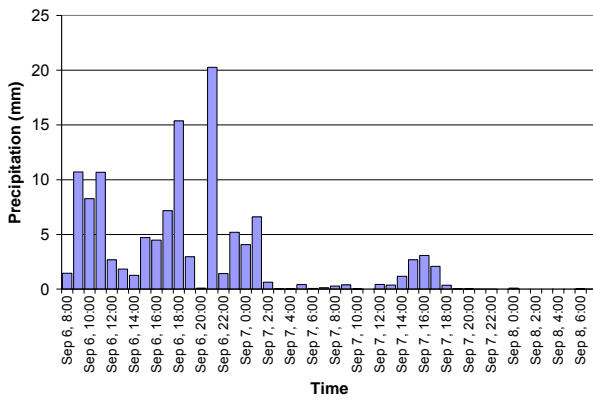
Figure C-26: Hyetograph of CCSRNIES B21 Event #1197 at Stratford
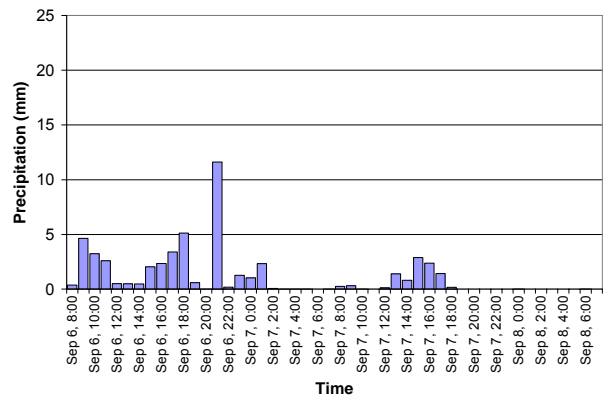
Figure C-27: Hyetograph of CCSRNIES B21 Event #1197 at Tavistock

143
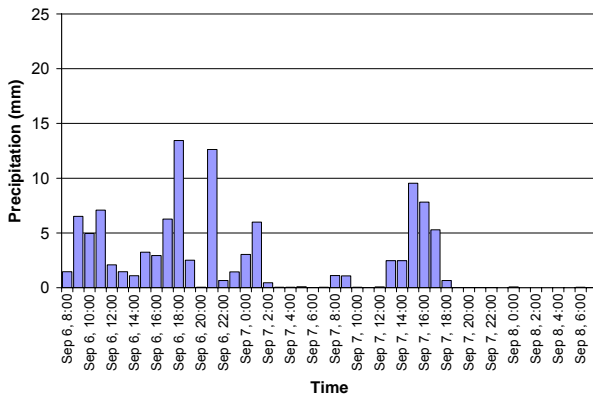
**Figure C-28: Hyetograph of CCSRNIES B21
Event #1197 at Waterloo**
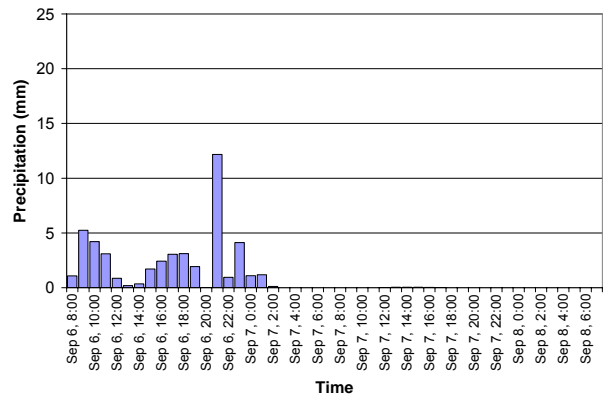
**Figure C-29: Hyetograph of CCSRNIES B21
Event #1197 at Woodstock**
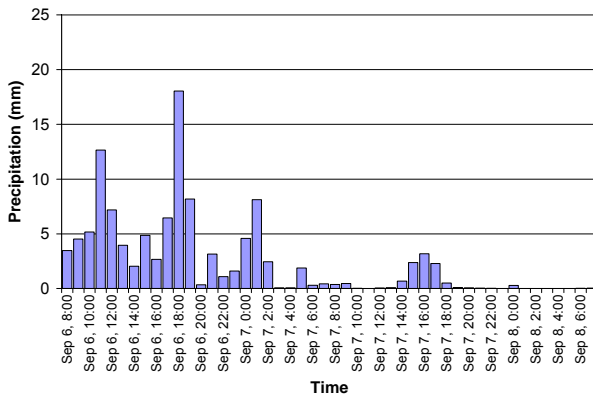
**Figure C-30: Hyetograph of CCSRNIES B21
Event #1197 at Wroxeter**

144

C.2 Isohyetal Plots for Selected Events

C.2.1 CSIROM2kb B11 Simulated Event #1403
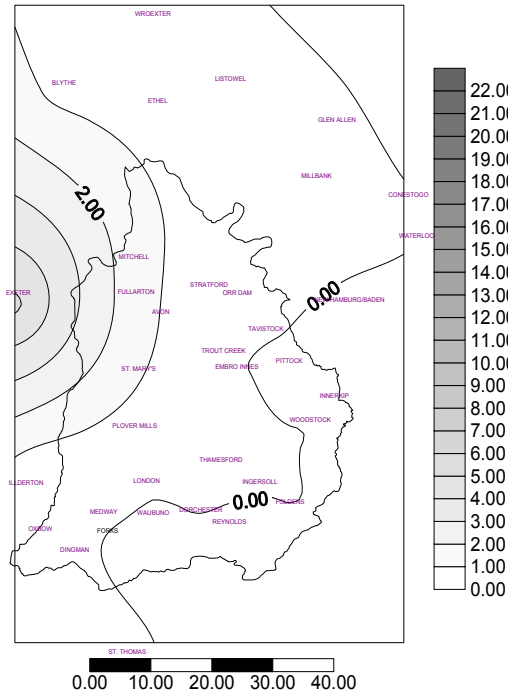
Figure C-31: Isohyets (mm) of July 15 at 08:00
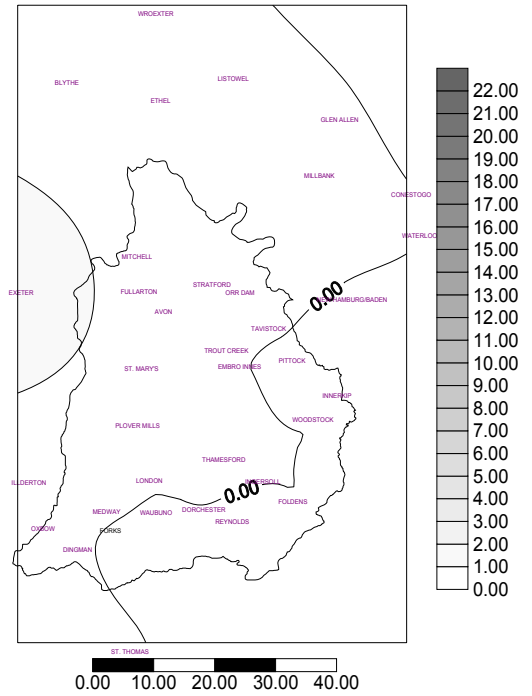
Figure C-32: Isohyets (mm) of July 15 at 09:00
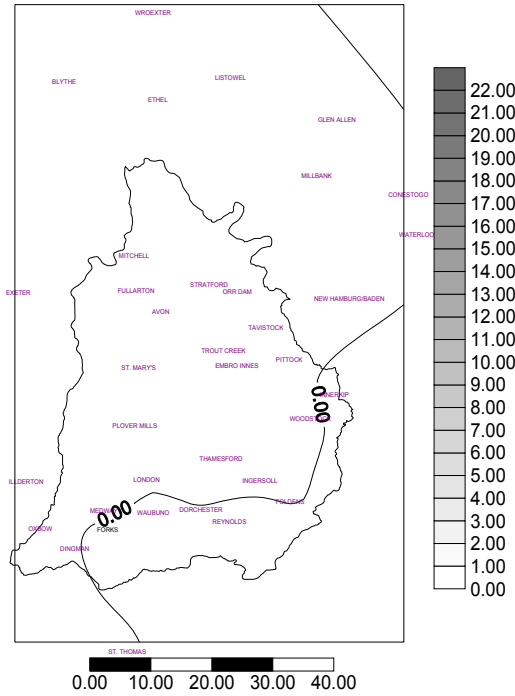
Figure C-33: Isohyets (mm) of July 15 at 10:00
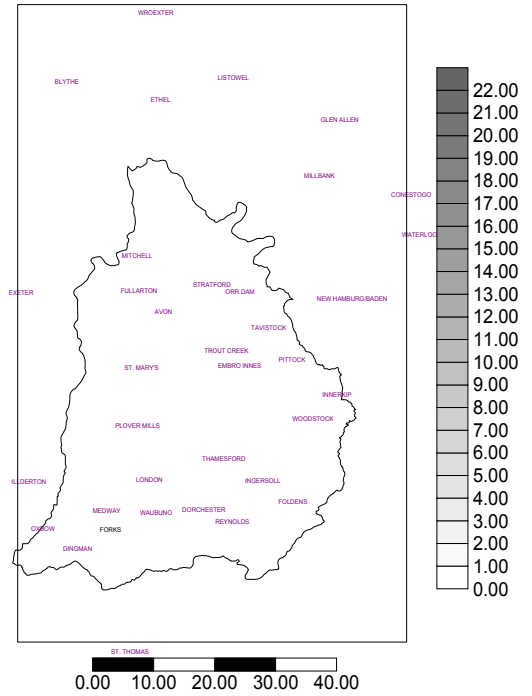
Figure C-34: Isohyets (mm) of July 15 at 11:00
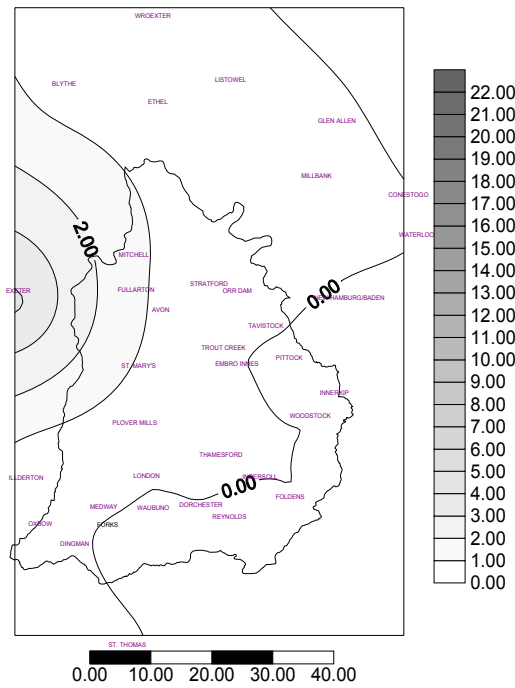
Figure C-35: Isohyets (mm) of July 15 at 12:00
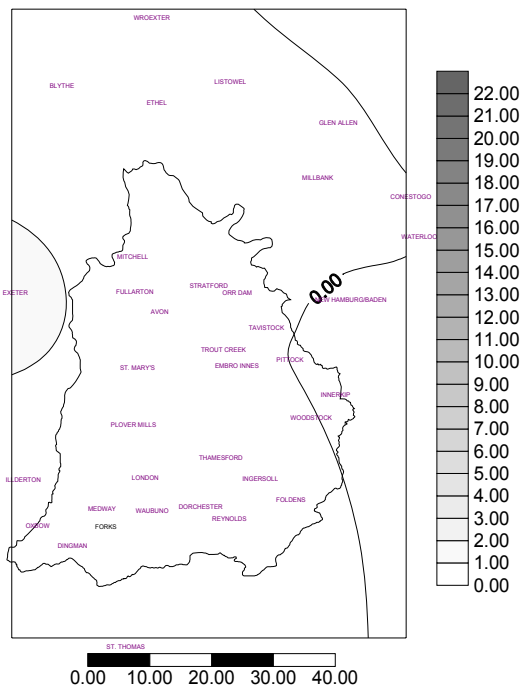
Figure C-36: Isohyets (mm) of July 15 at 13:00

146
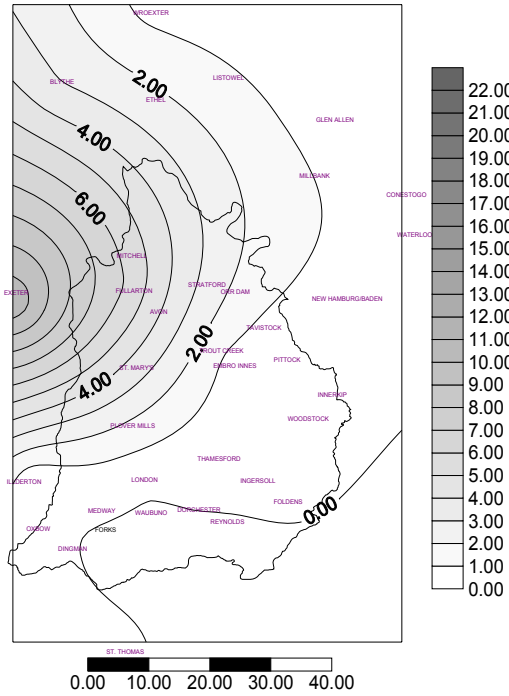
Figure C-37: Isohyets (mm) of July 15 at 14:00
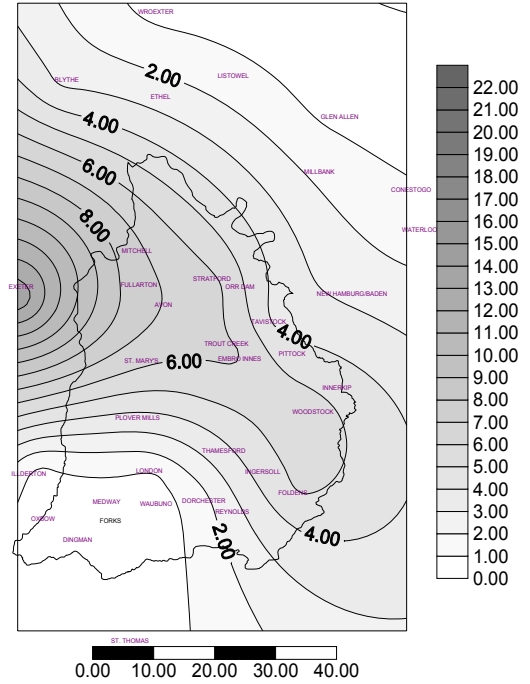
Figure C-38: Isohyets (mm) of July 15 at 15:00
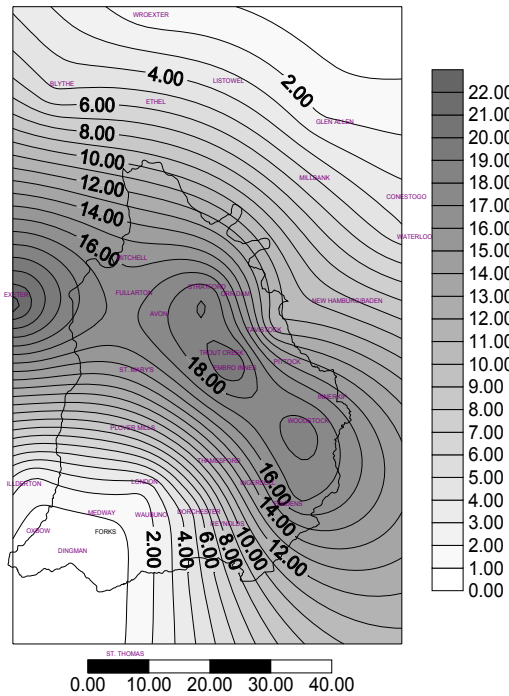
Figure C-39: Isohyets (mm) of July 15 at 16:00
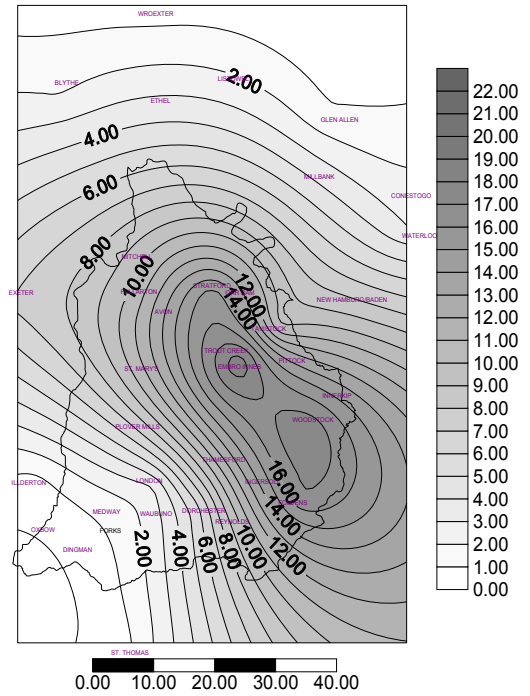
Figure C-40: Isohyets (mm) of July 15 at 17:00

147
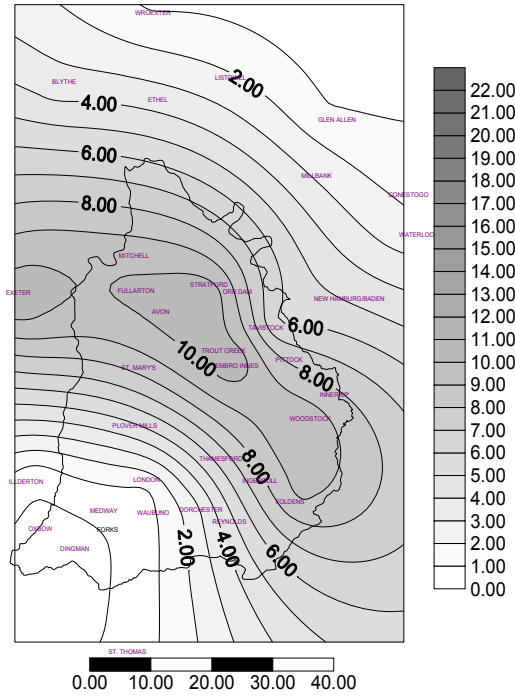
Figure C-41: Isohyets (mm) of July 15 at 18:00
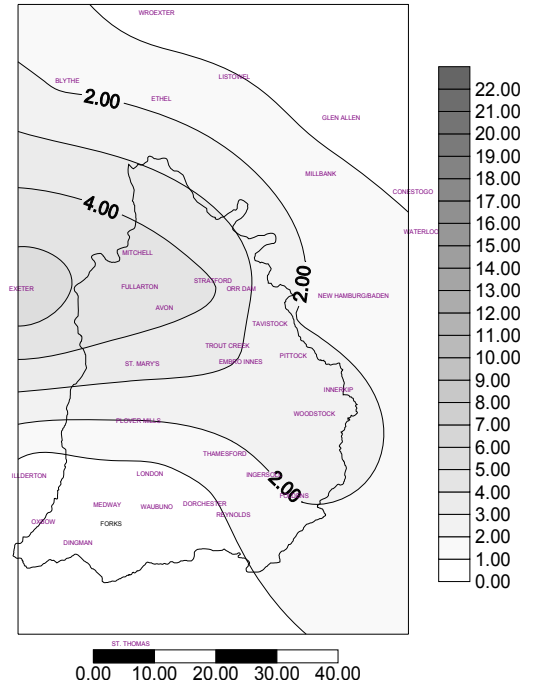
Figure C-42: Isohyets (mm) of July 15 at 19:00
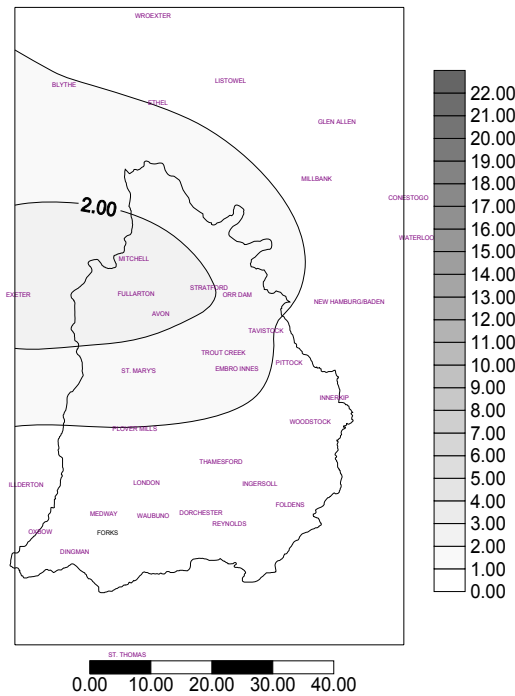
Figure C-43: Isohyets (mm) of July 15 at 20:00
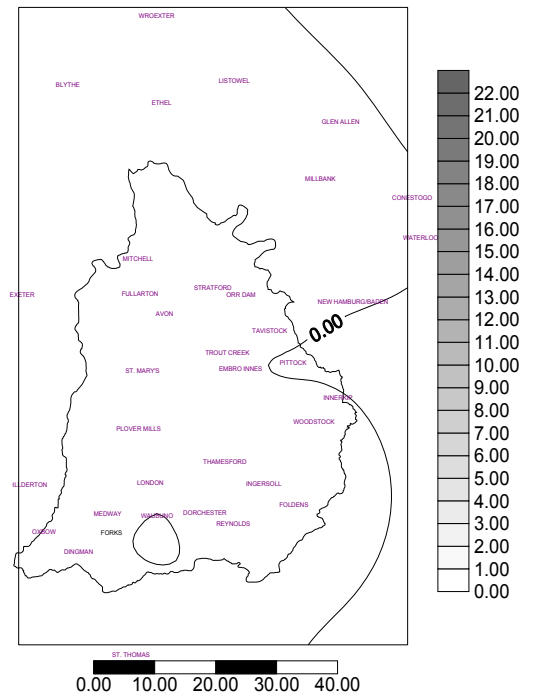
Figure C-44: Isohyets (mm) of July 15 at 21:00

148
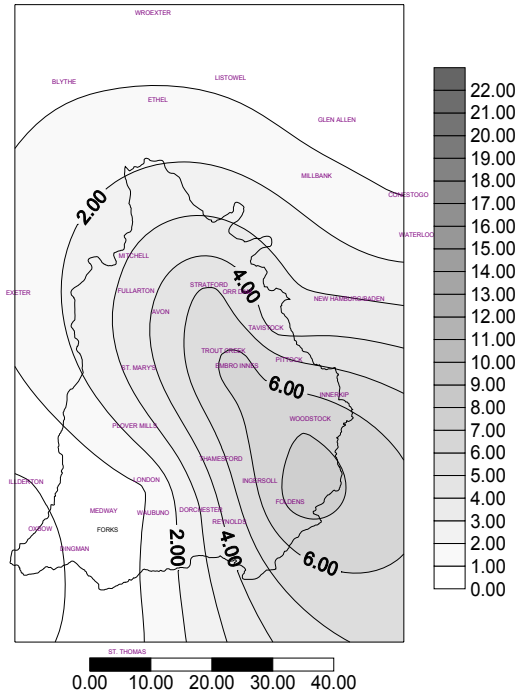
Figure C-45: Isohyets (mm) of July 15 at 22:00
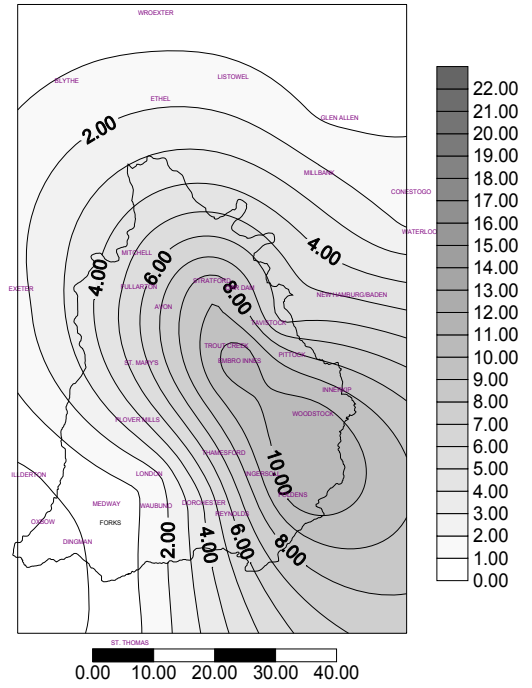
Figure C-46: Isohyets (mm) of July 15 at 23:00
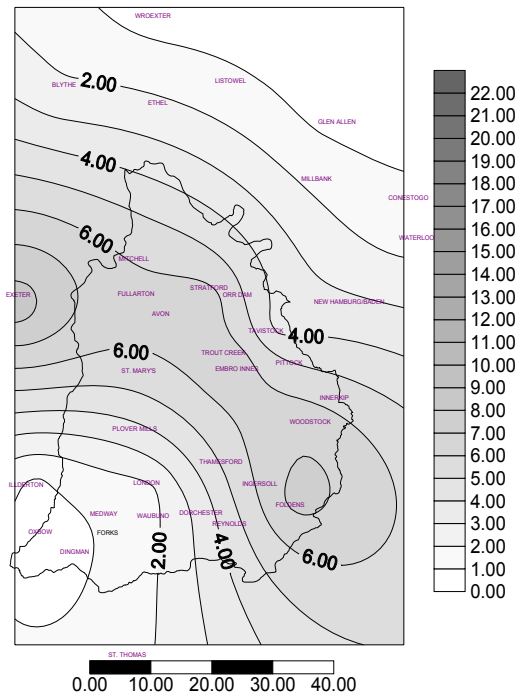
Figure C-47: Isohyets (mm) of July 16 at 00:00
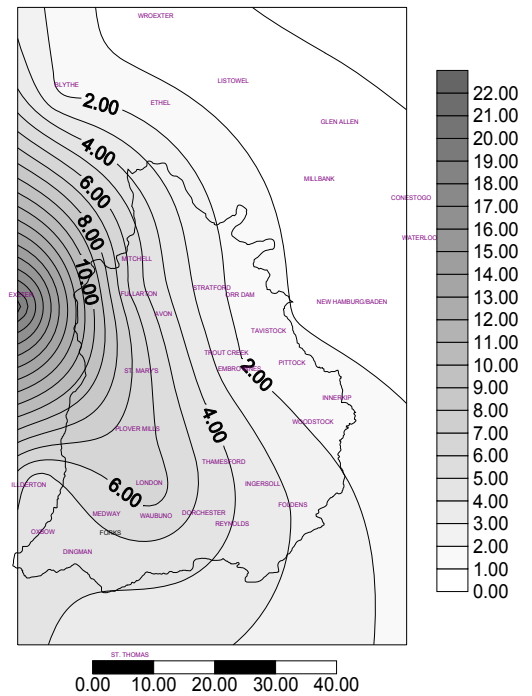
Figure C-48: Isohyets (mm) of July 16 at 01:00

149
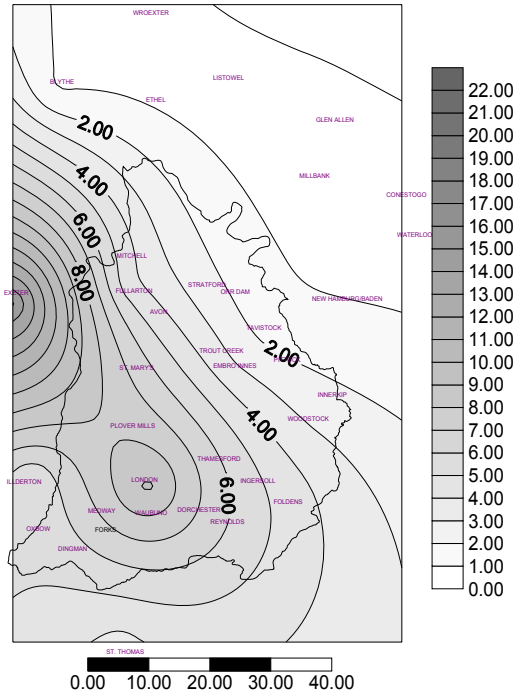
Figure C-49: Isohyets (mm) of July 16 at 02:00
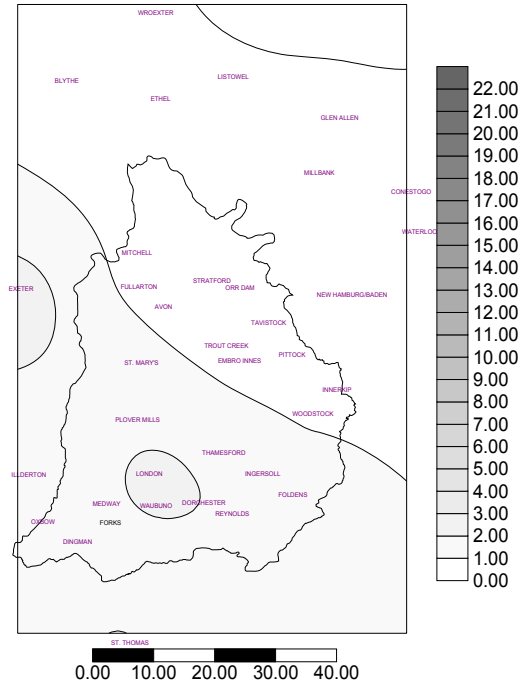
Figure C-50: Isohyets (mm) of July 16 at 03:00
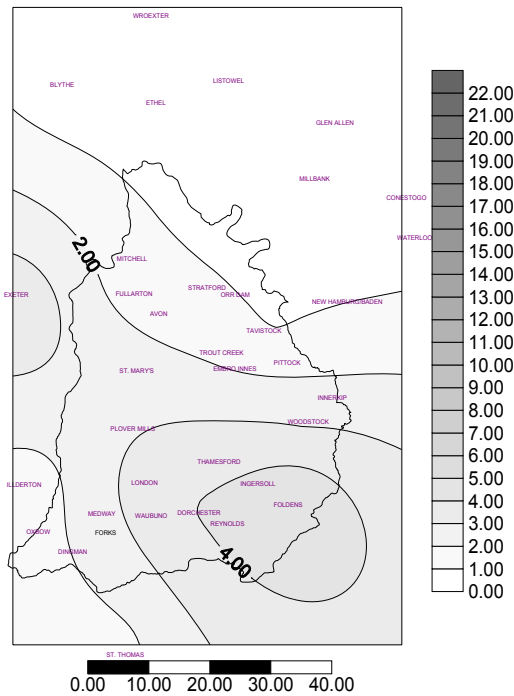
Figure C-51: Isohyets (mm) of July 16 at 04:00
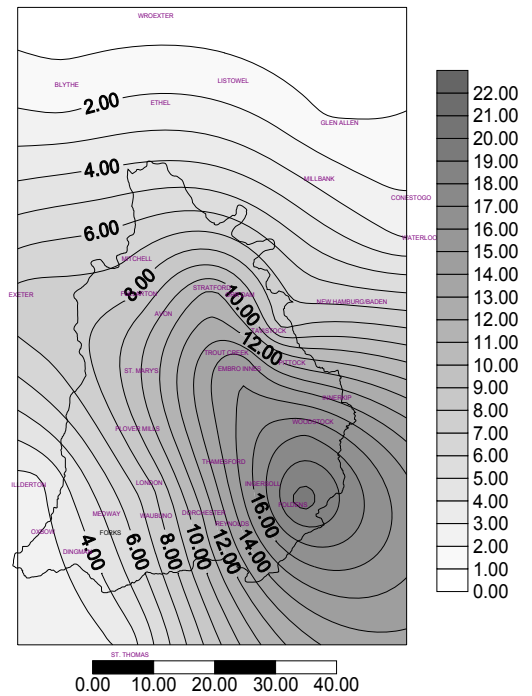
Figure C-52: Isohyets (mm) of July 16 at 05:00

150
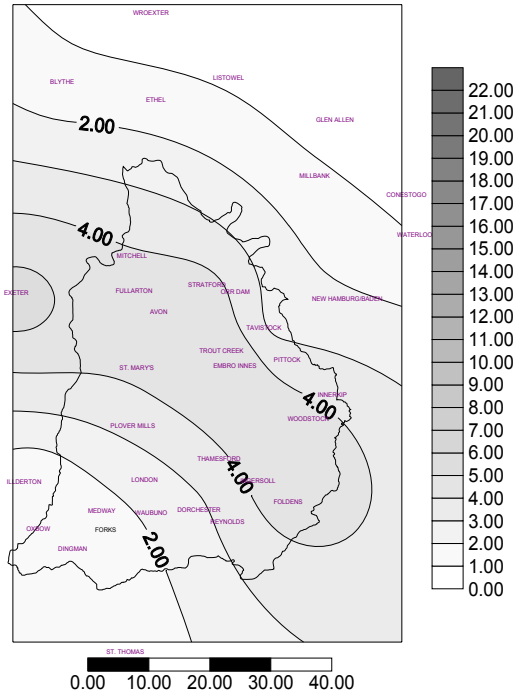
Figure C-53: Isohyets (mm) of July 16 at 06:00
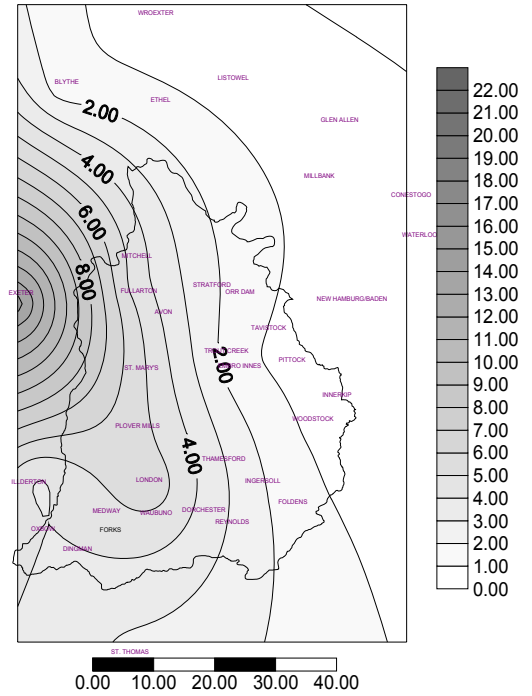
Figure C-54: Isohyets (mm) of July 16 at 07:00

151

C.2.2 CCSRNIES B21 Simulated Event #1197
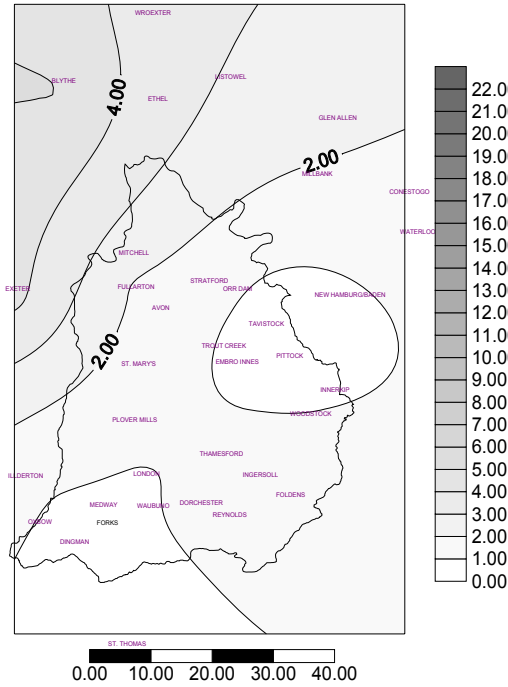
**Figure C-55: Isohyets (mm) of Sept. 6 at 08:00**
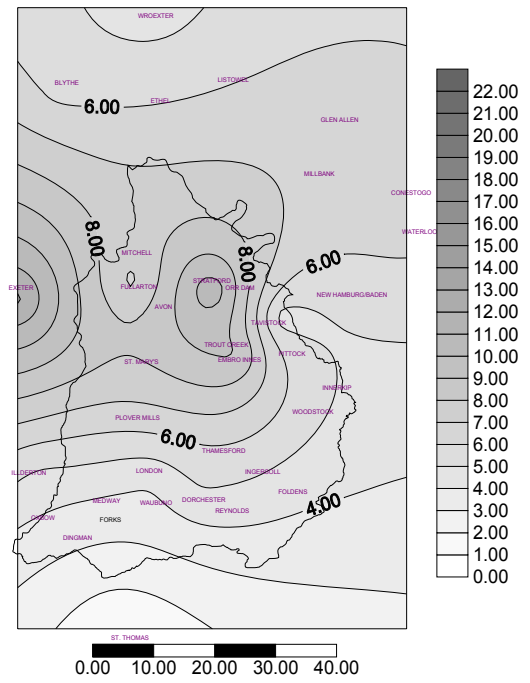
Figure C-56: Isohyets (mm) of Sept. 6 at 09:00
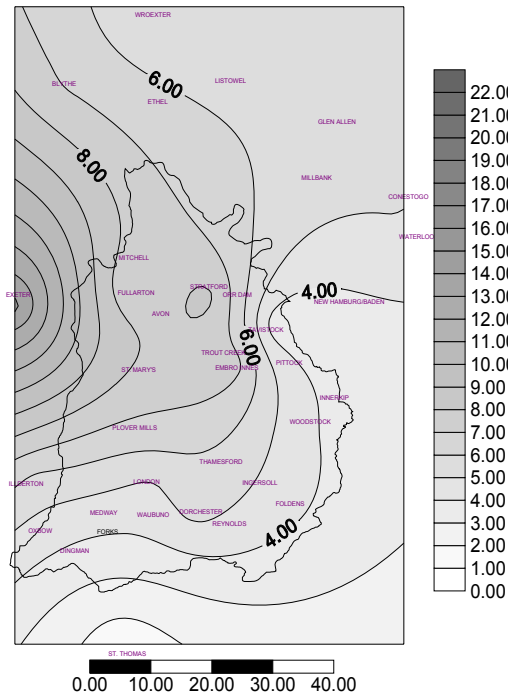
Figure C-57: Isohyets (mm) of Sept. 6 at 10:00
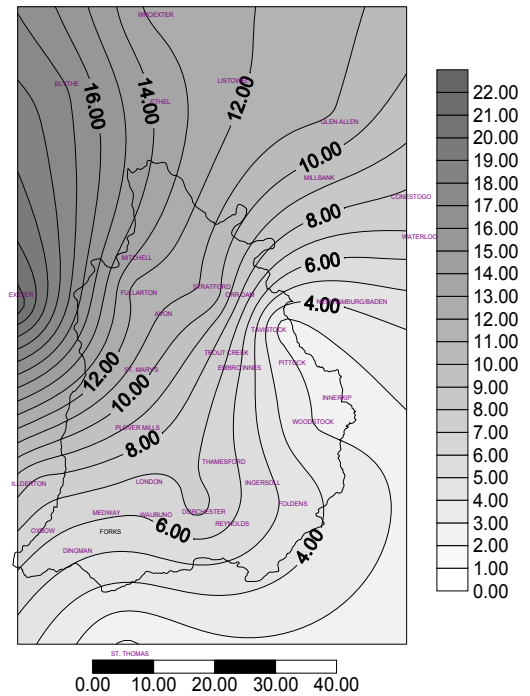
Figure C-58: Isohyets (mm) of Sept. 6 at 11:00

152
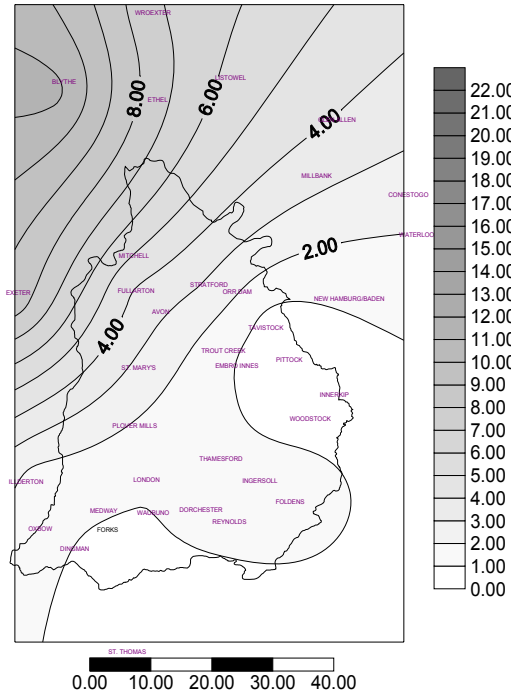
Figure C-59: Isohyets (mm) of Sept. 6 at 12:00
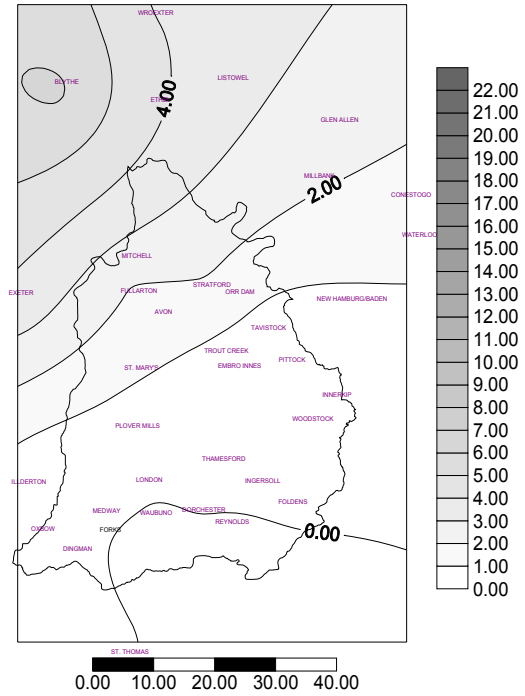
Figure C-60: Isohyets (mm) of Sept. 6 at 13:00
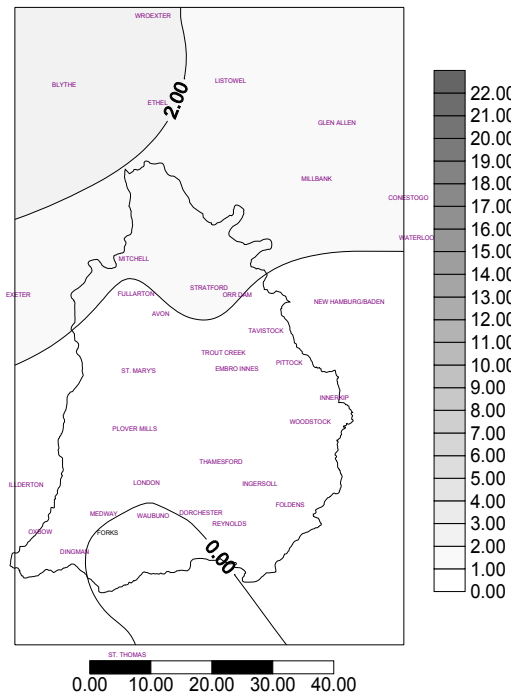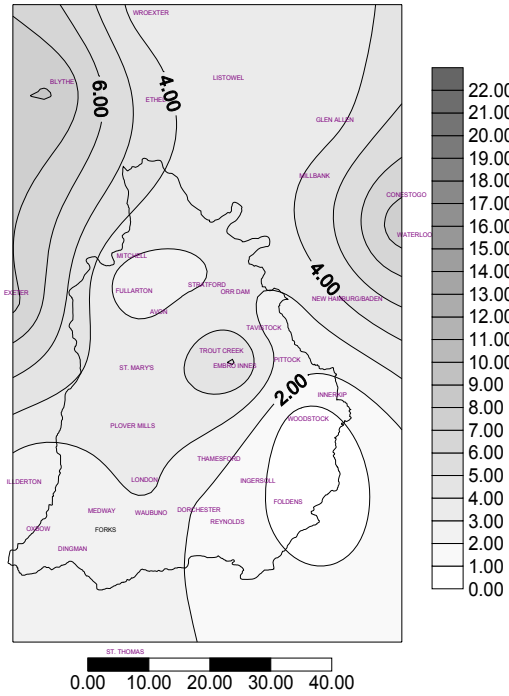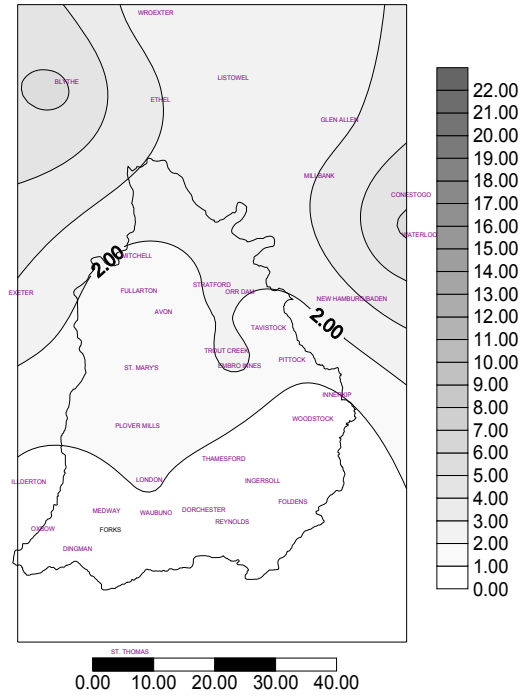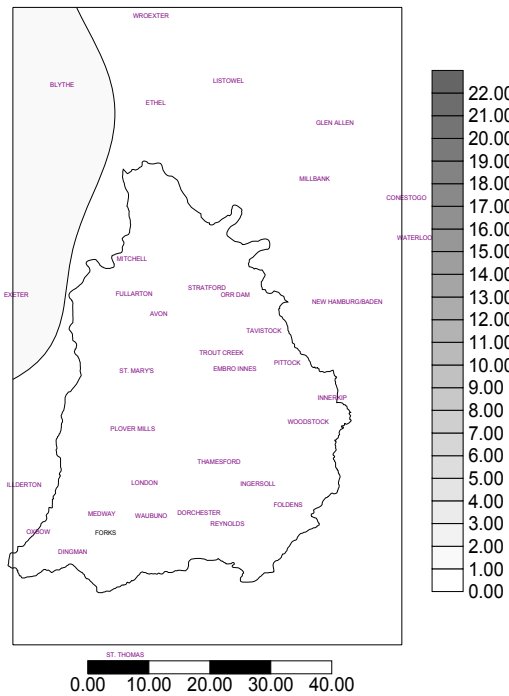

Figure C-61: Isohyets (mm) of Sept. 6 at 14:00
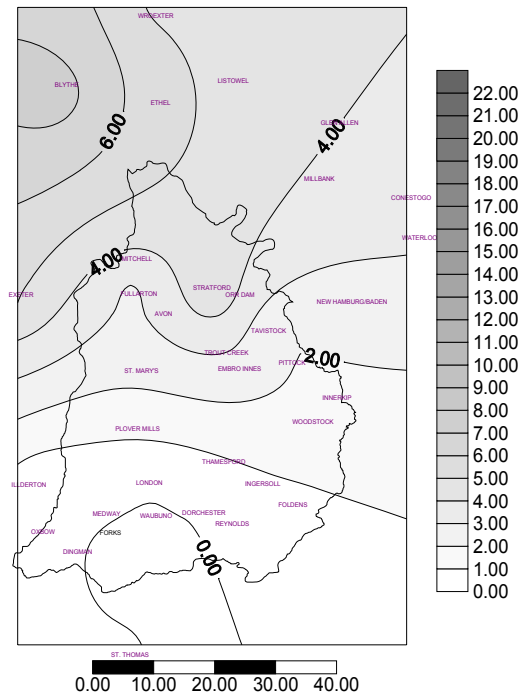
Figure C-62: Isohyets (mm) of Sept. 6 at 15:00

153
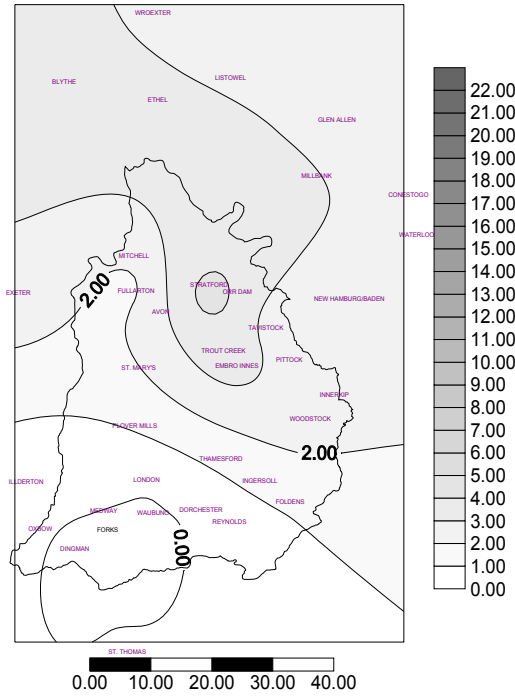
Figure C-63: Isohyets (mm) of Sept. 6 at 16:00
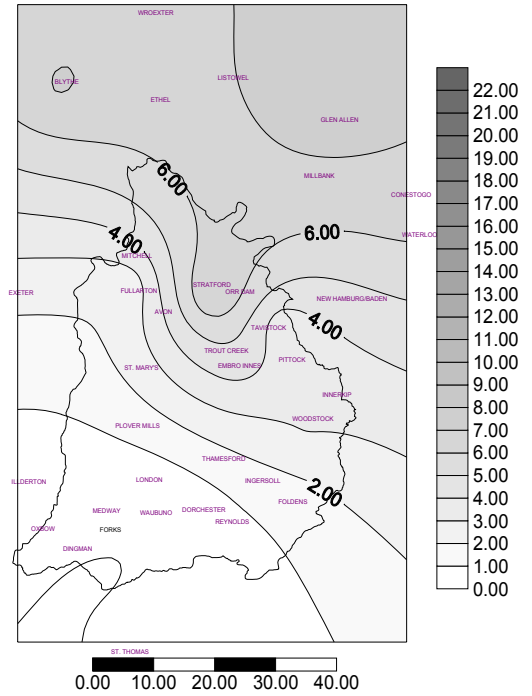
Figure C-64: Isohyets (mm) of Sept. 6 at 17:00
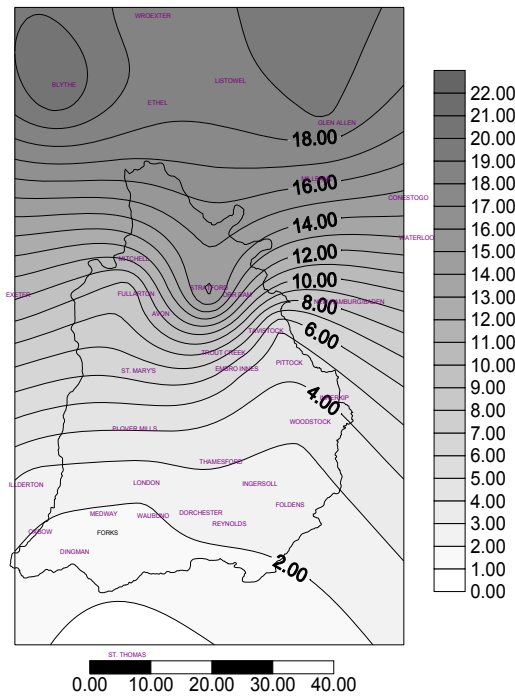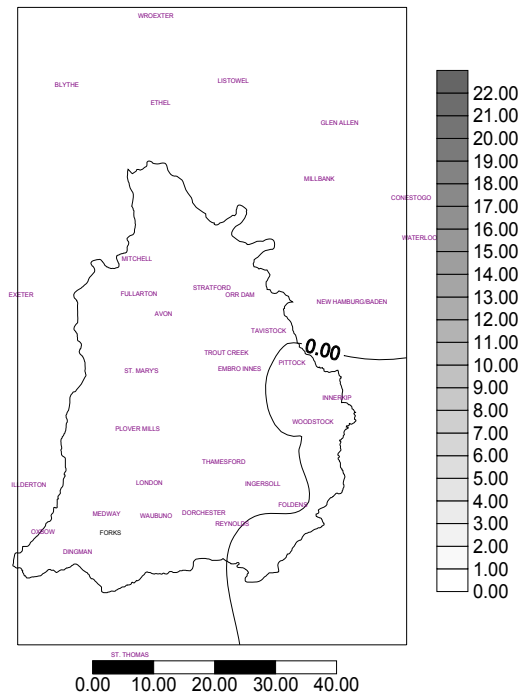

Figure C-65: Isohyets (mm) of Sept. 6 at 18:00
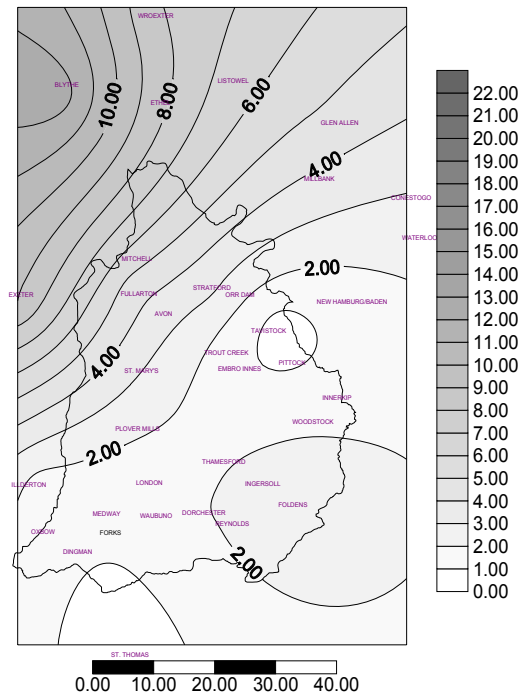
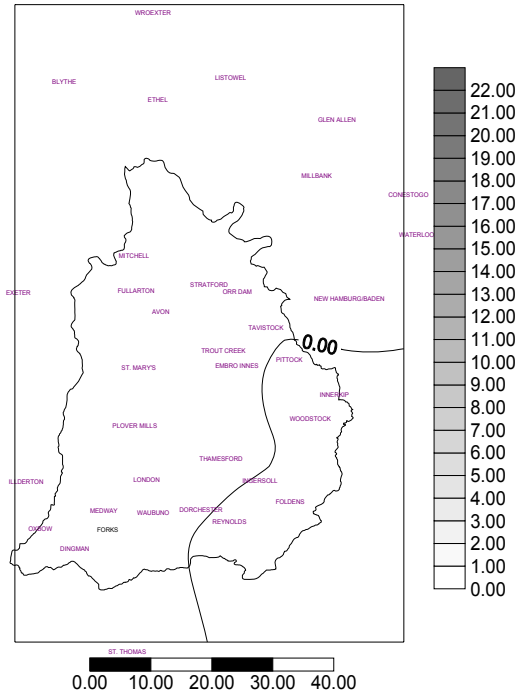**Figure C-66: Isohyets (mm) of Sept. 6 at 19:00**

154
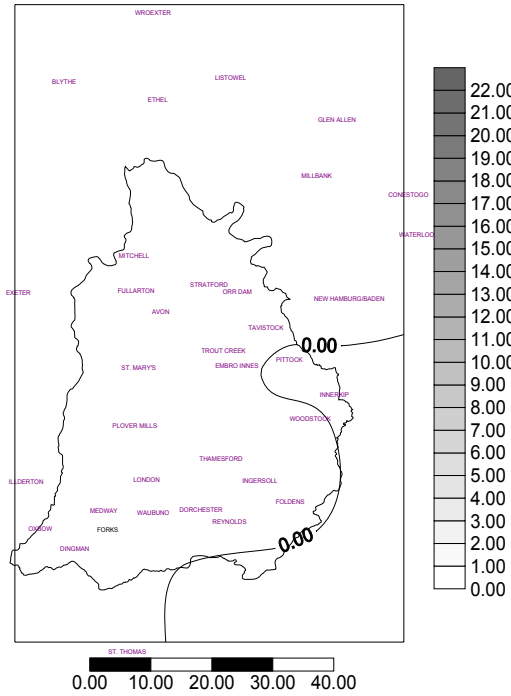
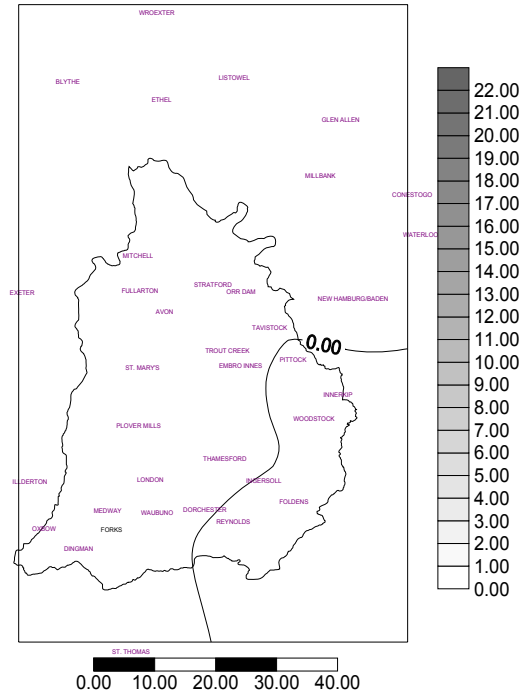**Figure C-67: Isohyets (mm) of Sept. 6 at 20:00**
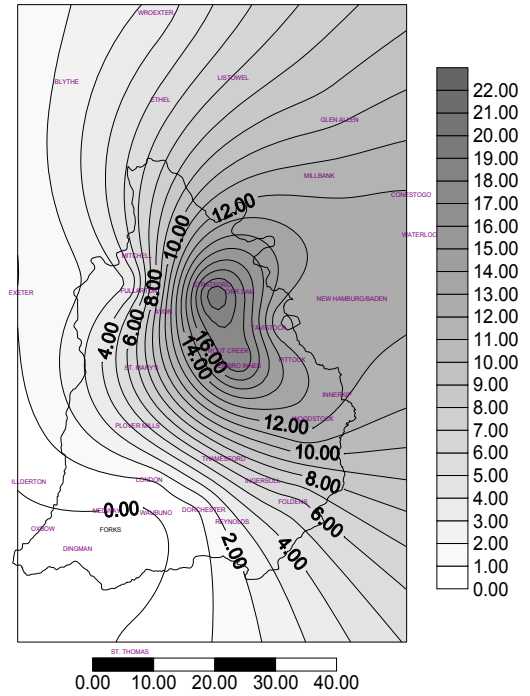
Figure C-68: Isohyets (mm) of Sept. 6 at 21:00
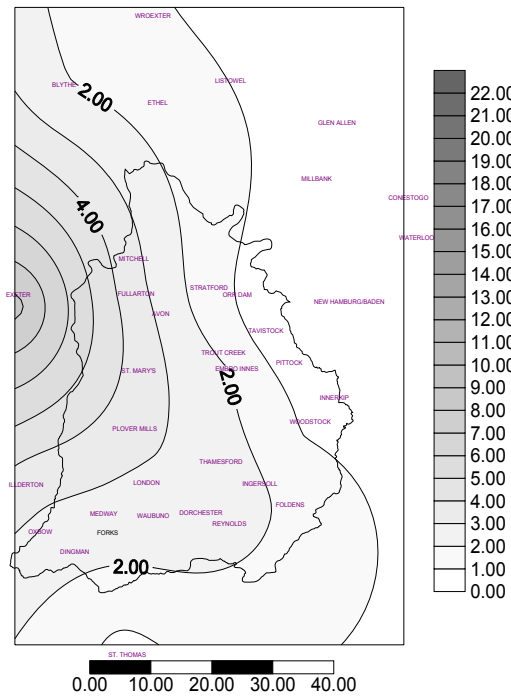
Figure C-69: Isohyets (mm) of Sept. 6 at 22:00
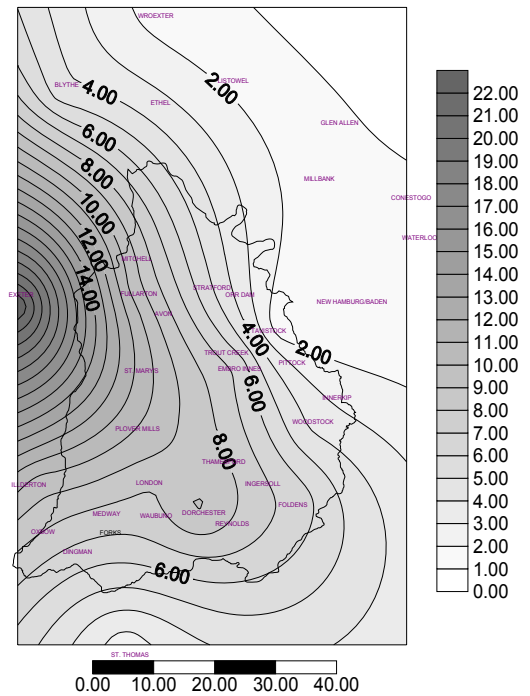
Figure C-70: Isohyets (mm) of Sept. 6 at 23:00

155
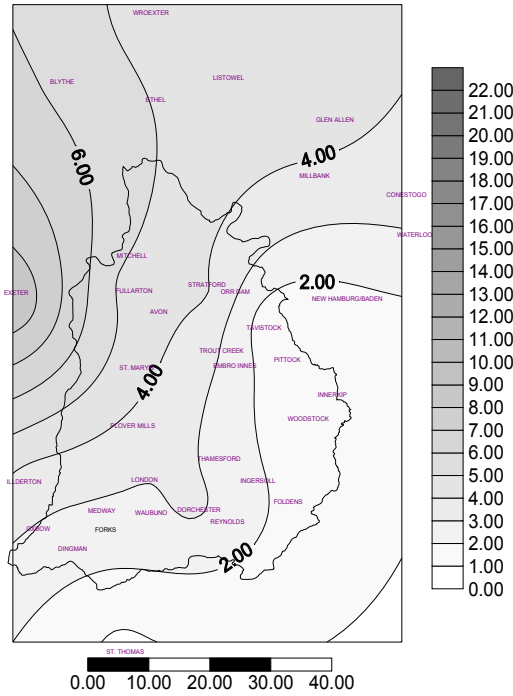
Figure C-71: Isohyets (mm) of Sept. 7 at 00:00
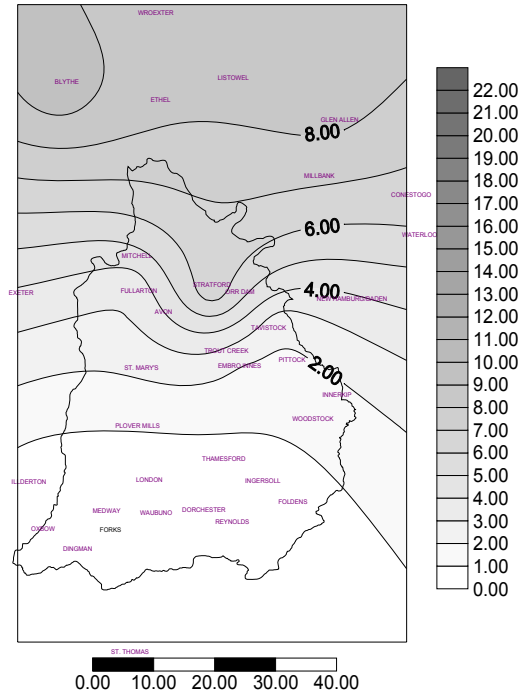
Figure C-72: Isohyets (mm) of Sept. 7 at 01:00
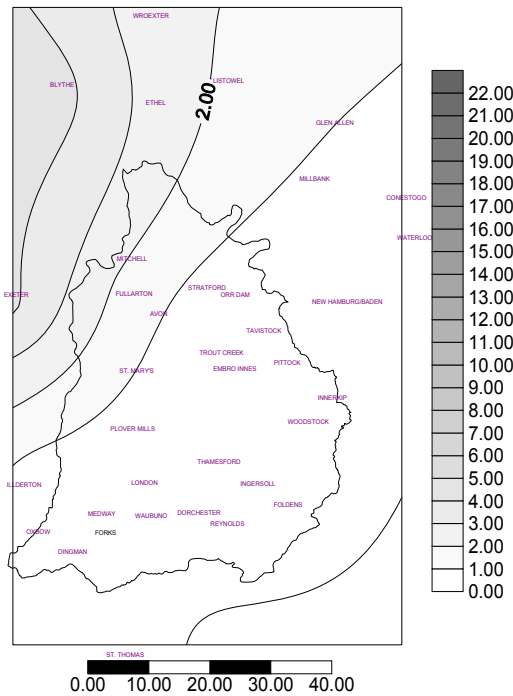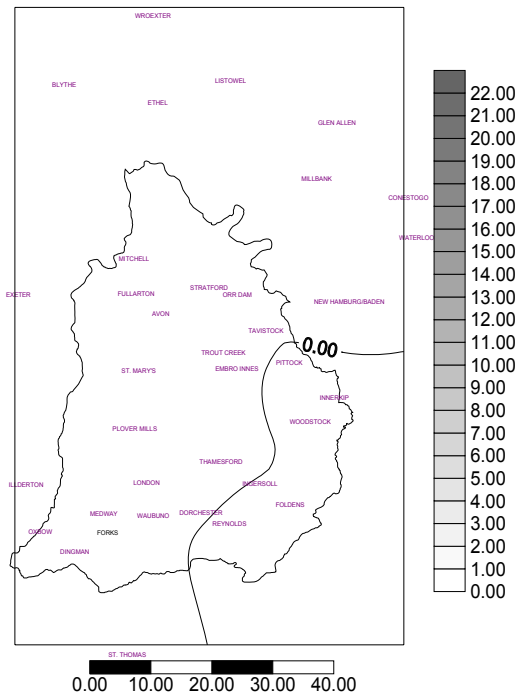

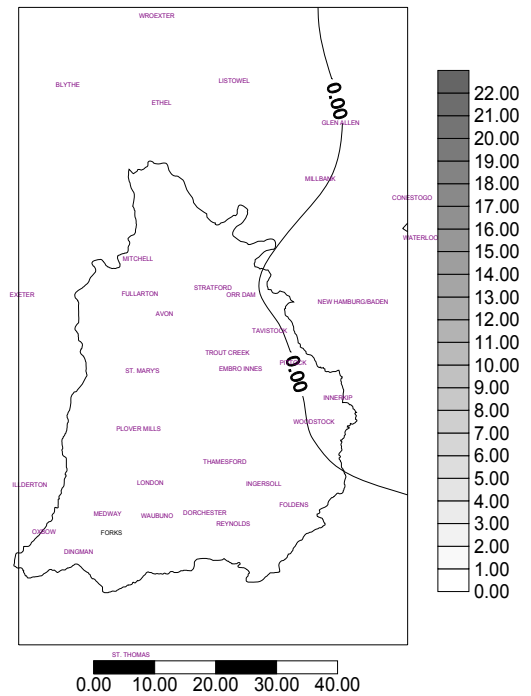**Figure C-73: Isohyets (mm) of Sept. 7 at 02:00**
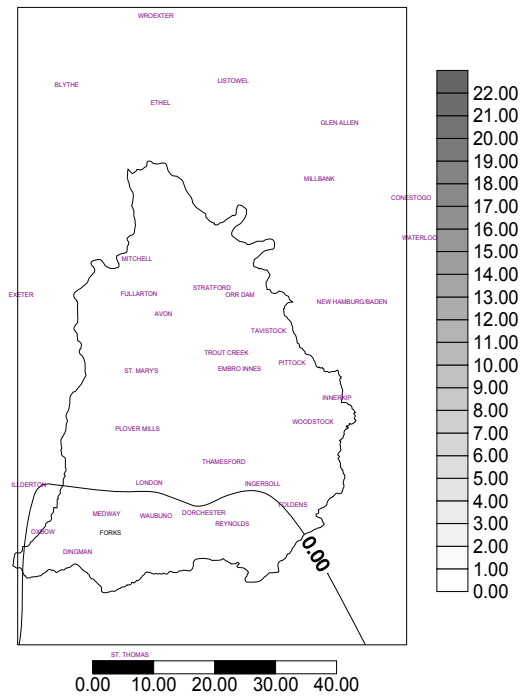
Figure C-74: Isohyets (mm) of Sept. 7 at 03:00

156
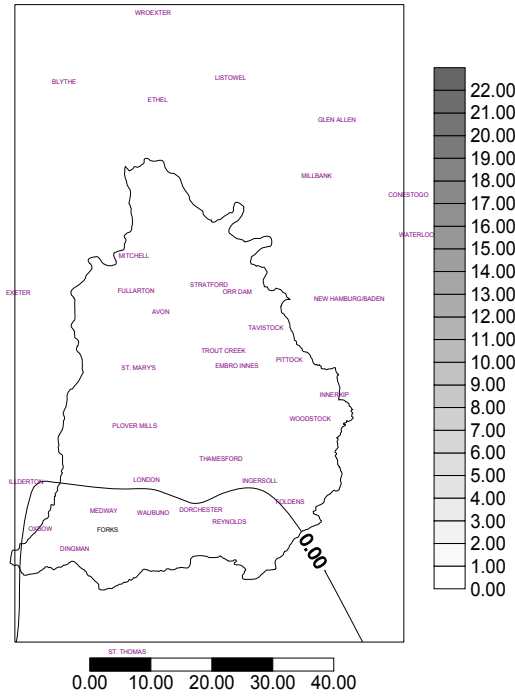
Figure C-75: Isohyets (mm) of Sept. 7 at 04:00
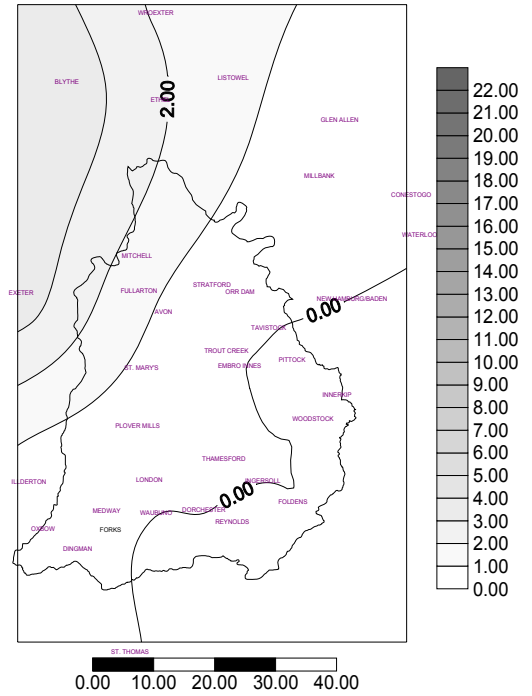
Figure C-76: Isohyets (mm) of Sept. 7 at 05:00
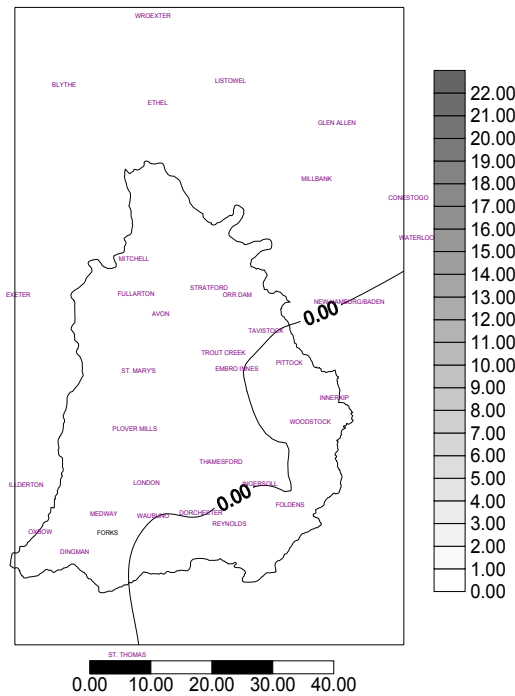
Figure C-77: Isohyets (mm) of Sept. 7 at 06:00
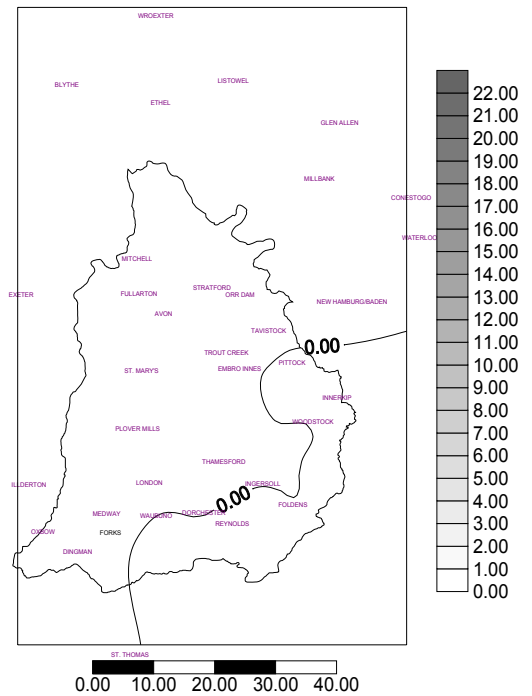
Figure C-78: Isohyets (mm) of Sept. 7 at 07:00

157
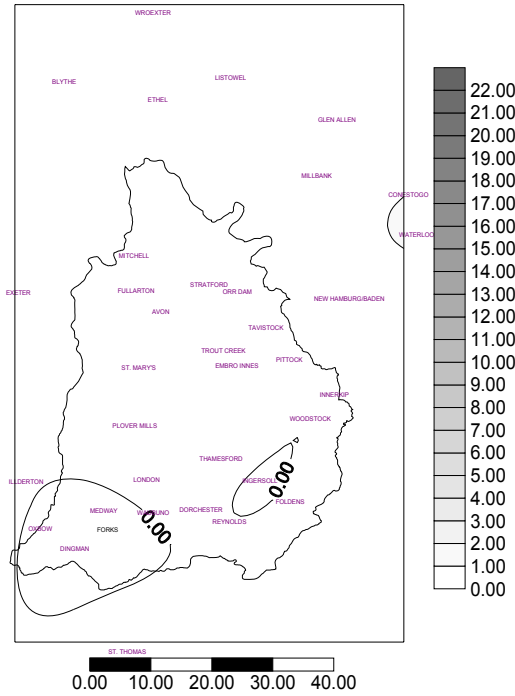
Figure C-79: Isohyets (mm) of Sept. 7 at 08:00
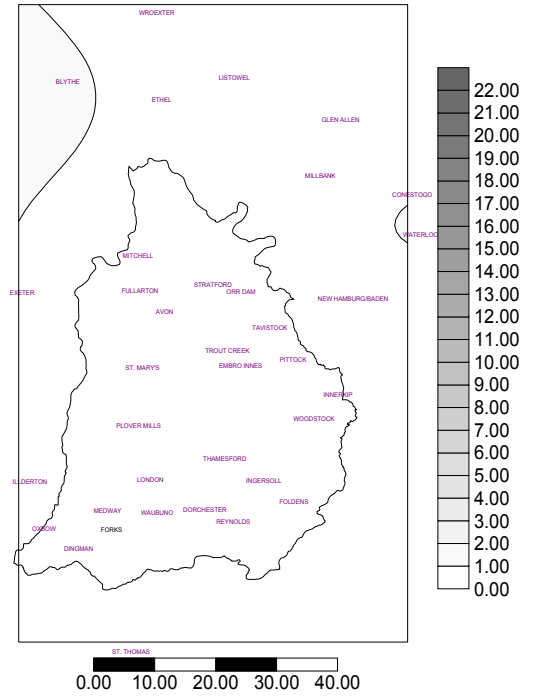
Figure C-80: Isohyets (mm) of Sept. 7 at 09:00
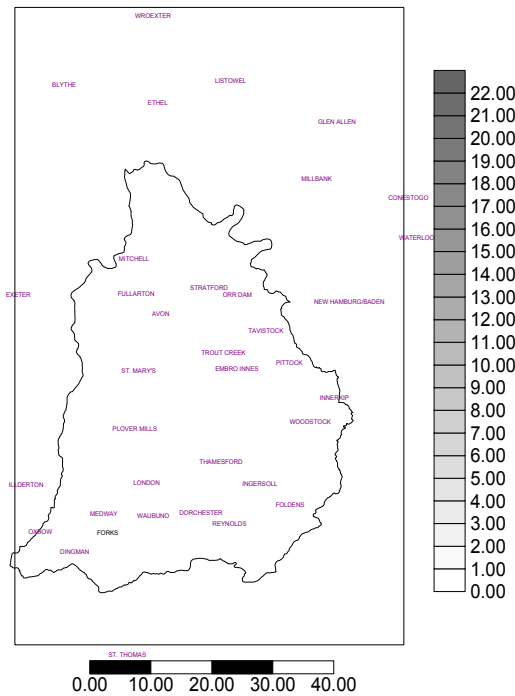
Figure C-81: Isohyets (mm) of Sept. 7 at 10:00
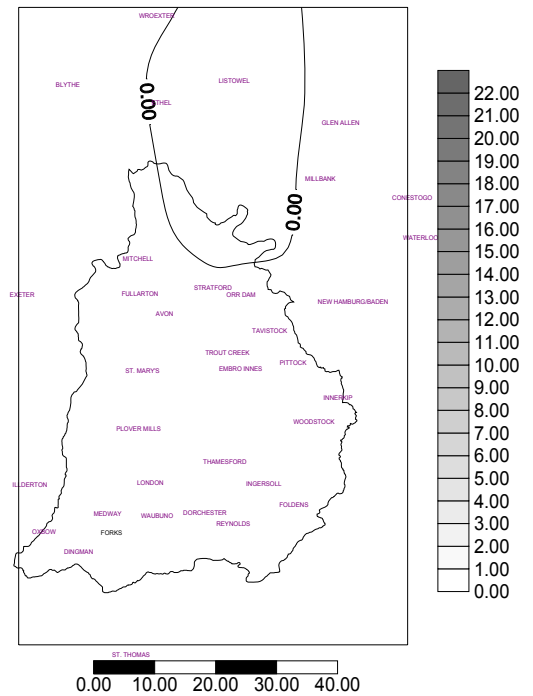
Figure C-82: Isohyets (mm) of Sept. 7 at 11:00

158
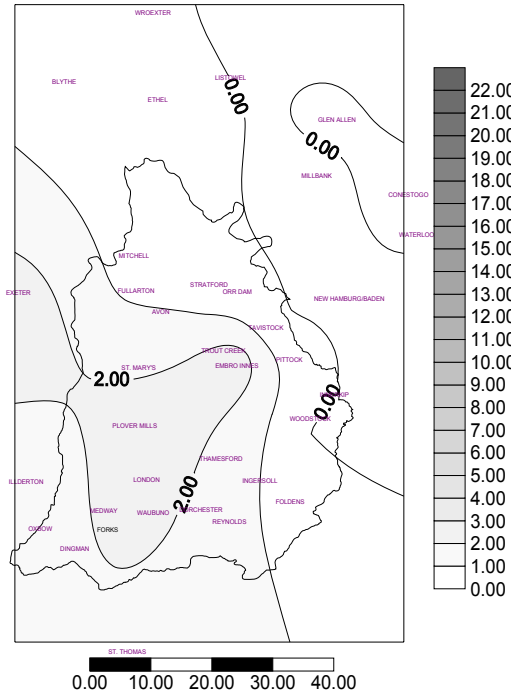
Figure C-83: Isohyets (mm) of Sept. 7 at 12:00
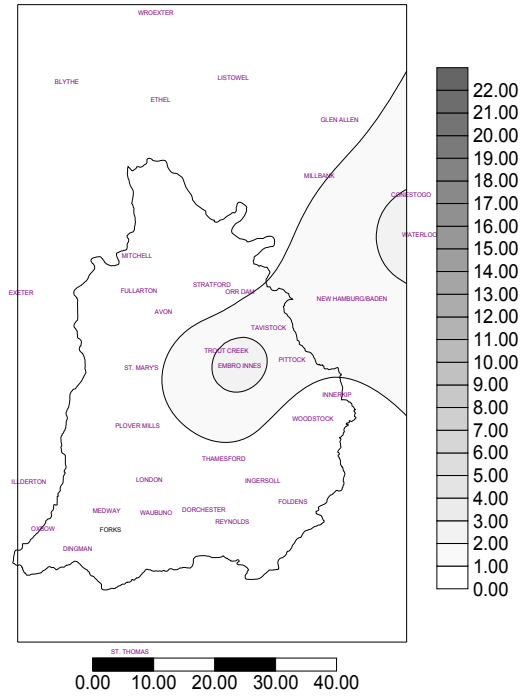
**Figure C-84: Isohyets (mm) of Sept. 7 at 13:00**
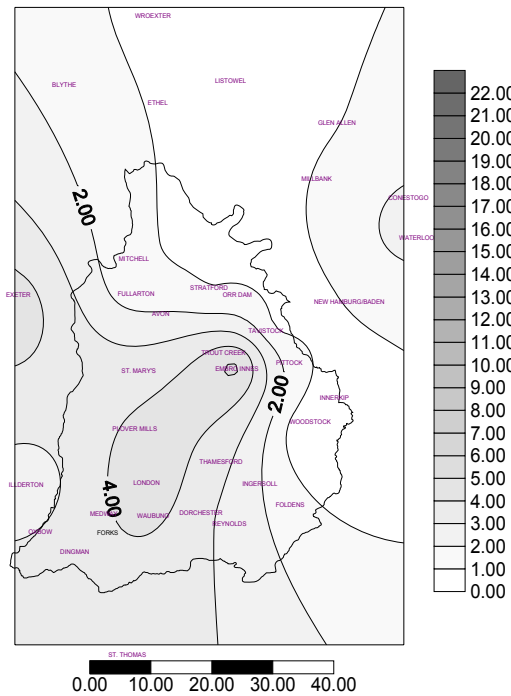

Figure C-85: Isohyets (mm) of Sept. 7 at 14:00
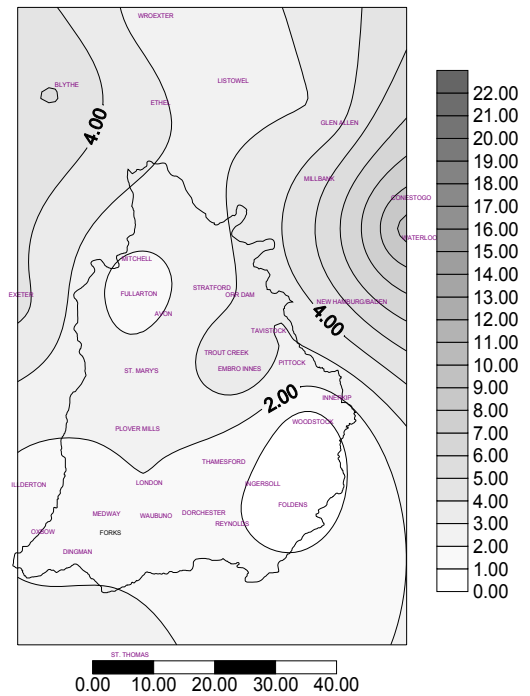

Figure C-86: Isohyets (mm) of Sept. 7 at 015:00

159

Figure C-87: Isohyets (mm) of Sept. 7 at 16:00

Figure C-88: Isohyets (mm) of Sept. 7 at 17:00

Figure C-89: Isohyets (mm) of Sept. 7 at 18:00

Figure C-90: Isohyets (mm) of Sept. 7 at 19:00

160

Figure C-91: Isohyets (mm) of Sept. 7 at 20:00

Figure C-92: Isohyets (mm) of Sept. 7 at 21:00

Figure C-93: Isohyets (mm) of Sept. 7 at 22:00

Figure C-94: Isohyets (mm) of Sept. 7 at 23:00

161
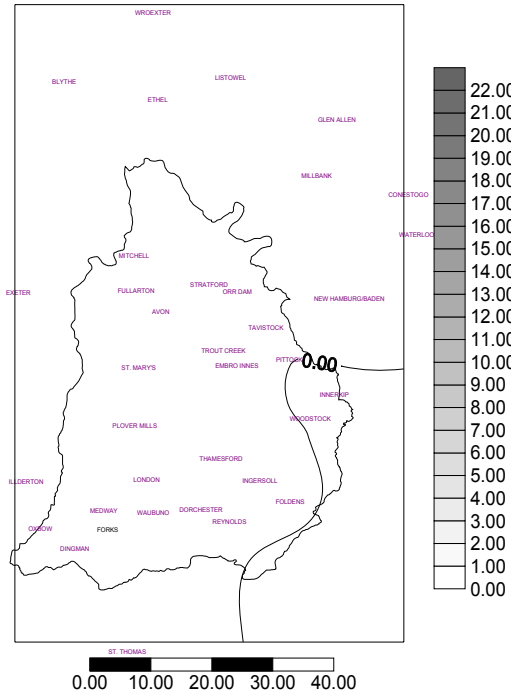
Figure C-95: Isohyets (mm) of Sept. 8 at 00:00
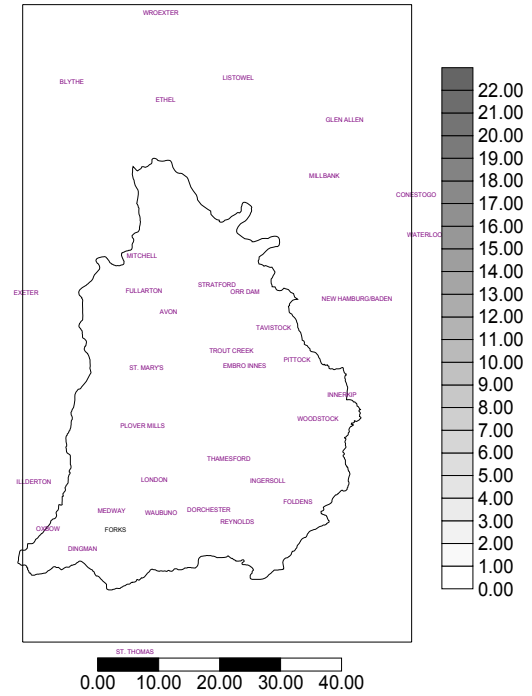
Figure C-96: Isohyets (mm) of Sept. 8 at 01:00
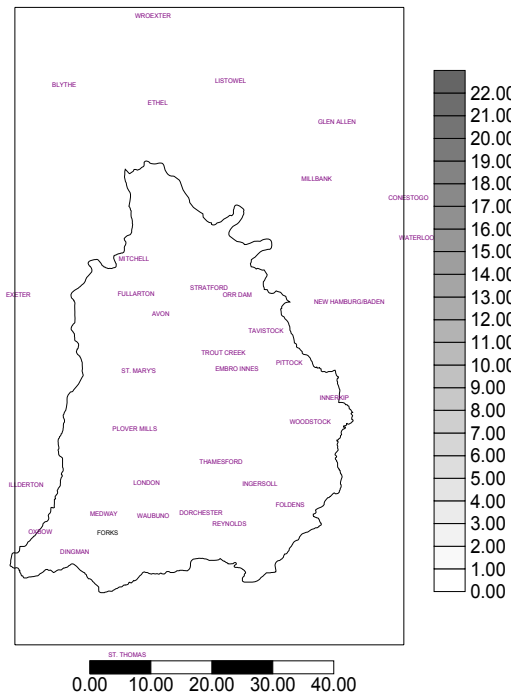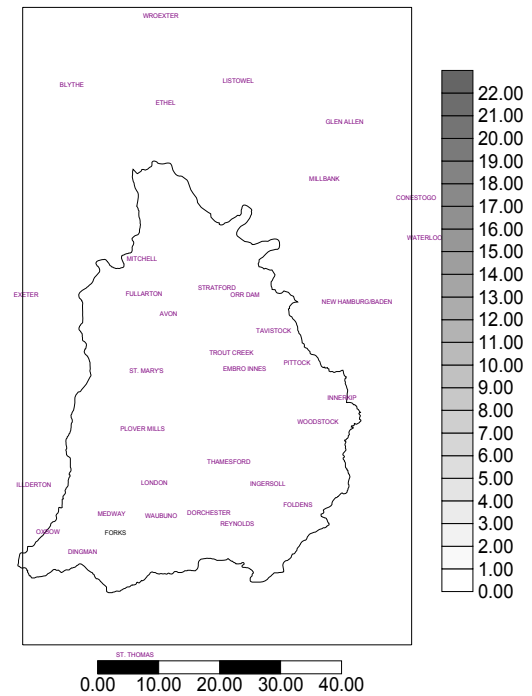

Figure C-97: Isohyets (mm) of Sept. 8 at 02:00
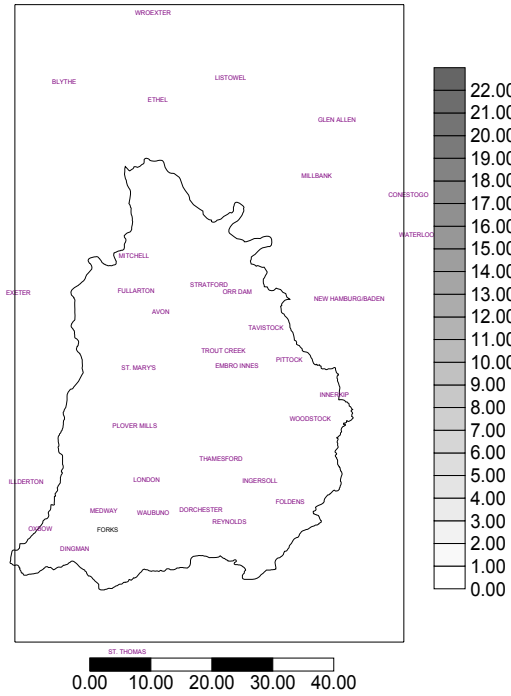

Figure C-98: Isohyets (mm) of Sept. 8 at 03:00

162

Figure C-99: Isohyets (mm) of Sept. 8 at 04:00
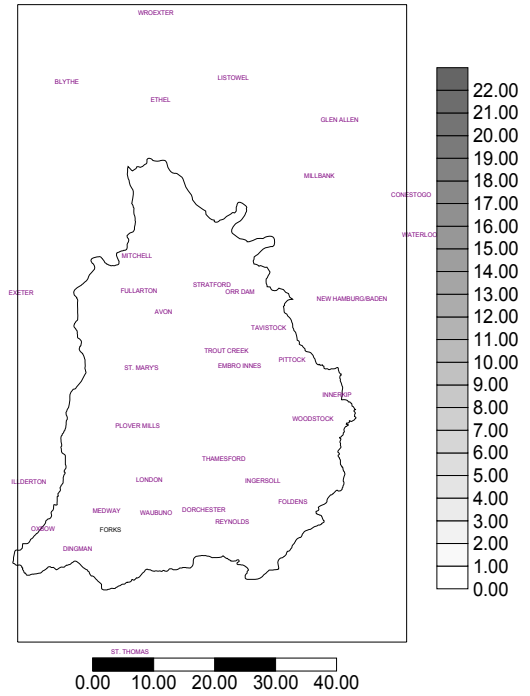

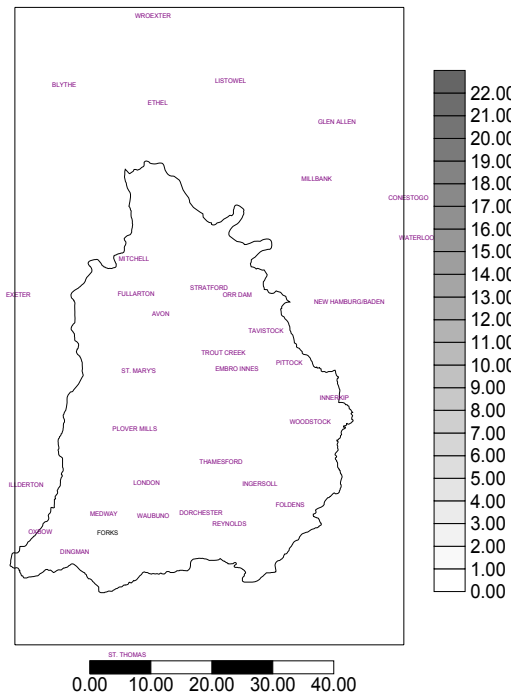**Figure C-100: Isohyets (mm) of Sept. 8 at 05:00**
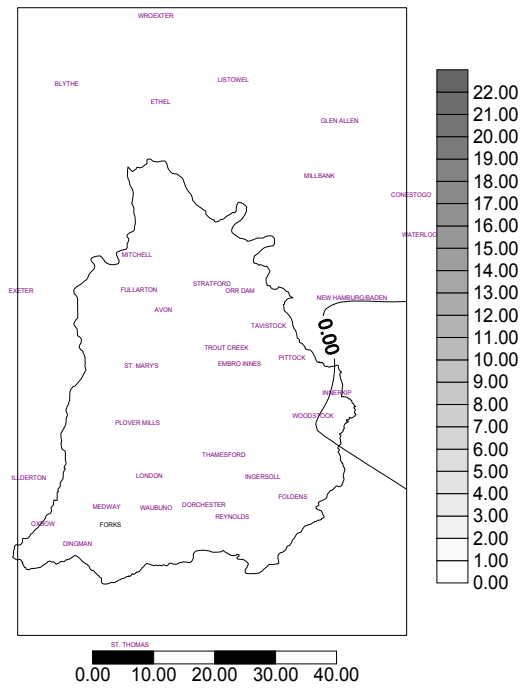

Figure C-101: Isohyets (mm) of Sept. 8 at 06:00

Figure C-102: Isohyets (mm) of Sept. 8 at 07:00

163